ABSTRACT

This project aims to investigate a fast and precise GPS processing algorithm suitable for short-baseline static deformation monitoring in short observation time-span. The slow displacement of static deformation can provide a fairly good *a priori* position determined in the previous measurements, which can be used as the approximate position for processing the new set of measurements. Ambiguity Function Method (AFM) is selected as the main data processing engine in this research. AFM has two advantages when applied to static deformation monitoring. Firstly, the search volume of AFM can be greatly reduced with a good *a priori* position, resulting in higher data processing efficiency. Secondly, Ambiguity Function is insensitive to cycle slips and computation of position using AFM does not require ambiguity resolution. However, AFM may result in an incorrect position when serious un-modeled errors and biases, such as multipath and ionospheric delay, are present in the measurements. Another disadvantage of AFM is that it has no direct and rigorous accuracy assessment for the positioning result.

In this research, two improved AFM GPS data processing algorithms are proposed to improve the GPS relative carrier phase positioning accuracy. They are the Combined AFM and Least Squares Method (LSM) with signal-to-noise ratio weighting (CALMS), and Signal-to-noise ratio Weighted Ambiguity function Technique (SWAT). Tests have been done and show that these two processing algorithms can effectively mitigate specular multipath as well as interference in GPS relative carrier phase measurements by using signal-to-noise ratio. Investigations

have also been made on an automatic and self-contained integrated GPS date processing algorithm, the integration of the above-proposed algorithms with Least-squares AMBiguity Decorrelation Adjustment (LAMBDA) method. The proposed integrated GPS data processing algorithm is applicable to process deformation measurements without a good *a priori* position. Test results show that integration of the above-proposed algorithms with LAMBDA can significantly reduce data processing time and provide extra statistical information on quality and reliability of processed results.

The proposed processing algorithms have been programmed using Visual Basic 5.0. The programs and test data sets collected on the roof of The Hong Kong Polytechnic University and in the construction site of the Hong Kong International Airport at Chek Lap Kok were used for verification of the proposed algorithms. Accuracy assessments are compared with pre-defined displacements on a X-Y-Z stage and results of the same set of data computed using Trimble's GPSurvey WAVE baseline processing software.

ACKNOWLEDGMENTS

I wish to thank Dr. Esmond C.M. Mok, my project chief supervisor, for his constructive criticisms, help in problems I came across and providing material, and his patience in supervising me. I want to extend my gratitude to the project co-supervisor Professor Y.Q. Chen and the other members of my departmental research committee, Dr. Z.L. Li (present chairman), Dr. Huseyin Baki Iz (ex-chairman), Dr. Jason C.H. Chao, and Dr. Guenther Retscher (returned Austria), and to the faculty and staff at the Hong Kong Polytechnic University for a fine education.

I am grateful to Mr. Ian Ayson, the Survey Manager of the Hong Kong New Airport Authority, for providing access to collect GPS data in the New Hong Kong Airport at Chek Lap Kok. Thank you Mr. Leslie Lam for his assistance in carrying out the fieldwork in Chek Lap Kok new airport site.

I am grateful to Mr. Steven Leung, the Chief Land Surveyor of the Hong Kong Mass Transit Railway Corporation for permission to acquire GPS data in the Tseung Kwan O construction site.

I appreciate very much the insights of LAMBDA given by Miss. Christian Tiberius.

I am grateful to Trimble Navigation Limited and PIL Systems Limited for GPS surveying instruments and support.

Finally, I want to thank all those who have contributed in any way to the completion of this project.

TABLE OF CONTENTS

LIST OF TABLES

LIST OF FIGURES

LIST OF SYMBOLS

A	- design matrix
a	- ambiguity vector
a	- partial derivative with respect to the receiver positions
b	- vector of position parameters, or observation
c	- velocity of light
D	- diagonal matrix
d	- multipath error
F	- F-distribution
f	- frequency
I	- ionospheric effect
L	- lower triangular matrix
l	- misclosure vector
M	- multipath error
m	- degree of freedom
N	- initial phase ambiguity
P	- weight matrix
Q	- variance-covariance matrix
S	- the number of satellites
T	- tropospheric effect
t	- time or epoch
v	- residual vector
W	- weight matrix

Z	- Z-transformation matrix
z	- Z-transformed ambiguity vector
Σ	- variance-covariance of parameters
λ	- wavelength of carrier phase (L1: ~19 cm; L2: ~24 cm)
φ	- carrier phase observable
ρ	- topocentric distance, or correlation coefficient
ε	- random measurement noise
σ	- standard deviation
α	- significance level
$\overset{km}{AB}$	- double differencing between two satellites (k and m) and two points (A and B)
$\wedge$	- approximate solution
$\vee$	- best estimated solution

LIST OF ABBREVIATIONS

AF	- Ambiguity Function value
AFM	- Ambiguity Function Method
AFR	- Ambiguity Function Ratio
C/A code	- Coarse/Acquisition code (1.023 MHz)
CALMS	- Combined AFM and LSM Method with Signal-to-noise ratio weighting
CNR	- Carrier-to-Noise Ratio
DD	- Double Differenced observable or Double Differencing
DoD	- Department of Defense
DOP	- Dilution of Precision
GDOP	- Geometric Dilution of Precision
GLONASS	- Global Navigation Satellite System
GPS	- Global Positioning System
GPSurvey	- Trimble's GPS data processing software
FARA	- Fast Ambiguity Resolution Approach
L1	- L1 carrier (1575.42 MHz)
L2	- L2 carrier (1227.6 MHz)
LAMBDA	- Least-squares AMBiguity Decorrelation Adjustment
LSAST	- Least Squares Ambiguity Search Technique
OTF	- On-The-Fly ambiguity resolution
PDOP	- Position Dilution of Precision

PLL	- Phase Lock Loop
RDOP	- Relative Dilution of Precision
RINEX	- Receiver INdependent EXchange format
SNR	- Signal-to-Noise Ratio
SWAT	- Signal-to-noise ratio Weighted Ambiguity function Technique
WGS-84	- World Geodetic System (1984)

CHAPTER 1

INTRODUCTION

This project aims to investigate a precise GPS data processing algorithm suitable for static deformation monitoring in small area coverage (baselines less than 10 km) with GPS data collected in short observation time.

Welsch [1996] defines that deformation monitoring is the measurement of displacement and distortion of an object, and Uren and Price [1994] state "deformation surveys can be used to measure the amount by which a structure moves both vertically and horizontally over regular time intervals". Chen and Chrzanowski [1986] describe that the two main purposes of a deformation monitoring are i) to give information on the geometrical status of a deformable body, the change in its position, shape, and dimensions; and ii) to give information on the physical status of a deformable body, the status of internal stress, and the load-deformation relationship.

Deformation monitoring is important because it provides useful deformation information of an object for deformation analysis and forecast. Therefore, necessary precautions can be taken to prevent loss of life and destruction of property due to, for example, earthquakes, volcanic eruptions, and collapse of structures such as dams and slopes.

Deformation can be classified by the response to movement. Welsch [1996] classifies deformation into dynamic, static and autonomous. Dynamic deformation is defined as the sudden movement of an object caused by accumulation of energy with

a time delay. Static deformation can be described as the external forces act on an object and causing it to move, but the movement stops when a new equilibrium position is reached. Other deformation, which is not caused by any external forces but disturbance noise, is classified as autonomous deformation.

1.1 Significance of Deformation Monitoring

Static deformation is important for civil engineering construction. Before, during and after construction, the movement of any structure must be monitored accurately and precisely so as to reduce possibility of collapse of structures such as buildings, bridges and other man-made structures. In addition to safety issues, deformation monitoring provides information on the stability of constructed structures and the suitability of further construction so it can keep the construction progress smooth and on time, otherwise, it may need more manpower, money and time for remedial work. Other static deformation monitoring applications include prediction of earthquakes, volcanic eruptions and land subsidence; hence we can take suitable safety measures to save life before accidents happen.

1.2 Deformation Measuring Techniques

It is possible to measure deformation by a number of different methods. The main measuring methods include:

i) conventional geodetic surveys;

ii) geotechnical and structural methods;

iii) photogrammetry; and

iv) satellite positioning techniques.

The selection of deformation measuring techniques is based on the following aspects:

i) the magnitude of movement;

ii) the required accuracy;

iii) the distance between the monitoring points involved;

iv) the measuring time;

v) the volume or area of the deformable body;

vi) intervisibility requirements;

vii) the deformation monitoring environment;

viii) absolute or relative displacement required;

ix) points or a network of points required; and

x) economical (cost effective) consideration.

1.2.1 Conventional Geodetic Surveys

Conventional geodetic surveys employ distances and angles for determining horizontal movements, and precise levelling for the height movement. These surveys are the most commonly used to determine deformations. They require line of sight intervisibility. Accuracy is deteriorated by distance between measuring points due to atmospheric refraction and instrumental errors such as scale error.

1.2.2 Geotechnical and Structural Methods

All of the geotechnical and structural methods are direct measurement methods. They involve determining changes in height, tilt, and length. Geotechnical methods measure changes in height by heave gauges or settlement gauges, in length by extensometers, in porewater pressure by piezometers, and in earth pressure using earth pressure cells. Structural methods measure changes in strain by a tensioned invar wire unit, strainmeters, or strain gauges, in inclination by inclinometers, and in tilt using tiltmeters. These high accuracy methods can yield millimetre results over short distances (<1 km) [Krakiwsky, 1986].

1.2.3 Photogrammetry

Photogrammetry is a powerful and rapid technique to collect deformation data. It utilizes metric-calibrated cameras in the terrestrial mode or aerial mode. The term "close-range photogrammetry" is generally used for terrestrial photographs having object distances up to about 300 m [Wolf, 1983]. The stereopairs of aerial or terrestrial photos contain the common photogrametric control points for determination of the coordinates of object points. Accuracies of a few millimetres can be achieved over short distances [Krakiwsky, 1986].

1.2.4 Satellite Positioning Techniques

Deformation monitoring data can be obtained with four satellite systems: i) The Doppler-Transit System; ii) Satellite Laser Ranging (SLR); iii) Very Long Baseline Interferometry (VLBI); and iv) Global Positioning System (GPS). Accuracies are shown in [Krakiwsky, 1986]. SLR and VLBI are high-accuracy but expensive. GPS is accurate and cost effective.

1.2.5 Summary of Techniques

Accuracies of the above measuring techniques deteriorate with increasing baseline length. Photogrammetry is powerful over short baselines. Geotechnical and structural methods are highly accurate over short distances. However, both photogrammetry and geotechnical and structural methods may not be suitable for monitoring large deformable bodies such as reclaimed land, or detecting local deformations inside the deformable body. Conventional geodetic surveys are next best over short distances but GPS is best for short baselines [Krakiwsky, 1986].

1.3 Conventional and GPS Technique on Deformation Monitoring

Movements of deformable bodies can be monitored by conventional angular and distance measurement techniques. These techniques usually require much manpower and time for observation of the whole monitoring network. Moreover, stations in the

monitoring network must be intervisible and therefore observation can only be made under good weather conditions.

For deformation surveys, a few millimetres or even less are measured and precisions of this order require the best surveying techniques to be used throughout a deformation monitoring. Remondi [1984] investigated using the Global Positioning System (GPS) for geodesy and found that the accuracy of GPS positioning was suitable for many surveys.

The Global Positioning System (GPS) was primarily designed by the U.S. Department of Defense for military navigation, velocity and time determination. The system consists of 24 operational satellites which can provide 24-hour and all-weather positioning capability worldwide above the earth surface.

Standard Positioning Service of GPS is available to international civil users and the use of GPS in surveying is growing rapidly. Application of GPS in surveying includes control survey, topographic survey, engineering survey, deformation survey and so forth. The use of GPS in deformation monitoring has received considerable interest in the last few years. Examples of GPS application or research in deformation monitoring can be found in [Ayson and Lang, 1996], [Bock et al., 1990], [Coulon and Caristan, 1990], [DeLoach, 1989], [Dong and Bock, 1989], [Hein and Riedl, 1995], [Lindquister et al., 1989] and [Rizos et al., 1996].

As GPS can take measurements anytime, anywhere and under all-weather condition, this makes continuous monitoring possible. Moreover, GPS observation has no limitation of inter-visibility between stations that causes problem in conventional monitoring methods. The size of GPS receivers becomes smaller and

less power consumption, which give extra merit in using GPS for deformation monitoring. Also, the growth of GPS receivers has high accuracy carrier phase observation capability, it makes GPS solution in centimetre accuracy possible. Advantages of using GPS over conventional technique in deformation monitoring are summarized in Table 1.1.

Table 1.1
Advantages of using GPS over conventional technique in deformation monitoring

	Conventional technique	GPS technique
All weather; anytime	Under good weather condition	Yes
Intervisibility between stations	Required	Not required
Instrumental size	Relatively large	Relatively small
Manpower	More	Less (can be one person)
Observation time	Usually longer (reciprocal and redundant observations required)	Shorter, can be a few minutes (depends on the GPS data processing algorithm)
Automation	No	Yes
Human error	Present	Less likely
Power consumption	Relatively more	Relatively less

GPS is not without problems and constraints. Satellite signals can only be received with a clear view to the sky. And GPS is an automatic operation system, so it causes reliability problems. Moreover, GPS receivers are too expensive; it is particularly true when using GPS for deformation monitoring. Deformation monitoring may have to be undertaken in very hostile environments. In such environments, the receivers may be damaged or lost when there are accidents such as collapse of structures. Despite these difficulties, GPS has been increasingly used for deformation monitoring.

1.4 Previous Work on Deformation Monitoring

GPS is increasingly used for control surveying, engineering surveying and deformation monitoring in Hong Kong. Geotechnical Engineering Office (GEO) of the Hong Kong Government, Survey section of the Airport Authority Hong Kong and some private surveying firms have used GPS for control surveying, topographic surveying, setting out, hydrographic surveying and deformation monitoring. For example, GEO applies GPS to deformation monitoring of sliding slope; Highways Department uses GPS for engineering surveying of highway constructions and deformation monitoring of the Tsing Ma Bridge; and Survey section of the Airport Authority Hong Kong employed GPS for control surveying, topographic surveying and setting out in the construction of the airport. Since the Hong Kong International Airport at Chek Lap Kok is built on a reclaimed land and it involved missive deformation monitoring and building construction in this area, the following discussion will be concentrated on deformation monitoring of this airport construction project.

Survey section of the Airport Authority Hong Kong used GPS almost for all surveying work including control surveying, stake out, setting out and horizontal deformation monitoring [Ayson and Lang, 1996]. Vertical deformation monitoring (or called settlement) was the deep concern of the Airport Authority Hong Kong as the Hong Kong International Airport at Chek Lap Kok is built on a newly reclaimed island (see Figure 1.1) [Ayson and Lang, 1996]. However, they did not use GPS for

settlement surveying. It is because they thought GPS technique was not reliable and accurate for vertical deformation monitoring.

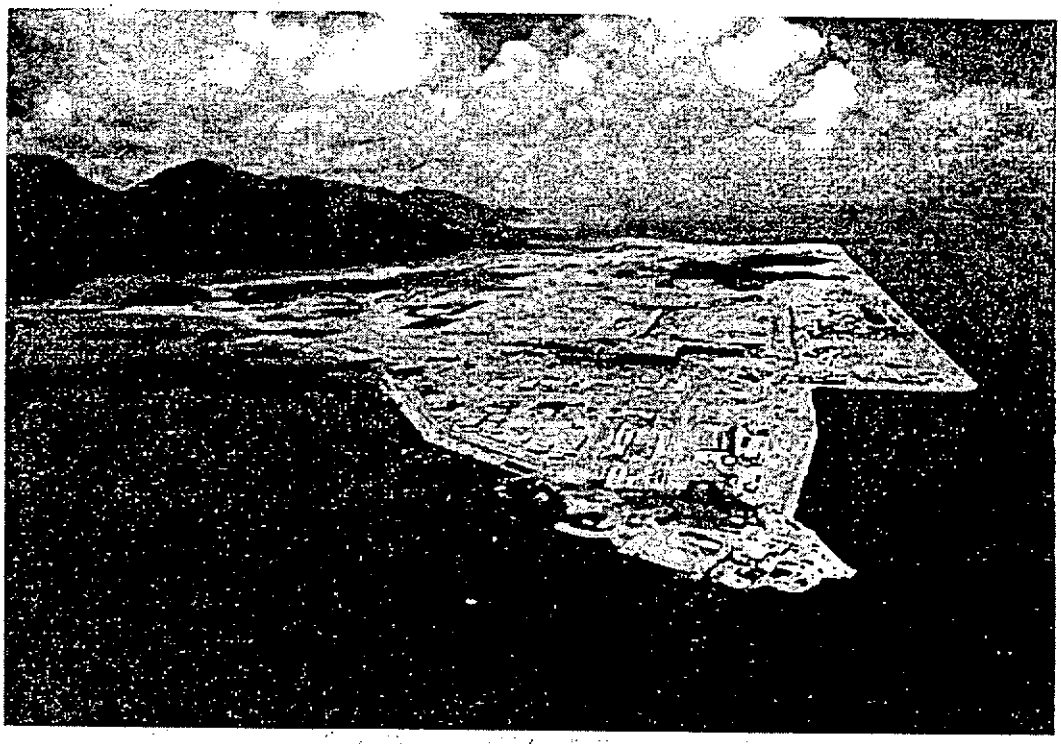

Figure 1.1
The newly reclaimed island of the New Hong Kong Airport at Chek Lap Kok

1.4.1 Background of Deformation Monitoring in the Airport

The Hong Kong International Airport at Chek Lap Kok is built on a newly reclaimed island. The reclamation was designed to ensure that permanent structures would not be adversely affected by settlement or deformation of the platform. To monitor this, extensive geotechnical investigations were undertaken prior to commencement of the reclamation. Deformation measurements of the reclamation were undertaken during and after construction. The results were compared with

design estimates of settlement and are used to make accurate prediction of future settlements.

There were nearly 2000 settlement markers and geotechnical instruments over the reclaimed island [Ayson and Lang, 1996]. They were measured either weekly or monthly by conventional precise levelling using high precision and fully digital levels. Besides, stable bench marks or datum piles (see Figure 1.2) were built over the island. They were about 1 km apart. Some of them reached down to a depth of 90 m. These important markers helped to determine deformation in all three planes. Keeping track of subsidence in newly reclaimed areas gave great workload to the surveyors of the authority.

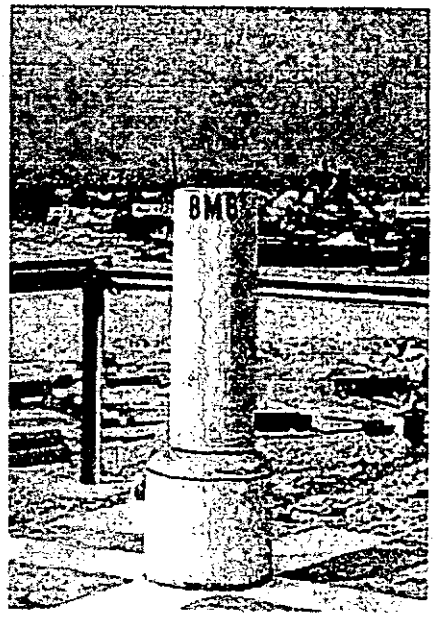

Figure 1.2
Bench mark and Datum pile, which are firmly anchored in bedrock

The daily responsibilities of the Airport Authority's Survey Section were control surveying, engineering surveying (setting out and check as-built) and settlement monitoring [Ayson and Lang, 1996]. Settlement monitoring of the authority was

done by precise levelling of various geotechnical instruments and settlement markers. It was hard and inefficient to run close-loop precise levelling around a 1,248ha island at about 2000 survey points. GPS technology was used for control surveying, setting-out and checking as-built. They were investigating the possibility of using GPS for settlement monitoring. So, if there was a precise and rapid GPS processing algorithm for deformation monitoring, it would not only benefit the Airport Authority's Survey Section but also all users of GPS deformation monitoring and height determination.

The positioning accuracy of GPS may be insufficient for deformation monitoring in centimetre accuracy, especially vertical accuracy. Achievable accuracy of the most accurate relative static GPS observation technique is ± 5mm, claimed by GPS receiver manufacturers such as Ashtech, Leica and Trimble. However, it is still far away from the 0.8 mm minimum ideal accuracy (IMA) defined and derived in section 2.3.2. Derivation of the 0.8mm IMA is based on a geodetic receiver capable to measure thousandth of carrier phase (L1 is about 190 mm and L2 is about 240 mm) [Lau and Mok, 1999b]. The limitation of GPS positioning accuracy is mainly due to multipath effect, ionospheric effect, tropospheric effect and receiver noise. Besides, signal strength (indicated in signal-to-noise ratio), cycle slip and correctness resolution of ambiguity will affect the GPS solution. Weak signal strength, cycle slip and multipath effect may become more significant errors when GPS deformation monitoring is carried out in engineering site. Engineering site is always piled with construction material, vehicles and power generators. Reflectivity of construction material (e.g. steel and other metallic substance) and vehicles cause multipath effect

for GPS measurement. Power generator and radio may make noise or interference to GPS signals. It leads to low signal strength (or SNR) or, even worse, causes cycle slip. The above problems were unavoidable when using GPS in the airport construction site; and might worsen because strong radio signal is emitted by the airport control centre.

In view of the above background of the airport construction project, the Airport Authority has established good deformation monitoring network, monitoring stations (see Figure 1.2) and settlement markers. It was therefore ideal to select the construction site of the Hong Kong International Airport at Chek Lap Kok as the site for deformation monitoring data acquisition in this project.

1.5 Significance of this Project

The improved GPS data processing algorithm makes GPS positioning more accurate, precise and reliable for high-accuracy GPS surveying such as control surveying, topographic surveying, setting out, and deformation monitoring in construction site and urban area. Rapid and precise measurement methodology, and accurate, precise and reliable GPS data processing algorithm (applied to high-accuracy deformation monitoring) provide us with accurate and reliable information for deformation analysis. So we can forecast movements, such as earthquakes and collapse of structures, and prevent disasters.

When single epoch data are used, the algorithm has great potential for rapid surveying and even precise vehicle navigation in urban area [Lau and Mok, 1999c].

1.6 Objective of this Project

This project is to investigate into the GPS data processing algorithm applied to deformation monitoring. It aims to improve the positioning accuracy of GPS for monitoring deformation in engineering site and other GPS applications, so factors affecting the accuracy are investigated. Since signal strength (indicated in signal-to-noise ratio), cycle slip, correctness resolution of ambiguity and multipath effect will affect GPS solution for short baselines (Figure 1.3), investigation into the GPS processing algorithm takes all these factors into account in order to give precise and reliable information for further deformation analysis.

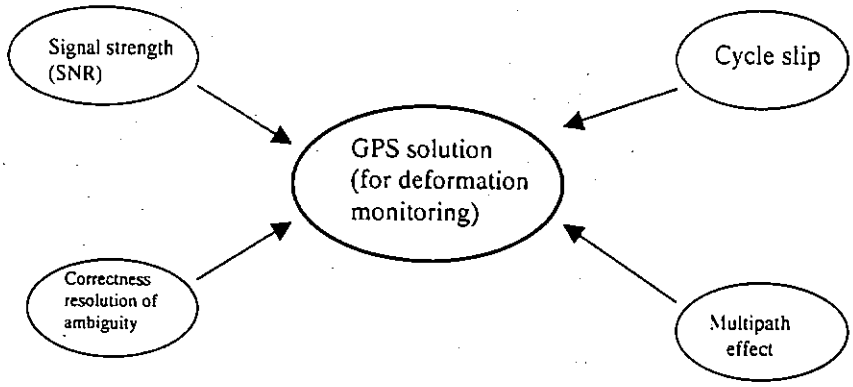

Figure 1.3
Factors affecting GPS solution in engineering site

In particular, this research examines the achievable accuracy of GPS for height determination (settlement monitoring). It aims at developing a technique to improve the accuracy and reliability of GPS for height determination. The overall objective of

the research is to develop a fast and reliable measurement methodology, and a rapid and precise GPS processing algorithm for deformation monitoring.

Development of the GPS data processing algorithm is based on Ambiguity Function Method (AFM). Programs written in Visual Basic 5.0 are used to implement the processing algorithm. In addition to implementation, they can validate the processing algorithm(s) at various stages.

Apart from development of methodology for rapid and precise measurement and processing algorithm, the project develops a GPS quality assurance procedure to keep the result reliable and accurate. Quality assurance procedure is to give specification of measurement, and quality of observation and solution [Mittag and Rinne, 1993].

1.7 Organization of the Thesis

Chapter 2 is the fundamental of GPS data processing. It briefly describes the GPS biases, errors, limitations and conditions in general and engineering site. Moreover, it describes and discusses the current GPS data processing algorithms and validation procedures. Chapter 3 investigates into the selected GPS data processing algorithms – AFM and LAMBDA method. Chapter 4 is dedicated to the proposed GPS data processing algorithms in this project. It describes the principles and procedures of the Combined AFM and LSM Method with Signal-to-noise ratio weighting (CALMS), Signal-to-noise ratio Weighted Ambiguity function Technique (SWAT), and an integrated GPS data processing algorithm. Chapter 5 is the description of test data

sets. Chapter 6 deals with the results and analyses of the proposed processing algorithms based on the test data sets. The performances of the algorithms are shown in this chapter. Finally, Chapter 7 concludes the significance of the proposed GPS data processing algorithms, describes the limitation of this research, and gives recommendations for future studies.

CHAPTER 2

FUNDAMENTAL OF GPS DATA PROCESSING

2.1 Biases, Errors, and Limitations of GPS

Bias is defined as the difference between the value of the parameter and the expectation of the estimator and it is equivalent to the term "systematic effect" or "systematic error" [Mikhail, 1976]. Biases of GPS are therefore the systematic error of GPS itself, its receiver and observation.

Wells et al. [1987] classified GPS biases into three categories. They are satellite biases, station biases, and observation dependent biases. Satellite biases consist of biases in the satellite ephemeris and satellite clock model. Station biases include receiver clock biases and reference station coordinates biases. Since this project is focused on relative positioning in small area coverage, satellite biases and receiver biases become relatively less important; these biases can be largely reduced or eliminated through the differencing techniques (see section 2.3.1). Only observation dependent biases are considered here. Observation dependent biases consist of ionospheric effect, tropospheric effect, and carrier phase ambiguity. Moreover, GPS positioning accuracy is affected by errors present during measurements. These errors include residual biases, cycle slips, multipath, antenna phase centre movement, and random observation error. Only cycle slip and multipath are considered in the following sections since the other error sources are either receiver or hardware dependent, or unavoidable. Besides, there are some limitations or conditions for GPS

to achieve geodetic accuracy and resolve ambiguity correctly. They are dilution of precision (DOP), baseline length, observation time, the number of satellites, satellite elevation angle and signal strength (indicated in signal-to-noise ratio).

2.1.1 Ionospheric Effect

The ionosphere starts 50 km above the Earth and extends in various layers 1000 km or more. Ultra-violet radiation from the sun ionises the gas molecules in this layer, thereby it is called ionosphere. The phase refractive index of the ionosphere is directly related to the number of free electrons along the path of the signal and inversely proportional to the square of frequency. Thus ionospheric effect is dispersive; it depends on the frequency. This characteristic causes code delay and phase advance when GPS signal passes through the ionosphere. It results in range errors. Examples and researches in the ionospheric effect can be found in [Abdalla and Fashir, 1991], [Davis et al., 1995], [Jakowski et al., 1995], [Komjathy et al., 1995], [Ou, 1995] and [Wanninger and Jahn, 1991].

2.1.2 Tropospheric Effect

The troposphere is the lower part of the earth's atmosphere. This layer is nondispersive, therefore its effect is frequency independent. However, tropospheric effect is temperature, humidity, and pressure dependent. Troposhere delays both code and carrier phase measurement. The total tropospheric delay can reach 2.0 to 2.5

metres in the zenith direction, and increases approximately with the cosecant of the elevation angle [Leick, 1995; Strang and Borre, 1997]. It yields about a 20-28 m delay at a 5° angle [Leick, 1995]. The nondispersive tropospheric error cannot be eliminated by dual-frequency observation. [Davis et al., 1995; Geiger et al., 1995; Ou, 1995]

2.1.3 Carrier Phase Ambiguity

When GPS signal is initially locked by a receiver (Figure 2.1), the receiver register starts to count the incoming signal. The fractional cycle ($\Delta\lambda$) of the signal at the first measurement epoch (t = 1) is precisely recorded. An arbitrary value (A) is set at the first epoch (t=1). And then the register counts the integer cycles ($I_{2...}n$) and fractional cycle (f) in the following measurement epochs (time = 2...n).) However, the initial integer cycles (N) between the satellite S and the receiver R are unknown. It is called integer ambiguity of the satellite S and the receiver R.

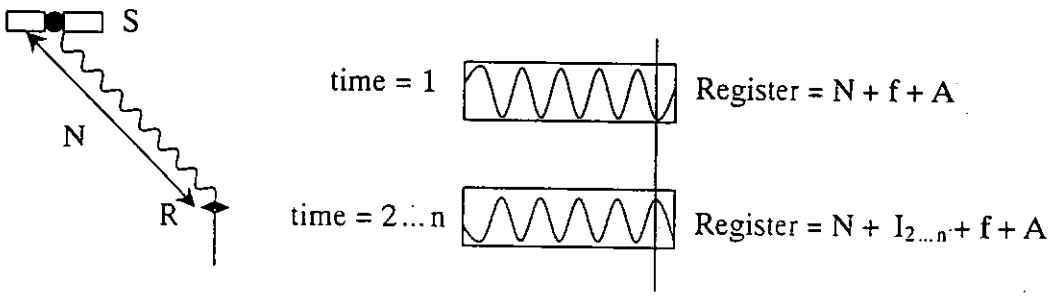

Figure 2.1
Carrier phase ambiguity

Ambiguity resolution is the determination of the integer value of the ambiguity. The resolved ambiguity has included the arbitrary value A; that is why the ambiguity may be negative (see Table 3.8 and Appendix II). A similar description can be found in [Leick, 1995, pp.326] and it states that in the hypothetical case of no ionospheric and tropospheric delays and the complete absence of all other errors (including the "register setting" of the carrier phase counter of the receivers is zero or an initial constant is subtracted from the carrier phase observations during preprocessing), the computed ambiguity would equal the topocentric distance. Once the ambiguity has been resolved, high accuracy GPS positioning becomes theoretically achievable (if a minimum of four satellites are available). However, incorrect resolution of ambiguity can cause serious positioning error. Han and Rizos [1997a and 1997b] stated that ambiguity resolution becomes a key procedure for centimetre accuracy GPS positioning. Moreover, ambiguity resolution is very time-consuming as it may involve search of possible solutions. Efficiency in ambiguity resolution efficiency has become more crucial for real-time kinematic (RTK) processing algorithms.

2.1.4 Cycle Slips

Cycle slips would affect the GPS solution because an unknown number of integer phase cycles will impose on the carrier phase measurement. Cycle slip errors can be caused by

i) obstruction of the satellite-to-receiver signals by, for example, trees, buildings, bridges (Figure 2.2)

ii) low signal-to-noise ratio due to bad atmospheric conditions, multipath, or low elevation satellite

iii) sudden and rapid change in velocity

Failure to repair cycle slips will cause incorrect positioning. Investigation on cycle slip can be found in [Hilla, 1986; Lichtenegger and Hofmann-Wellenhof, 1990].

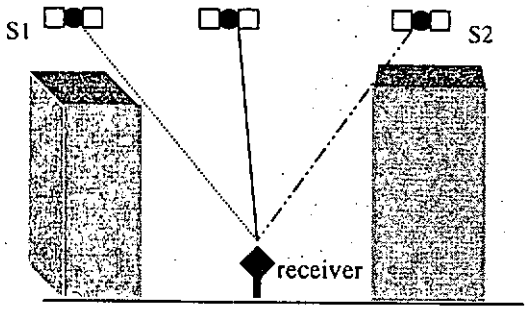

Figure 2.2
GPS signal tracking problems caused by obstructions

2.1.5 Multipath

Cohen [1996] and Lightsey [1996] expressed that multipath effect accounts for at least 90 percent of the total error budget in relative carrier phase measurement. Multipath effect is therefore a major source of error in GPS positioning. Multipathing is caused by the mixing of the direct signal with unwanted signals reflected from surfaces near the receiver site. The reflected signal, also called indirect path or secondary path, when combined with the direct signal, will form a composite signal (mixing of direct and reflected signal). The change in the phase value of the composite signal will lead to inaccurate or incorrect positioning results.

The multipath error can be explained mathematically as follows:

The direct signal can be expressed as

$$A_0\cos\varphi \tag{2.1}$$

The reflected signal (multipath)

$$\beta A_0\cos(\varphi+\Delta\varphi) \tag{2.2}$$

When the two signals are combined, the superimposed signal will become

$$A_0\cos\varphi + \beta A_0\cos(\varphi+\Delta\varphi) \tag{2.3}$$

where A_0 and φ denote the amplitude and the phase of the direct signal, β is the damping factor and $\Delta\varphi$ is the phase shift; the above equations ignored receiver noise. If M represents the multipath error caused by a single satellite, reflector and antenna (as expression (2.2)), then under the conditions that total multipath error for $a=1,2,..j$ number of antennae, $s=1,2,..k$ number of satellites in view, $r=1,2,..l$ number of reflectors related to the measurement environment, and $t=1,2,...i$ number of measurement epochs, the total multipath errors can be expressed as

$$\text{Total multipath error for single epoch} = \sum_{a=1}^{j}\sum_{s=1}^{k}\sum_{r=1}^{l} M \tag{2.4}$$

$$\text{Total multipath error for epochs} = \sum_{t=1}^{i}\sum_{a=1}^{j}\sum_{s=1}^{k}\sum_{r=1}^{l} M \tag{2.5}$$

The total multipath error on GPS solution is very complicated since it is different from site to site, therefore differencing techniques cannot eliminate this error. In processing the baseline vector, total multipath error at known (fixed) station will transfer to the unknown station. Therefore, the total multipath error of known station incorporates in that of unknown station, yielding the resultant total multipath error of $d_{km}^{pq}(t)$ in the general DD phase observation equation:

$$\varphi_{km}^{pq}(t) = \varphi_{km}^{p}(t) - \varphi_{km}^{q}(t) + N_{km}^{pq} + I_{km}^{pq}(t) + \frac{f}{c}T_{km}^{pq}(t) + d_{km}^{pq}(t) + \varepsilon_{km}^{pq} \qquad (2.6)$$

where N_{km}^{pq} denotes the DD integer ambiguity,

$I_{km}^{pq}(t)$ denotes the DD ionospheric delay at epoch t,

$T_{km}^{pq}(t)$ denotes the DD tropospheric delay at epoch t,

$d_{km}^{pq}(t)$ denotes the resultant or net multipath error after DD at epoch t,

ε_{km}^{pq} is the random carrier phase measurement noise, and

$\varphi_{km}^{p}(t)$ *and* $\varphi_{km}^{q}(t)$ denote between-receiver single-differenced carrier phase data..

Multipath effect is a random process [Strang and Borre, 1997] and has a non-zero mean [Van Nee, 1992], therefore smoothing and averaging of measurements cannot effectively reduce this type of error. Due to the above multipathing properties, investigating a method to reduce the multipath errors existing in the GPS data is needed.

2.1.6 Limitations and Conditions of GPS positioning

In addition to the errors and biases, GPS positioning is also subject to some limitations and conditions that would affect the accuracy, correctness and reliability of ambiguity resolution. They are Dilution Of Precision (DOP), baseline length, observation time, the number of satellites, satellite elevation angle, and signal strength (indicated in signal-to-noise ratio).

2.1.6.1 Dilution of Precision (DOP)

DOP is the purely geometrical contribution to the uncertainty in a position fix [Strang and Borre, 1997]. It indicates the effect of the satellite-receiver geometric distribution on the accuracy of the code solution. DOP values are simple functions of the diagonal elements of the covariance matrix of the adjusted parameters [Leick, 1995]:

$$Q_x = \left(A^T A\right)^{-1} = \begin{bmatrix} \sigma_x^2 & \sigma_{xy} & \sigma_{xz} & \sigma_{xt} \\ \sigma_{xy} & \sigma_y^2 & \sigma_{yz} & \sigma_{yt} \\ \sigma_{xz} & \sigma_{yz} & \sigma_z^2 & \sigma_{zt} \\ \sigma_{xt} & \sigma_{yt} & \sigma_{zt} & \sigma_t^2 \end{bmatrix} \tag{2.7}$$

Geometric dilution of precision, GDOP = $\sqrt{\sigma_x^2 + \sigma_y^2 + \sigma_z^2 + \sigma_t^2}$ (2.7.1)

Position dilution of precision, PDOP = $\sqrt{\sigma_x^2 + \sigma_y^2 + \sigma_z^2}$ (2.7.2)

For definition of the other DOPs, please refer to [Hofmann-Wellenhof et al., 1994, pp. 253 and Leick, 1995, pp 253].

Measurements with the DOP less than eight are normally considered as an acceptable level. Many receiver manufacturers advise users to stop taking measurement when DOP (GDOP or PDOP) is greater than eight because measurements with DOP higher than this threshold will yield relatively weak geometry, thus affecting the positional accuracy σ, which is the function of the DOP and the measurement accuracy [Hofmann-Wellenhof et al., 1994, pp. 253 and Leick, 1995, pp 253]:

$$\sigma = \sigma_o DOP \tag{2.8}$$

where σ is the standard deviation of the position or the positioning accuracy,

σ_o is the standard deviation of measurement or measurement accuracy, and

DOP is the dilution of precision

2.1.6.2 Baseline Length

Baseline length is another factor that affects the positioning accuracy. It is because the advantage of using differencing techniques to reduce ionospheric and tropospheric effects will deteriorate with the increase in baseline length. If the height variation between two stations is not great, and the baseline length is within 10km,

the ionospheric and tropospheric error can be greatly reduced due to the similarity of these effects at both stations. When the baseline is longer than about 10 km, ionospheric and tropospheric corrections may be applicable but it has the risk of having big modelling error. Therefore for long baseline it is advised to use ionospheric-free solution or ionospheric solution [Mader, 1992]. In addition to ionospheric and tropospheric effect, reference frame and orbital errors are the dominant error sources for the baseline range from 10 to 10^3 km [Bock, 1998].

2.1.6.3 Duration of Observation

Short observation period can affect the correctness of ambiguity resolution and significantly affect the effectiveness of reducing multipathing by averaging or estimation. Even though reduction of multipath effect of data observed in short time span may be achieved by, for example, choke ring antenna or modelling of the multipath effect, the observation period must be long enough for correct ambiguity resolution. Lau [1995] carried out a test on the effect of observation period on GPS positioning with Leica GPS System 300 and SKI GPS data processing software version 1.09. According to this test, ambiguity resolution generally requires at least 2 minutes data in 15 seconds measurement interval. It is of course subject to many factors such as the baseline length and number of satellites. Once the ambiguities have been correctly determined, centimetre-accuracy positioning results can be achieved. Before the minimum observation time is reached, sub-metre accuracy can be achieved using the float solution. It was also found that the longer the observation

period, the higher the accuracy, because of the significant change in satellite geometry and in-view satellites.

2.1.6.4 Elevation Angle

GPS data quality would be affected by the incident angle of the satellite signal. Firstly, ionospheric effect and tropospheric effect become unstable, therefore it is difficult to predict when the elevation angle is low. Secondly, the multipath effect becomes serious when low elevation satellite is observed. Therefore it is generally advised that at least 10° to 15° of elevation angle (mask angle) should be configured in the GPS receiver hardware.

2.1.6.5 Signal Strength

Hatch [1991] states that the noise level of the measurements is very important to the number of potential solutions in ambiguity resolution. High noise level data may cause less accurate or even incorrect solution, and reduce the data processing efficiency.

Noise can be divided into environmental noise and receiver internal noise. High noise level implies low signal-to-noise ratio (SNR). Low SNR may stem from bad weather condition such as the effect of thunderstorm, strong multipathing, man-made noise such as noise from nearby engine and radio signals, and the effects of troposphere and ionosphere. Lau [1995] carried out an experiment to investigate the

effect of weak signal strength on GPS positioning. A Leica System 200 GPS receiver was set up under a tree and GPS data was collected. His results showed that the GPS positioning accuracy was significantly affected by low SNR GPS observations.

Besides, SNR ratio is almost directly proportional to elevation angle if the environment does not cause too much noise [Lau and Mok, 1999a]. Sleewaegen [1997] shows that there is a linear relationship between standard derivation of multipath and satellite elevation angle. He also relates phase multipath and SNR by their standard deviation. Investigation on the relationship between signal-to-noise ratio and multipath can also be found in Comp and Axelrad [1996], Langley [1997], and Lau and Mok [1999a].

Johannessen [1997], and Spilker and Natali [1996] discussed the sources of interference, and concluded that interference of signal is indicated in the signal level or SNR. Moreover, Comp and Axelrad [1996], Langley [1997] and Sleewaegen [1997] described in detail the relationship between multipath and SNR ratio. Hartinger and Brunner [1998] and Talbot [1988] used SNR ratio to mitigate multipath error. Based on their investigation results, SIGMA-ε and PC-PHASER models were introduced respectively.

2.2 Relationship among Signal-to-Noise Ratio, Carrier-to-Noise Ratio and Multipath Effect

This section describes the relationship between signal-to-noise ratio and carrier-to-noise ratio, and how they relate to multipath.

2.2.1 Signal-to-Noise Ratio and Carrier-to-Noise Density Ratio

Signal-to-noise ratio is the ratio of signal power to noise power at the receiver output. It is sometimes referred to as the post detector or destination signal-to-noise ratio. SNR can be expressed as,

$$S/N = P_S/P_N \tag{2.9}$$

where P_S is the signal power in watts, P_N is the noise power in watts and S/N is the signal-to-noise ratio.

Carrier-to-noise density ratio (C/N_0) is the ratio of carrier power to noise power at the demodulator input so it is the real power ratio received at the GPS antenna.

$$C/N_o = P_C/P_N \tag{2.10}$$

where P_C is the carrier power in watts, P_N is the noise power in watts and C/N_0 is the carrier-to-noise ratio.

2.2.2 Relationship between CNR and SNR

Carrier-to-noise ratio and signal-to-noise ratio are related through the receiver processing gain; Roddy [1995] expressed this relationship in decibel form as:

$$10\log_{10}\frac{S}{N} = 10\log_{10}\frac{C}{N_o} + 10\log_{10}K_R \tag{2.11}$$

where S/N is the SNR, C/N_o is the CNR and K_R is the receiver processing gain.

For a Costa loop (frequency multiplication avoided) GPS receiver, Langley [1997] expressed jitter in carrier-tracking loop (or Phase Lock Loop, PLL) as:

$$\sigma_{PLL} = \sqrt{\frac{B_P}{c/n_o}\left[1+\frac{1}{2Tc/n_o}\right]}\frac{\lambda}{2\pi} \tag{2.12}$$

where σ_{PLL} is the jitter in PLL (mm), B_P is the equivalent phase lock loop bandwidth (Hz), T is the predetection integration time (sec.), c/n_0 is the CNR and λ is the wavelength of the carrier (m).

For normal signal strength ($C/N_0 \geq 35$dB-Hz, where C/N_0 is the signal strength in dB-Hz):

$$\sigma_{PLL} \approx \sqrt{\frac{B_P}{c/n_o}}\frac{\lambda}{2\pi} \tag{2.13}$$

$$c/n_o = 10^{(C/No)/10} \tag{2.14}$$

$$\because \frac{c/n_o}{B_P} = 10^{(S/N)/10} \tag{2.15}$$

$$\therefore S/N = 10 \cdot \log\left(\frac{c/n_o}{B_P}\right) \tag{2.16}$$

Eqn. 2.16 shows the relationship between SNR and CNR where S/N is the SNR, c/n_0 is the CNR and B_P is the carrier loop noise bandwidth (Hz).

According to the relationship between SNR and CNR in eqn. 2.16, using either SNR or CNR for weighted least squares method described in Chapter 4 will have the same effect on the solution, provided that L1 and L2 signal processor have the same B_P. It is common for most GPS receivers to have the same B_P on L1 and L2 signals. For example, Trimble 4000SSi receiver has 10 MHz B_P for both L1 and L2. SNR is readily available to users through GPS receiver display or NMEA-0183 GSV output format, therefore it is practically feasible to be used for weighting the data quality.

2.2.3 Relationship between Multipath and Signal-to-Noise Ratio

It was discussed in section 2.1.5 that noise due to multipathing would cause phase delay ($\Delta\varphi$), changes in amplitude and frequency of the direct signal. The strength of the signal with respect to the noise is the signal-to-noise ratio. If multipath is the dominant noise, this ratio is called the signal-to-multipath ratio (SMR). Obviously, the larger the SMR, the stronger is the signal.

Section 2.1.6.5 described the relationship between multipath and SNR. Further discussions can be found in [Sleewaegen, 1997], [Comp and Axelrad, 1996], [Langley, 1997], and [Lau and Mok, 1999a].

2.3 GPS Observables

GPS observables are the pseudoranges and carrier phases. Due to the 1 to 5 metres achievable accuracy for Differential GPS using pseudorange data, this type of observable is normally applied for marine navigation and other positioning applications, where the positioning accuracy requirement is low. High accuracy positioning can only be achieved by using carrier phase measurements. The achievable positioning accuracy using carrier phase observable is about 5 mm, which is subject to baseline length, satellite-to-receiver geometry, the number of in-view satellites, types and level of errors exist in the data, observation and sampling period.

2.3.1 Double Differenced Phase Observable

Assuming the two receivers k and m observe to the two satellites p and q at the same time (see Figure 2.3), the DD phase observable is:

$$\varphi_{km}^{pq}(t) = \varphi_{km}^{p}(t) - \varphi_{km}^{q}(t) + N_{km}^{pq} + I_{km}^{pq}(t) + \frac{f}{c} T_{km}^{pq}(t) + d_{km}^{pq}(t) + \varepsilon_{km}^{pq} \qquad (2.17)$$

where N_{km}^{pq} is the DD integer ambiguity,

$I_{km}^{pq}(t)$ is the DD ionospheric delay at epoch t,

$T_{km}^{pq}(t)$ is the DD tropospheric delay at epoch t,

$d_{km}^{pq}(t)$ is the DD multipath at epoch t, and

ε_{km}^{pq} is the DD random carrier phase measurement noise.

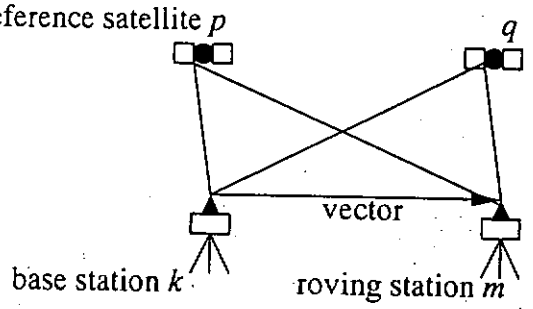

Figure 2.3
The double difference

DD integer ambiguity is very important because it reduces the number of ambiguities to be resolved. Moreover, DD technique can effectively reduce common biases during measurement such as satellite clock bias, receiver clock bias, ionospheric effect and tropospheric effect in short baseline. Therefore DD technique is commonly employed in GPS data processing software and GPS data processing algorithms. DD technique is used in the proposed algorithms to be described in Chapter 4.

2.3.2 Ideal Minimum Accuracy (IMA) for Carrier Phase Data

GPS positioning accuracy is subject to the presence and effect of biases, errors and other factors, as described in Section 2.1, during measurement. In order to derive the achievable positioning accuracy of GPS DD carrier phase measurement in a

hypothetical case of the complete absence of all biases and errors, the author would like to propose a term "Ideal Minimum Accuracy (IMA)". The following discussion aims to show the IMA of relative positioning in the hypothetical case and compare the real and hypothetical achievable accuracy.

IMA is defined as the minimum achievable accuracy for carrier phase data in the vacuum ideal (complete bias and error free) environment, without any obstruction, and that the receivers have no internal noise. Under this ideal environment, biases or errors (as described in session 2.1) will not affect the quality of GPS data used to determine positions. IMA is therefore directly related to the tracking precision of receivers' signal processing system. If the tracking precision of a receiver is in the order of 10^{-3}, the ideal minimum accuracy of a topocentric distance measured by carrier phase will be about ± 0.2 mm (or more precise: L1 will be ± 0.19 mm and L2 will be ± 0.24 mm). Figure 2.4 shows the principle of IMA. In Figure 2.4(a), the accuracy of the measured topocentric distance under the ideal condition would be ± 0.2 mm, that is +/- 0.2mm from the "true" position at the centre of the circle in the figure. When more than one satellites are available (Figure 2.4(b)), the distance between the best intersecting point and the "true" position would be less than ± 0.2 mm. Therefore, it is called the minimum accuracy.

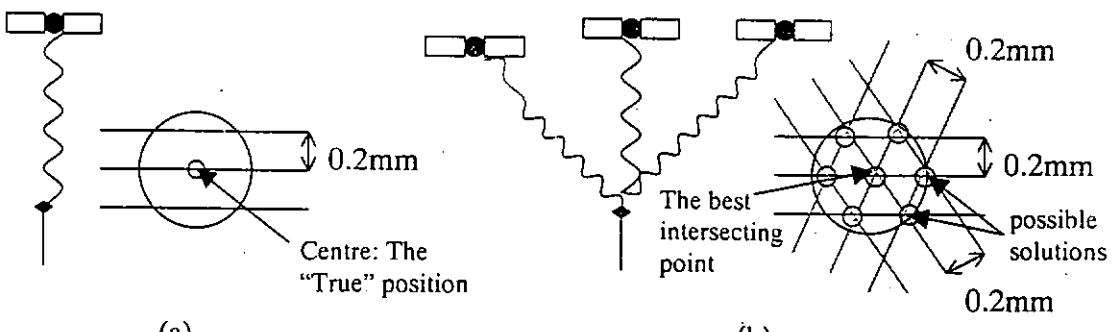

Figure 2.4
Ideal Minimum Accuracy (IMA)

How is the ideal minimum accuracy related to the tracking precision? According to Allan [1993], precision is defined as "the degree of agreement between the measures, and accuracy as the difference between the best estimate and the true value"; Leick [1995] defines precision as the closeness of the observations to the true value, and accuracy as the closeness of repeated observations to the sample mean. Relative positioning is our major concern, thereby the coordinates of one site are known and the position of the other site is to be determined relatively to the known site [Hofmann-Wellenhof et al., 1994, pp. 130]. In the ideal case of IMA, the "true" position of the unknown point would be only relative to the known point (Figure 2.5), therefore the positioning accuracy of the unknown point would be determined by the accuracy of the baseline vector from the known point to the unknown. The accuracy of the relative baseline vector would purely depend on the precision of carrier phase observable in the ideal case.

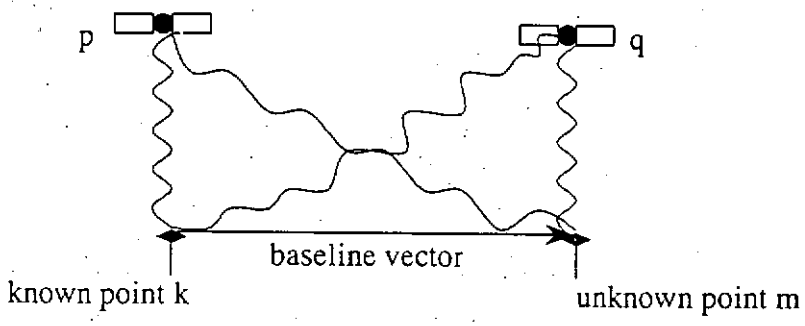

Figure 2.5
Relative positioning technique

Let us derive the IMA for DD according to the "Uncertainty in sums and Differences (Provisional Rule)" in [Taylor, 1997, eqn. (3.4) on pp. 50 and section

3.5 in pp. 57-60], the error propagation law is not applicable since the ± 0.2 mm precision is neither a random variance nor a standard error.

If carrier phase data φ_k^p and φ_k^q has a range error of ± 0.2 mm, then for a single-differenced observables φ_k^{pq},

$$\varphi_k^{pq} = \varphi_k^p - \varphi_k^q \tag{2.18}$$

the uncertainty (or maximum error) of single-differenced observable becomes

$$\delta\varphi_k^{pq} = \delta\varphi_k^p + \delta\varphi_k^q = 0.4mm \tag{2.19}$$

and the uncertainty of DD phase observable:

DD phase: $$\varphi_{km}^{pq} = \varphi_k^{pq} - \varphi_m^{pq} \tag{2.20}$$

DD uncertainty: $$\delta\varphi_{km}^{pq} = \delta\varphi_k^{pq} + \delta\varphi_m^{pq} \tag{2.21}$$

$$\because \delta\varphi_k^{pq} = \delta\varphi_m^{pq} = 0.4mm$$

$$\therefore \delta\varphi_{km}^{pq} = 0.8mm$$

The achievable positioning accuracy for DD carrier phase data of most high precision GPS receivers is about 5 mm, which is far from the IMA – 0.8 mm. It is

due to the satellite geometry and the presence of biases and errors. The major factor affecting GPS positioning accuracy is believed to be the multipath effect, and this type of error cannot be eliminated or reduced using the differencing techniques.

In reality the ideal case of IMA never exists, therefore IMA can never be achieved. If ideal conditions were present, relative positioning technique would not exist!

2.4 Linear Combination of Carrier Phases

Generally, the linear combination of two carrier phases φ_{L1} and φ_{L2} is defined by

$$\varphi_{LC} = n_1\varphi_{L1} + n_2\varphi_{L2} \tag{2.22}$$

where φ_{LC} is the linear combined phase, and

n_1, n_2 are arbitrary numbers.

The substitution of different n_1 and n_2 will result in different linear combined wavelengths. For example, linear combination of carrier phases, according to [Teunissen, 1995], can be formed by analog

$$\begin{bmatrix} \varphi_{1,1} \\ \varphi_{1,-1} \end{bmatrix} = \begin{bmatrix} 1 & 1 \\ 1 & -1 \end{bmatrix} \begin{bmatrix} \varphi_{L1} \\ \varphi_{L2} \end{bmatrix} \tag{2.23}$$

where φ_{L1} denotes L1 carrier phase observable,

φ_{L2} denotes L2 carrier phase observable,

$\varphi_{1,1}$ denotes narrowlane linear combination of carrier phases observable (wavelength = 10.7 cm), and

$\varphi_{1,-1}$ denotes widelane linear combination of carrier phases observable (wavelength = 86.2 cm).

Widelane observable has a relatively longer wavelength of about 86 cm. It is useful to speed up ambiguity resolution or search in position domain. Hofmann-Wellenhof et al. [1994, pp. 214] states that the increased widelane wavelength provides an increased ambiguity spacing and this is the key to easier resolution of the integer ambiguities. Moreover, this observable has relatively low noise behaviour, and reasonable small ionospheric effect [Teunissen, 1995a]. However, widelane (and other linear combination of carrier phases) observable may amplify multipath effect and therefore lower the accuracy of solutions [Hofmann-Wellenhof et al., 1994, pp. 127]. Another disadvantage of linear combination is that the linear combined ambiguity may no longer an integer.

In addition to the above linear combinations of carrier phases observables, Mok [1998] described other possible linear combinations of carrier phases observables. Teunissen [1995a] suggested that linear combinations should preserve the information content of the original L1 and L2 carrier phase observables by proposing the use of invertible integer linear combination of carrier phases. It is very important since it can preserve the integer property of ambiguities after linear combination or

transformation, and it guarantees a one-to-one correspondence between the original and transformed ambiguities.

Linear combination of carrier phases can be used to solve the ionospheric effect. The ionospheric-free linear combination of carrier phases data is [Leick, 1995]:

$$\varphi^{p}_{k,IF}(t) \equiv \frac{f_1^2}{f_1^2 - f_2^2}\varphi^{p}_{k,1}(t) - \frac{f_1 f_2}{f_1^2 - f_2^2}\varphi^{p}_{k,2}(t) \qquad (2.24)$$

where $\varphi^{p}_{k,IF}(t)$ denotes ionospheric-free linear combination of carrier phases between the satellite p and the receiver k at epoch t,

$\varphi^{p}_{k,1}(t)$ denotes L1 carrier phase observable between the satellite p and the receiver k at epoch t,

$\varphi^{p}_{k,2}(t)$ denotes L2 carrier phase observable between the satellite p and the receiver k at epoch t, and

f_1 and f_2 are the frequencies of L1 and L2 carrier phase respectively.

Eqn. 2.24 is a very useful expression to eliminate ionospheric effect mathematically.

2.5 GPS Data Processing Algorithm

GPS data processing algorithms can be divided into search in the ambiguity domain and search in the position (physical) domain. Ambiguity search algorithms aims to solve integer ambiguities before position determination. Physical domain search algorithm usually refers to the Ambiguity Function Search Method (AFM), which will be discussed in more details in section 3.1. Basically speaking, AFM does not need to fix the ambiguities. Position determination is achieved by searching the correct position among a set of trial positions within a defined search volume.

There are many GPS data processing algorithms presented by various authors, examples can be found in standard textbooks like [Hofmann-Wellenhof et al., 1994] and [Leick, 1995]. Several approaches are briefly described here as far as their capabilities in static and kinematic observation. Most of them are based on DD phase observable (described in section 2.3.1) [Remondi, 1985; Dong and Bock, 1989].

2.5.1 The Classical GPS Data Processing Procedure

Classical processing procedure is typically based on four steps. They are summarised below.

(i) Estimation of initial ambiguity parameters as real values in a least squares float solution.

(ii) Fixing initial real ambiguities to integer values based on their estimated accuracy or by general ordering search strategy.

(iii) Introduction of ambiguity parameters as known quantities into the least squares observation equation to perform a fixed solution.

(iv) Validation by evaluating the adjusted results and the *a posteriori* statistical quantities, such as residuals and variance-covariance matrix.

A variety of methods have been developed to fix real-valued estimates to integer quantities. The correctness and efficiency of these techniques based on ordering search strategy are mainly dependent on the number of fixed ambiguity sets evaluated to make the final choice. A full search over all possible combinations is optimal as far as reliability is concerned but it is definitely not efficient. Evaluation of only a few sets will take a risk that the correct set has not been selected. This classical approach can be improved by using the statistical and geometrical information normally available during GPS data processing. Examples include the algorithm proposed by [Beutler et al., 1984] and [Bock et al., 1986], the Fast Ambiguity Resolution Approach (FARA) [Frei, 1991; Frei and Beutler, 1990], the Least Squares Ambiguity Search Technique (LSAST) [Hatch, 1991] and the Least squares AMBiguity Decorrelation Adjustment (LAMBDA) method [Teunissen, 1995b].

2.5.2 Fast Ambiguity Resolution Approach (FARA)

This technique is based on the information provided by an initial adjustment. The information are coordinates, real-valued ambiguity estimates and the corresponding

variance-covariance matrix. For the details of FARA, please see [Frei and Beutler, 1989; Frei and Beutler, 1990; Frei, 1991; Erickson, 1992].

The FARA ambiguity resolution method is summarised below:

(i) to select the search range by using statistical information from initial adjustment

(ii) to reject ambiguity sets by analysing variances and covariances and to perform statistical test

(iii) to select the correct set of integer ambiguities by statistical hypothesis test

FARA normally requires five minutes of observations. Lau [1995] showed that FARA could resolve ambiguities successfully using two minutes of L1 and L2 measurements, with the baseline within about 10 km, the average GDOP equal to 4.5, and five in-view satellites. This investigation shows that FARA can perform correct ambiguity resolution using data observed in short time span, say about 5 minutes, but it may not be able to effectively solve for ambiguities if only a few epochs of observations are available. Moreover, the processing time will dramatically increase when only single frequency measurements are available because of the increase in the number of possible ambiguity sets [Han and Rizos, 1997a].

2.5.3 Least Squares Ambiguity Search Technique (LSAST)

Hatch [1991] described the least squares ambiguity search technique to solve ambiguities in kinematic mode. This method of course can be applied to static case.

The technique is divided into three procedures. Firstly, the initial position and standard deviation of differential code range measurements are determined by the least squares method. The search volume is then established by defining the uncertainty region around the initial position. The primary group of four satellites with reasonably good GDOP is used to generate a set of potential ambiguity solutions. Finally, the remaining satellite group is used to eliminate the incorrect potential solutions [Hatch, 1991].

LSAST was proposed for instantaneous ambiguity resolution, however, its processing time is about a few seconds to a few tens of seconds [Han and Rizos, 1997a]. It was expected that the increase in the number of redundant satellites should reduce the number of potential solutions, however Han and Rizos [1997a] showed that there was a great increase in the number of candidates and processing time under this condition.

The author doubts the reliability of the LSAST solution. LSAST assumes that the correct set of ambiguities must be contained in the potential solutions. If the potential solutions generated by the primary group does not contain the correct ambiguity set, then the test of secondary group will become meaningless, as the final solution will be incorrect. The selection of primary group of satellites is therefore very crucial.

From the point of view of the author, the redundant satellites should not be used to eliminate the incorrect potential solutions only. The redundant satellites should act as redundant measurements (more degree of freedom) to strengthen the solution.

Besides, the low accuracy code solution (the first procedure of LSAST) will increase the search volume and the number of potential solutions generated by primary group of satellites, and thus increase the processing time.

2.5.4 LAMBDA Method

A processing algorithm, namely Least-squares AMBiguity Decorrelation Adjustment (LAMBDA) was developed by Teunissen [1995b]. The algorithm generally follows the following three steps (the details of LAMBDA method will be described in Chapter 3):

(i) float solution,

(ii) integer ambiguity estimation and

(iii) fixed solution.

The main characteristic of the algorithm is the efficient integer ambiguity estimation by LAMBDA method. The LAMBDA method consists of:

(i) the decorrelation of the ambiguities by a reparametrization of the original ambiguities to new ambiguities, and

(ii) the actual ambiguity estimation

The high efficiency of LAMBDA method comes from the decorrelation step (see Figure 2.6) [Jonge and Tiberius, 1995; Pachelski, 1995; Teunissen, 1995c]. This step transforms the original ambiguities to the less correlated new ambiguities. The ambiguity search space is forced to become more sphere-like and the transformed ambiguities are more precise than the original ambiguities.

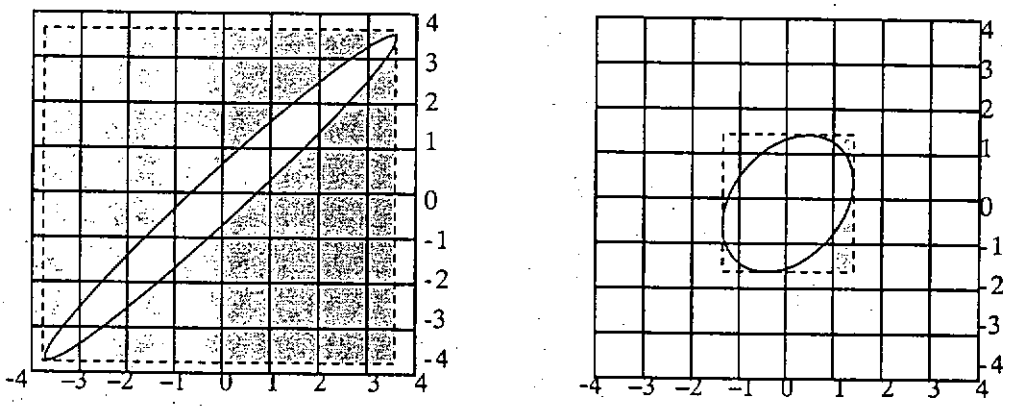

Figure 2.6
Decorrelation
(a) Original Ambiguity Search Space, (b) Transformed Ambiguity Search Space

LAMBDA method can resolve ambiguities in less than a second or a few seconds. The processing time depends on the number of ambiguities, the searching bounds χ^2, and the inputted maximum number of candidates; the details of these factors will be described in Chapter 3 and can be found in [Jonge and Tiberius, 1996]. The number of measurements does not affect the processing time of LAMBDA since the ambiguity transformation step and integer ambiguity estimation by search step consider the ambiguity parameters and its variance-covariance matrix only. From the point of view of the author LAMBDA is currently the most efficient ambiguity resolution technique, however, it is not quite suitable to correctly resolve ambiguities if only one or a few epochs of data is available. It is because a few measurements can only give very little information for LAMBDA to decorrelate and resolve the ambiguities successfully.

2.5.5 Ambiguity Function Method (AFM)

Ambiguity Function Method (AFM) was first introduced by Counselman and Gourevitch [1981]. Remondi [1984] and Mader [1992] further investigated this technique. This method is not mainly used for solving ambiguities, even though it can serve such purpose (will be described in section 3.1.4). The correct set of ambiguities can be computed after the correct position has been determined by search in the coordinate space.

AFM determines the solution by searching for the trial position with maximum Ambiguity Function Value (AFV) within a search volume (see Figure 2.7). AFV is a function of phase residual, which will be described in section 3.1. In terms of the DD observables, it is expressed as

$$AF(X,Y,Z) = \sum_{L=1}^{2}\sum_{R=1}^{i}\sum_{S=1}^{j} \cos\{2\pi[\frac{f_L}{c}\rho_{km,c}^{pq}(t) - \varphi_{km,L,b}^{pq}(t)]\} \qquad (2.23)$$

where $AF(X,Y,Z)$ is the ambiguity function of the trial position X,Y,Z,

f_L is the carrier frequency,

$\rho_{km,c}^{pq}(t)$ denotes computed DD geocentric range at epoch t,

$\varphi_{km,L,b}^{pq}(t)$ denotes observed DD carrier phase measurement of L1 or L2 at epoch t,

c is the velocity of light,

L is the number of carrier phases,

R is the number of receivers from 1 to i, and

S is the number of satellites in view from 1 to j.

Details on the AFM algorithm can be found in Mader [1992], Mok and Cross [1996], Lau [1997] and the next chapter.

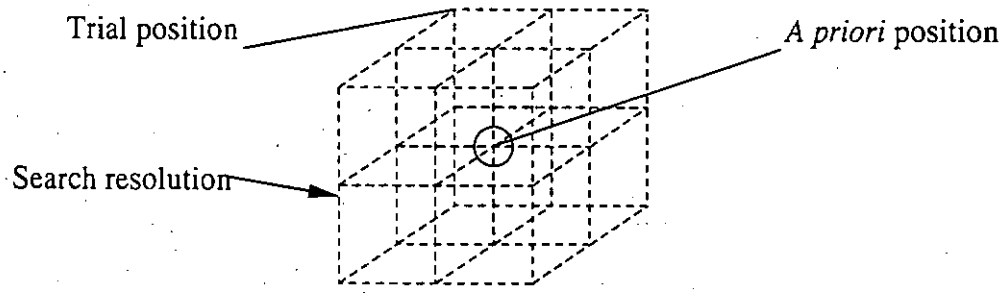

Figure 2.7
Search volume of ambiguity function method

According to recent investigations, AFM can be used to process short observation time-span measurements and even single-epoch measurement. Remondi [1991] used AFM for pseudo-kinematic GPS without static initialization. Corbett and Cross [1995] and Mok [1998] applied AFM for single-epoch solution. When using AFM to process more than one epoch measurements, it has an advantage of the insensitivity to integer cycle slips. However, AFM requires a good *a priori* position to construct a search volume and it has no quality measure to the solution. The processing time of AFM depends on the size of search volume and the number of measurements; it is not efficient. Investigation on AFM will be shown in the next chapter.

2.5.6 Validation Criteria

To ensure that the ambiguities or position determined is correct, validation criteria for the solution should be set in the quality assurance procedure. There are many quality assurance approaches proposed by different authors, and some general approaches are described here.

In ambiguity float solution, the test of complete sets of ambiguities can be applied, according to [Leick, 1995] as

$$\frac{\Delta V^T PV}{V^T PV}\frac{n-u}{s} \sim F_{s,n-u,\alpha} \tag{2.24}$$

where V denotes the residual vector of the float solution,

P denotes the weight matrix of the float solution,

$(n\text{-}u)$ denotes the degree of freedom of the float solution,

s denotes the number of ambiguities of the float solution, and

$F_{s,n-u,\alpha}$ denotes the corresponding F distribution.

Many GPS post-processing software packages (e.g. Leica's SKI and Trimble's GPSurvey) test the ratio of the best to the second best solution against the F-distribution, or a critical value,

$$\frac{\left(V^T PV\right)_{2ndBest}}{\left(V^T PV\right)_{Best}} > F_{\alpha,m1,m2} \text{ or critical value} \qquad (2.25)$$

where V denotes the residual vector of the fixed solution,

P denotes the weight matrix of the fixed solution,

$m1$ and $m2$ denotes the degree of freedom of the fixed best and second best solution respectively, and

$F_{\alpha,m1,m2}$ denotes the corresponding F distribution.

In other GPS data processing algorithms involving ambiguity function method, the following ratio test may be applied

$$\frac{AF_{2ndMax}}{AF_{Max}} > F_{\alpha,m1,m2} \qquad (2.26)$$

where AF_{2ndMax} denotes the second maximum ambiguity function yielded by the second best position,

AF_{Max} denotes the maximum ambiguity function yielded by the best position,

$m1$ and $m2$ denotes the degree of freedom of the best and second best position respectively, and

$F_{\alpha,m1,m2}$ denotes the corresponding F distribution.

2.6 Ambiguity Function Method Applied to Deformation Monitoring

Different GPS data processing algorithms have been described in last section. They have advantages and disadvantages for different applications. In order to tailor the processing algorithm for deformation monitoring, the processing algorithm must make good use of the features of deformation monitoring.

Features of deformation monitoring are applied to the GPS processing algorithm in this project. By taking these advantages, the processing algorithm can be faster and more precise to find the solution. The advantages are:

(i) For deformation monitoring in engineering site, the reference station is always close to the monitoring markers (roving station). Since GPS satellites are at the altitude of about 20,200 km and the receivers are only a few kilometres apart, the two signal paths of a satellite reaching the two receivers of relative positioning would be very similar. Therefore, the effects of ionosphere and troposphere on the two receivers are very close and can be greatly reduced by differential positioning.

(ii) Taking observations of a monitoring station at the same time can greatly reduce multipath effect. It is because the similar satellite geometry at same observation time (sidereal time) and similar position of the monitoring marker and reference station (receiver locations) would have similar multipath effect on the antennas. This is the similar satellite-antenna-reflector geometry. So relative displacement between observation epochs would be close to the real movement. Of course, it is only true for deformation

monitoring. However, it may not be practical. This project aims to find other solutions to reduce multipath effect.

(iii) For static deformation in reclaimed area, the magnitude of displacement is likely to be little and slow. Thus, after the first measurement of a monitoring station, the determined position of the station can act as *a priori* position for the processing of next measurement. The *a priori* position can narrow down the search volume of ambiguity function and other ambiguity resolution techniques. The smaller the search volume, the faster the processing algorithm for GPS solution.

In view of the above advantages and the present GPS processing algorithm, ambiguity function method is adopted as the engine for developing GPS processing algorithm in this project.

The concept of ambiguity function is that it computes the AF values of the trial positions within the search volume; when the correct position is reached, it would yield the minimum residuals, which are maximized by cosine of the residuals. The correct position, in theory, would yield the maximum AF for all measurements, which are DD observations in this project. Ambiguity function method has the advantage of not being affected by cycle slip and integer ambiguities do not have to find. The position yielding the maximum AF is the most possible correct position. However, even at the correct position, AF is only close to an integer because the small DD ionospheric delay, tropospheric delay, and multipath are present, but they are not listed in eqn. 2.23.

The advantages of adopting ambiguity function method for static deformation monitoring:

(i) although ambiguity function method does not take the bias of ionospheric effect and tropospheric effect into account, it will not introduce too much bias to the AFM solution in this project since this project does not need to take these biases into account; it is because these un-modelled bias of ionospheric effect and tropospheric effect are greatly reduced by DD in short baseline.

(ii) *a priori* position, determined by solution of the last measurement, is a good estimate position of the new measurement; it narrows down the search volume, making fast and precise processing algorithm possible.

(iii) ambiguity function method is insensitive to cycle slips; it is important to rapid processing algorithm because it saves the time for cycle slip detection and correction.

However, ambiguity function method does have disadvantages in general. The disadvantages are:

(i) solution of incorrect position may occur when serious un-modelled errors are present on the measurements.

(ii) the correct position must be contained in the search volume, otherwise, no solution can be found.

(iii) each trial position must be taken into computation; it is inefficient.

Despite the disadvantages of ambiguity function method, it is very beneficial to adopt the method as the engine of the developing processing algorithm. It is because

that ambiguity function method has the capability of single epoch solution that is very useful for fast deformation monitoring [Mok, 1998].

Based on the disadvantages, the project is going to find solutions or strategies to overcome them, e.g., early exit strategy and more accurate *a priori* position can overcome the disadvantage (iii). It concentrates more on the disadvantage (iii) since the general disadvantages of ambiguity function method (i) and (ii) are overcome by the advantages of adopting ambiguity function method for static deformation monitoring (i) and (ii) respectively.

CHAPTER 3

A CRITICAL ANALYSIS OF GPS PROCESSING ALGORITHMS

3.1 Investigation into Ambiguity Function Method

Ambiguity Function Method (AFM) was first introduced by Counselman and Gourevitch [1981]. Remondi [1984] and Mader [1992] further investigated this technique. AFM is a position domain algorithm; the solution is determined by searching the trial positions in a defined search volume with the GPS carrier phase measurements. The principle of AFM is described below.

The observable used in this project is DD carrier phase measurements (eqn. 3.1), so the following derivation and description of AFM will be based on DD carrier phase measurement. Let DD ionospheric effect, tropospheric effect, multipath and measurement noise be $DD\delta$ (double-differenced biases and errors), and convert the two single-differenced carrier phase measurements to DD topocentric distance, then rewrite eqn. 3.1 to eqn. 3.2 with replacing the dimension cycle by radians.

$$\varphi_{km}^{pq}(t) = \varphi_{km}^{p}(t) - \varphi_{km}^{q}(t) + N_{km}^{pq} + I_{km}^{pq}(t) + \frac{f}{c} T_{km}^{pq}(t) + d_{km}^{pq}(t) + \varepsilon_{km}^{pq} \tag{3.1}$$

$$2\pi\varphi_{km}^{pq}(t) = 2\pi\left[\frac{f}{c}\rho_{km}^{pq}(t) + N_{km}^{pq} + \delta_{km}^{pq}(t)\right] \tag{3.2}$$

In Figure 3.1, a search volume is constructed by defining trial positions around the a priori position, which can be determined by code solution, float solution, or input by user. Search volume can be a cube or an ellipsoid. The size of search volume can be defined by variance of initial solution or pre-defined by fixed distance from the a priori position. Space between the trial positions is search resolution or interval. The search resolution can be determined by initial solution or fixed to a value. Therefore, the coordinates of all trial positions are known.

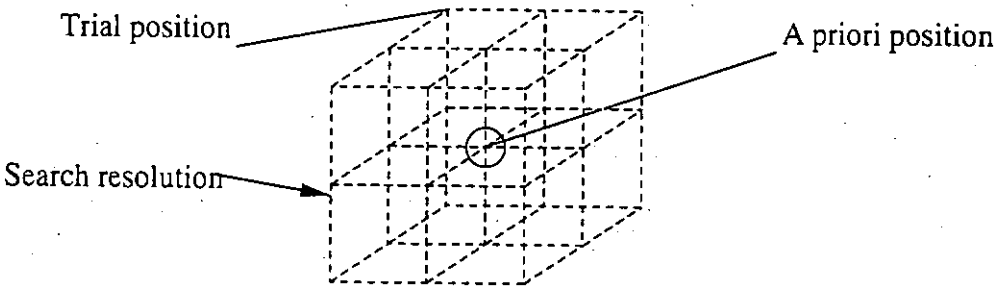

Figure 3.1
Search volume of AFM

Since the coordinates of trial positions are known, the topocentric distance can be computed from known reference station and satellites. Assuming point k as a known reference point and m as a trial position, and putting the known terms to the left-hand side of the eqn. 3.2, it gives:

$$2\pi \varphi_{km}^{pq}(t) - \frac{2\pi f}{c} \rho_{km}^{pq}(t) = 2\pi N_{km}^{pq} + 2\pi \delta_{km}^{pq}(t) \qquad (3.3)$$

Since N_{km}^{pq} is an integer, applying cosine or sine function to $2\pi N_{km}^{pq}$ will cause a special character of AFM. Therefore, eqn. 3.3 is placed into the complex plane by

raising the whole equation to the exponential function e^{i} where i is the imaginary unit:

$$e^{i\left\{2\pi\varphi_{km}^{pq}(t)-\frac{2\pi f}{c}\rho_{km}^{pq}(t)\right\}} = e^{i\left\{2\pi N_{km}^{pq}+2\pi\delta_{km}^{pq}(t)\right\}} \tag{3.4}$$

which may be written as

$$e^{i\left\{2\pi\varphi_{km}^{pq}(t)-\frac{2\pi f}{c}\rho_{km}^{pq}(t)\right\}} = e^{i2\pi N_{km}^{pq}} e^{i2\pi\delta_{km}^{pq}(t)} \tag{3.5}$$

Eqn. 3.5 can be expressed in an Argand diagram:

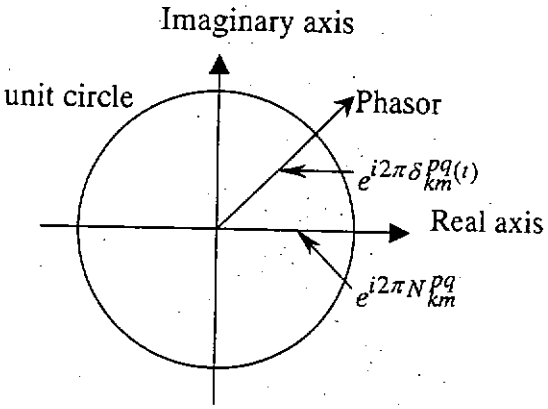

Figure 3.2
Argand diagram: unit vector in the complex plane

Since Euler's formula defines:

$$e^{i\alpha} = \cos\alpha + i\sin\alpha \tag{3.6}$$

the integer ambiguity term in eqn. 3.5 becomes:

$$e^{i2\pi N_{km}^{pq}} = \cos(2\pi N_{km}^{pq}) + i\sin(2\pi N_{km}^{pq}) = 1 + i \cdot 0 \tag{3.7}$$

The result in eqn. 3.7 is due to that the cosine of an integer ambiguity equals one, and the sine of an integer equals zero, and 2π is a complete revolution on the Argand diagram.

Hence, substituting result of eqn. 3.7 into eqn. 3.5 gives:

$$e^{i\left\{2\pi\varphi_{km}^{pq}(t) - \frac{2\pi f}{c}\rho_{km}^{pq}(t)\right\}} = e^{i2\pi\delta_{km}^{pq}(t)} \tag{3.8}$$

The left-hand side of eqn. 3.8 is defined as an ambiguity function of a DD carrier phase measurement.

When applying Euler's formula (eqn. 3.6) to the left-hand side of eqn. 3.8:

$$\cos[2\pi\varphi_{km}^{pq}(t) - \frac{2\pi f}{c}\rho_{km}^{pq}(t)] + i\sin[2\pi\varphi_{km}^{pq}(t) - \frac{2\pi f}{c}\rho_{km}^{pq}(t)] \tag{3.9}$$

the real function of the unit vector in the complex plane becomes:

$$\cos[2\pi\varphi_{km}^{pq}(t) - \frac{2\pi f}{c}\rho_{km}^{pq}(t)] \tag{3.10}$$

therefore, the ambiguity function for a DD carrier phase measurement is:

$$AF = \cos[2\pi \varphi_{km}^{pq}(t) - \frac{2\pi f}{c} \rho_{km}^{pq}(t)] \tag{3.11}$$

Finally, factorizing eqn. 3.11 becomes:

$$AF = \cos 2\pi[\varphi_{km}^{pq}(t) - \frac{f}{c} \rho_{km}^{pq}(t)] \tag{3.12}$$

It is the ambiguity function of a DD carrier phase measurement. When considering all DD carrier phase measurements at epoch t, a general expression for ambiguity function is obtained:

$$AF(X,Y,Z) = \sum_{L=1}^{2} \sum_{R=1}^{i} \sum_{S=1}^{j} \cos\{2\pi[\frac{f_L}{c} \rho_{km,c}^{pq}(t) - \varphi_{km,L,b}^{pq}(t)]\} \tag{3.13}$$

where $AF(X,Y,Z)$ is the ambiguity function value (AFV) of the trial position X,Y,Z,

f_L is the carrier frequency,

$\rho_{km,c}^{pq}(t)$ denotes computed double difference topocentric range at epoch t,

$\varphi_{km,L,b}^{pq}(t)$ denotes observed double difference carrier phase measurement of L1 or L2 at epoch t,

c is the velocity of light,

L is the number of carrier phases,

R is the number of receivers from 1 to i, and

S is the number of satellites in view from 1 to j.

Note that the phase residual $[\frac{f_L}{c}\rho^{pq}_{km,c}(t) - \varphi^{pq}_{km,L,b}(t)]$ of eqn. 3.13 is (computed – observed) while that of eqn. 3.12 is (observed – computed); it has no difference since the cosine of a positive or negative number is the same.

AFM determines the maximum AFVs (local maxima) of the trial positions within a search volume (see Figure 3.1 and 3.3). A trial position yielding the maximum AFV (global maximum) is considered as the "correct" position (see eqn. 3.13). This global maximum AFV is the maximum value of cosine function of the phase residuals after conversion to cycles [Counselman and Gourevitch, 1981; Mader, 1992; Remondi, 1984].

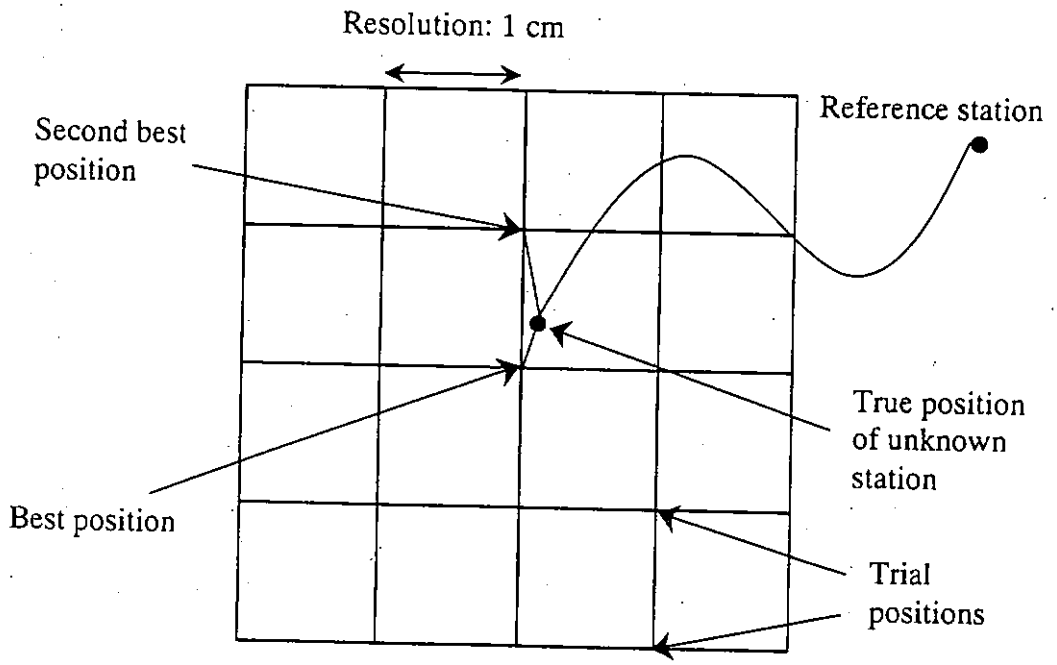

Figure 3.3
2-D representation of an AFM search volume

In Figure 3.3, the phasor (phase residual in AFM) computed with the best position is close to the real axis of Argand diagram (see Figure 3.2), which is shown in Figure 3.4(a). However, the phasor computed with the second best position is less close to the real axis of Argand diagram, which is shown in Figure 3.4(b). The phase residual of the best position will be smaller than that of the second best position theoretically. Therefore, the AFV of the best position will be greater than that of the second best position. It is because the cosine function of a smaller phase residual yields a greater AFV. In theory, the AFV equals one when a trial position reached the true position (the phasor is on the real axis of Argand diagram). However, the maximum AFV may not equal one in practice since there are some un-modelled biases or errors. AFM does not take ionospheric effect, tropospheric effect, multipath effect and random measurement noise into account. It is the reason for using DD carrier phase measurement in this AFM based project.

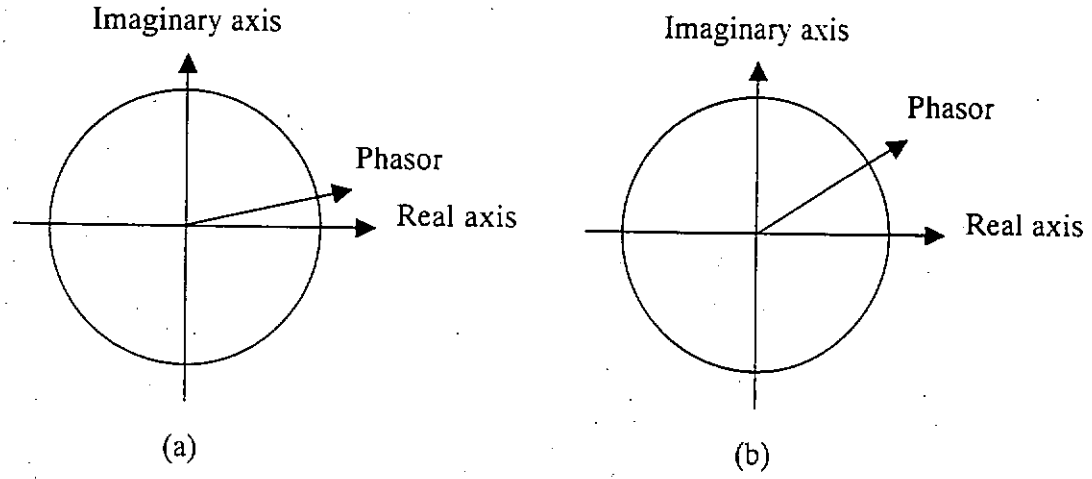

Figure 3.4
(a): phasor of the best position, (b): phasor of the second best position

The solution of AFM can be strengthened when more satellites, receivers, carrier frequencies and measurement epochs are observed. It is because the possible "correct" positions (intersecting points in Figure 3.5) have to fulfil the additional measurements. For example, three satellites' data yield nine possible solutions in Figure 3.5a, however, the number of possible solutions reduces to four when observing to one more satellite in Figure 3.5b. The effect of more receivers, carrier frequencies and measurement epochs is analogous to the effect of more satellites.

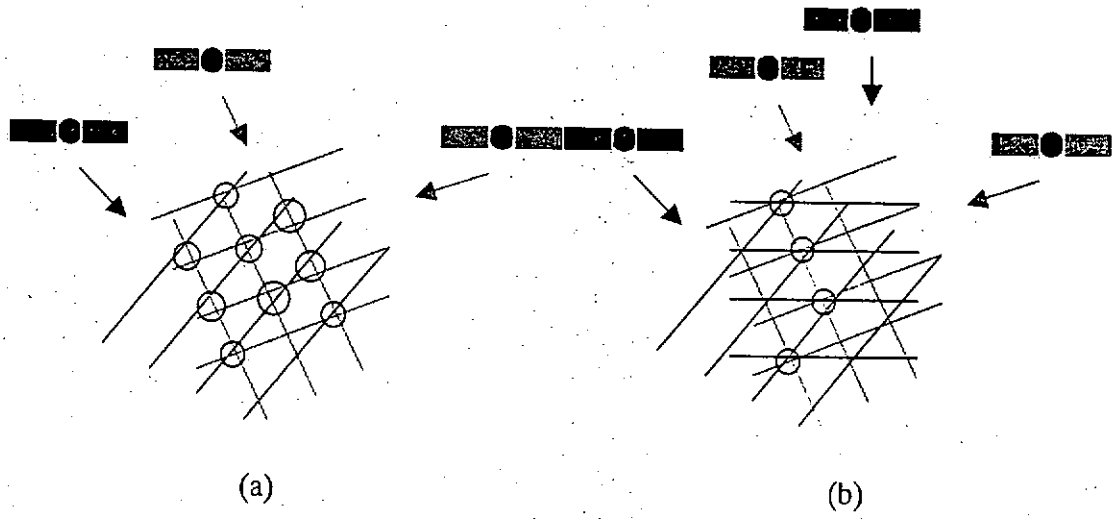

Figure 3.5
(a) nine possible solutions when observing to three satellites, (b) four possible solutions when observing to four satellites.

Therefore, the more unique AFM solution can be found by:

$$AF(X,Y,Z) = \sum_{t=1}^{g} \sum_{L=1}^{h} \sum_{R=1}^{i} \sum_{S=1}^{j} \cos\{2\pi[\frac{f_L}{c}\rho_{km,c}^{pq}(t) - \varphi_{km,L,b}^{pq}(t)]\} \qquad (3.14)$$

where $AF(X,Y,Z)$ is the AFV of the trial position X,Y,Z,

f_L is the carrier frequency,

$\rho^{pq}_{km,c}(t)$ denotes computed double difference topocentric range at epoch t,

$\varphi^{pq}_{km,L,b}(t)$ denotes observed double difference carrier phase measurement at epoch t,

c is the velocity of light,

L is the number of carrier phases from 1 to h,

R is the number of receivers from 1 to i,

S is the number of satellites in view from 1 to j, and

t is the measurement epochs from 1 to g.

AFVs of each trial position are computed by eqn. 3.14 during data processing by AFM. An example of AFVs of 1 m^3 search volume and 1mm resolution is shown in Figure 3.6; it is generated by data collected from seven satellites, 15 second measurement interval, 15° mask angle and 3 m baseline. In the example, there are 1 million trial positions. The central local maximum is considered as the correct maximum, which contains the correct position, since it is prominent to the other local maxima. At the correct position, all measurements yield their maximum AFV theoretically and sum up constructively, thus normalized AFV:

$$Normalized\ \ AF(X,Y,Z) = \frac{\sum_{t=1}^{g}\sum_{L=1}^{h}\sum_{R=1}^{i}\sum_{S=1}^{j}\cos\{2\pi[\frac{f_L}{c}\rho^{pq}_{km,c}(t) - \varphi^{pq}_{km,L,b}(t)]\}}{\sum_{t=1}^{g}\sum_{L=1}^{h}\sum_{R=1}^{i}\sum_{S=1}^{j}1} \quad (3.15)$$

will be clearly greater than the other trial positions. The effect of measurements at the correct position and a trial position on AFVs is shown in Figure 3.7.

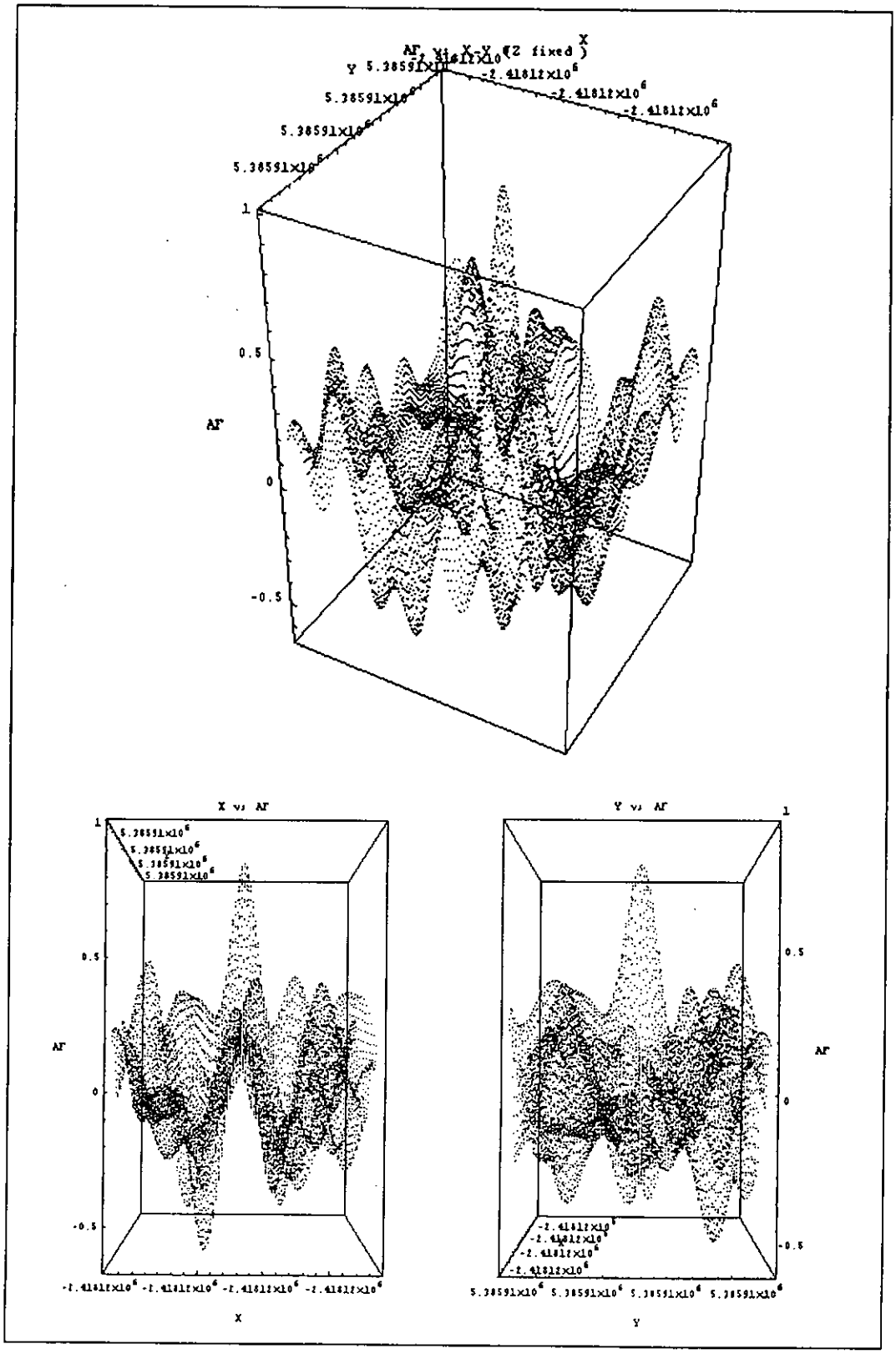

Figure 3.6
Example of AFVs of trial positions in a search volume

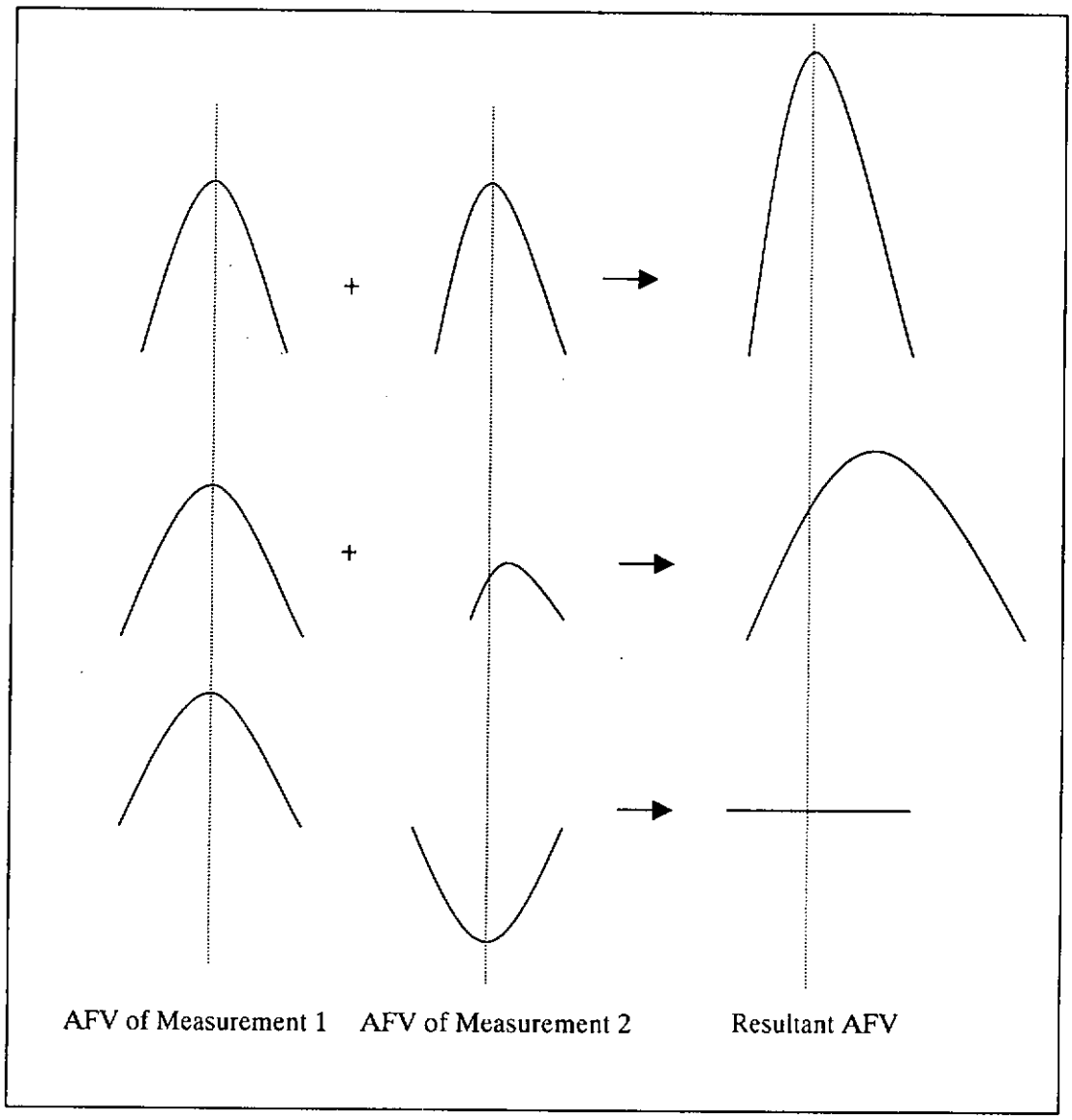

Figure 3.7
Top: Constructive AFV at the correct position; Middle: Partial constructive AFV in the correct local maximum; Bottom: Destructive AFV at the incorrect trial position

In theory, the more GPS measurements for data processing the more reliable the AFM solution. More measurements can be achieved by more observing satellites, more receivers and more carrier phase observable.

More observing satellites can be done by lowering the mask angle (less than 15°), however, low elevation satellite may cause problem to AFM. At low elevation,

where atmospheric condition is unstable, biased measurements may yield lower AFV even at the correct position. It may cause wrong solution. Besides, two or more reference receivers can increase measurements, which may strengthen AFM solution. It is multiple baseline solution.

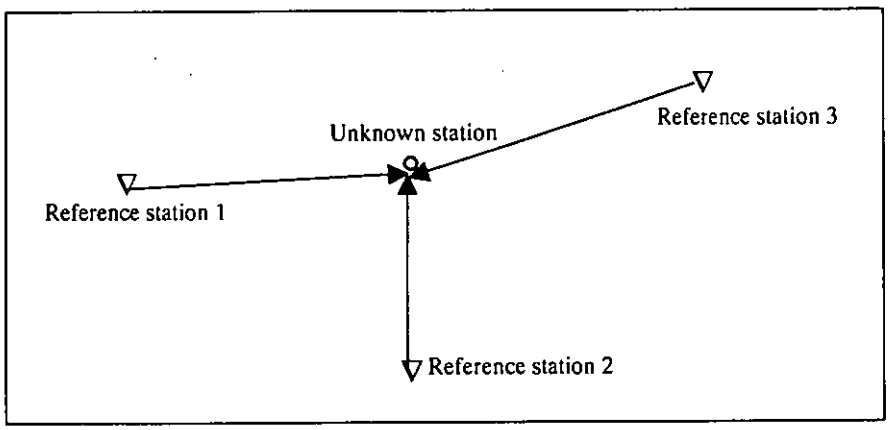

Figure 3.8
Multiple-baseline technique

Increasing carrier phase observable is impossible in user segment because of the hardware of GPS. Linear combination of L1 and L2 (widelane or narrowlane) may be considered as the additional observable, however, Chen (1996) stated that linear combination of L1 and L2 would enlarge multipath effect and measurement noises. Undoubtedly, linear combination of L1 and L2 (widelane) can increase the speed of searching when dealing with large search volume of AFM. Carrier phase observable may be increased in the future. Divis (1997) stated that the Department of Defense (DoD) and the Department of Transportation (DoT) agreed to develop a second frequency with coarse-acquisition code and navigation message for civil use. L5 or even LM, which may be the new military signal, will be usable as an additional carrier phase observable.

As stated above, AFM has to search all trial positions inside search volume; it is very time-consuming. It is because AFM requires trial and error to determine the correct position. Computation of all observations and trial positions will take a long time to complete. Since most of trial positions are far from the "correct" position (see Figure 3.6), it is possible to speed up the search process by using combination of coarse and fine search volumes, ambiguity function threshold test and using linear combination observables such as widelane observable. Search by using combination of coarse and fine search volumes and linear combination observables are investigated in Section 3.1.1 and 3.1.2, respectively. However, the ambiguity function threshold test does not discuss or apply in this project. It is because that even one bad DD measurement (from one satellite at an epoch), which may be caused by ionospheric effect, multipath and low elevation satellite, can cause a low AFV that cannot pass the threshold test and finally may reject the "correct" position. The detailed description on the ambiguity function threshold test can be found in [Leick, 1995, pp. 377] and [Mok and Cross, 1996].

3.1.1 Search by Coarse and Fine Resolutions

Search interval is the spacing between the neighbouring trial positions inside a search volume, it always sets to uniform among the whole search volume (see Figure 3.1 and 3.3). Search interval is very important for correct and accurate AFM solution since the positioning accuracy is directly related to it. The smaller the search interval (high resolution) will yield higher positioning accuracy. Figure 3.9 shows two cases

of search resolutions; one is 1 cm interval (solid line), another is 2 cm interval (dotted line). It is obvious that the distance between the true position to the best position of the 1 cm search resolution is less than that of the 2 cm one. Thus, the 1 cm search resolution (fine) has higher accuracy than the 2 cm search resolution (coarse).

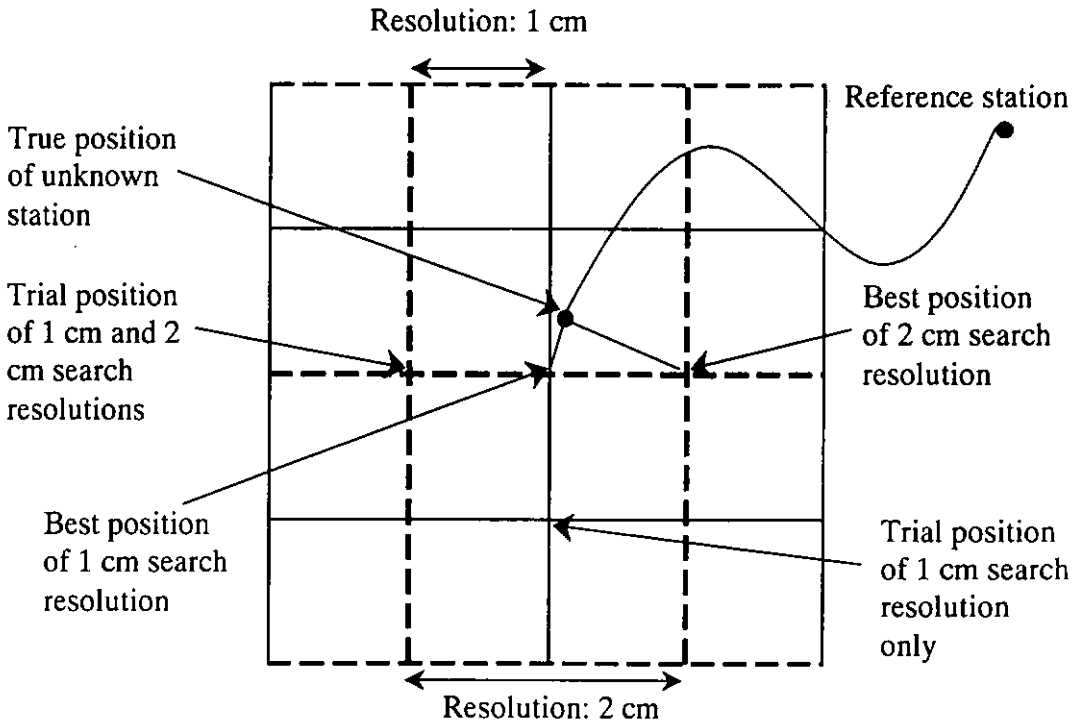

Figure 3.9
Effect of the AFM search resolutions

Although coarse searching solution is less accurate, it requires less processing time. Coarse searching solution can therefore act as a good approximate for fine search to speed up AFM process. Combined coarse and fine search technique finds a local maximum, which can be separated from the other local maxima by the search interval, by coarse search first. Fine search is then carried out in the local maximum

for further refinement. For example, a local maximum is isolated from the other local maxima in Figure 3.10; the local maximum is extracted for fine search.

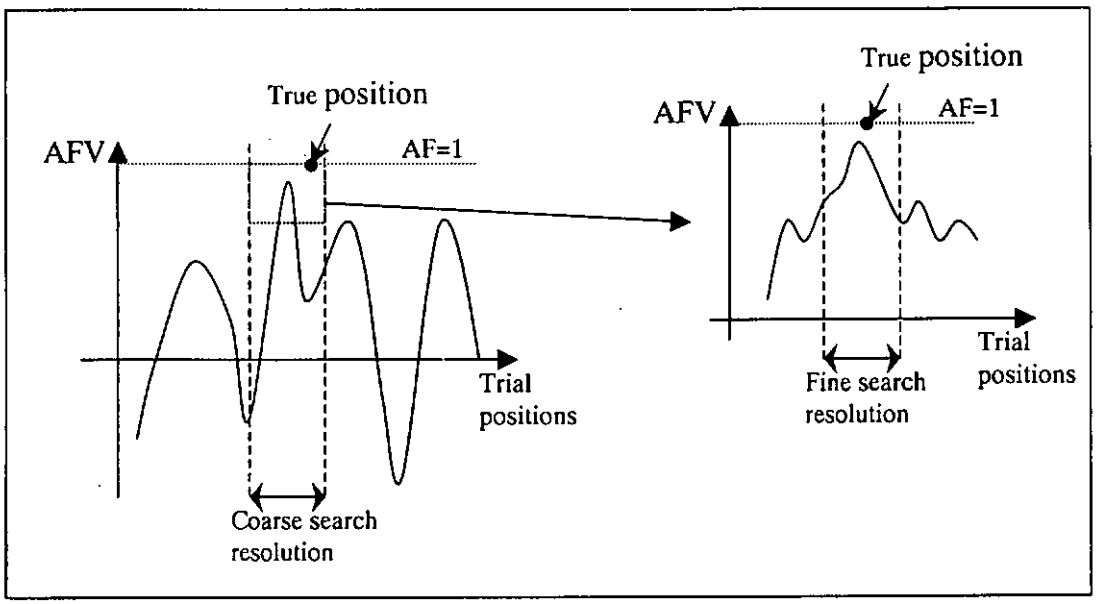

Figure 3.10
Combined coarse and fine search technique

Three-stepped searching of cubic volumes is investigated in this section. The search volumes are set to different sizes and searching intervals. The different combinations of search volumes and intervals will vary the processing time because of the different number of trial positions. The search interval should be selected as small as possible since it affects the accuracy of the determined position.

Different combinations of search volumes and resolution were tested, and the results are shown in Table 3.1. They yielded about the same position with respect to their search intervals. In order to get the same accuracy of 1mm, the third searching were carried out in combination 2,5,6 and 7. After the third searching, they all came up with the same position. The third searching does not affect the processing time too

much because it searches a very small cube only. Therefore, the combination 6 is selected as the setting of AFM in this project. This test was performed in a 133 MHz computer. The baseline length is about 2.2 km, the measurement epochs are six.

Table 3.1
Combinations of search volume and resolution

	Length of a side of the cube	Resolution	Total no. of trial positions	AF value	Processing time (sec.)	Remark
1						
First searching	1m	2cm				
Second searching	4cm	1mm	189,000	0.9747533262	>240	
2						
First searching	1m	2cm				
Second searching	4cm	2mm	133,000	0.9747533261	70	
3						
First searching	1m	1cm				
Second searching	2cm	1mm	1,008,000	0.9747532257	180	
4						
First searching	1m	1cm				
Second searching	4cm	1mm	1,064,000	0.9747533261	>240	
5						
First searching	1m	2cm				
Second searching	4cm	4mm	126,000	0.9747533246	30	
6						
First searching	1m	2cm				
Second searching	4cm	5mm	125,512	0.9747533264	20	Fastest
7						
First searching	1m	2cm				
Second searching	5cm	5mm	126,000	0.9747533256	23	

A 1 m^3 search volume with the a priori position as the centre of the search cube is constructed first. In the first stage searching, the resolution is set to 2 cm. The correct position, which produces the highest AFV in the first searching, acts as the centre of the second search volume (as in Figure 3.10). For the second stage, the search

volume is 6.4E-5 m^3 and the resolution is 5 mm. Search volume and resolution of the third searching are 1E-6 m^3 and 1 mm respectively.

Test on accuracy of the adopted combination of coarse and fine AFM searching

Table 3.2 shows the comparison of six-epoch solution (10 seconds measurement interval and 10° mask angle) of the AFM to solutions (10° and 15° mask angle, 6 and 1392 epochs' data) of Trimble GPSurvey software. The selected baseline is about 2.5 km in the new airport. 10 seconds measurement interval and 10° mask angle were set in the field. The differences in plane coordinates system are shown in Table 3.2.

Table 3.2
Difference of the processing algorithm solution from Trimble GPSurvey solution

Epochs	1392 (about 4 hrs)	6 (60 sec.)	1392 (about 4 hrs)	6 (60 sec.)
Mask angle (degree)	15	10	10	15
δN (mm)	-15	-5.6	-16	-5.6
δE (mm)	-6.5	-7.5	-6.7	-7.5
δH (mm)	0	-7	2	-7

Moreover, 14 six-epoch measurements were extracted from about 4 hours of observations, at 15 minutes intervals, and were processed with the AFM. The results were compared with the Trimble GPSurvey software's solution, which processed all measurements above 15° elevation angle, and to its mean. The coordinate differences from Trimble GPSurvey's solution in millimetre are shown in Table 3.3 and Figure 3.11, and the standard deviations of different epochs are shown in Figure 3.12.

Table 3.3
Coordinate differences of different epochs

Time (min)	1.5	15	30	45	60	75	90	105	120	135	150	175	190	205
ΔN (mm)	-16	-9.7	-8.3	-2.6	-14	3.8	-3.1	-14	-13	-4.5	-1.8	4.2	5	0.3
ΔE (mm)	-6.5	-5.9	7.8	-1.9	-16	0.1	-5.8	-9	-3.9	-9.5	-12	0.7	-9.5	1.7
ΔH (mm)	0	26	22	8	-3	6	9	-6	8	39	-20	18	-10	41

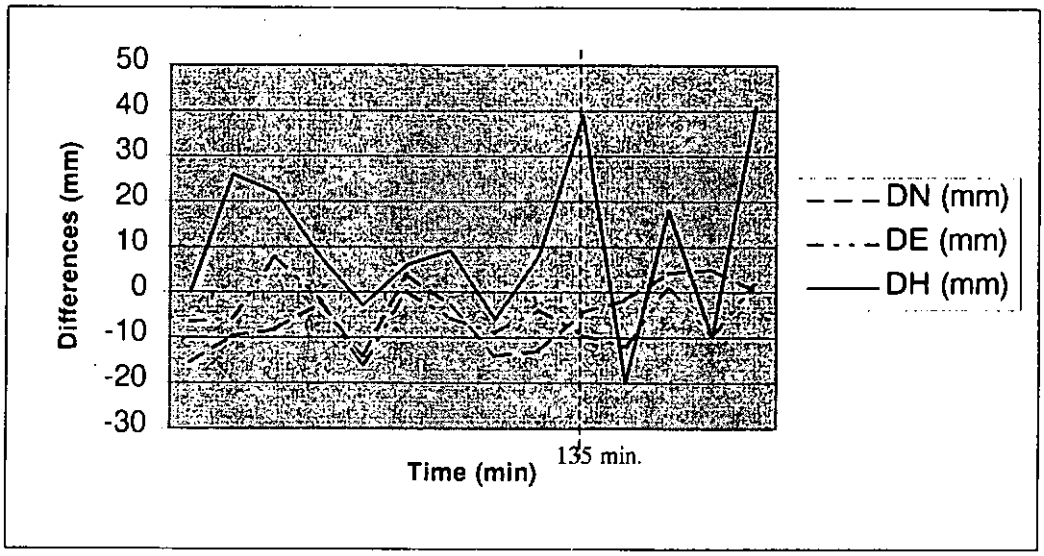

Figure 3.11
Coordinate differences of different epochs

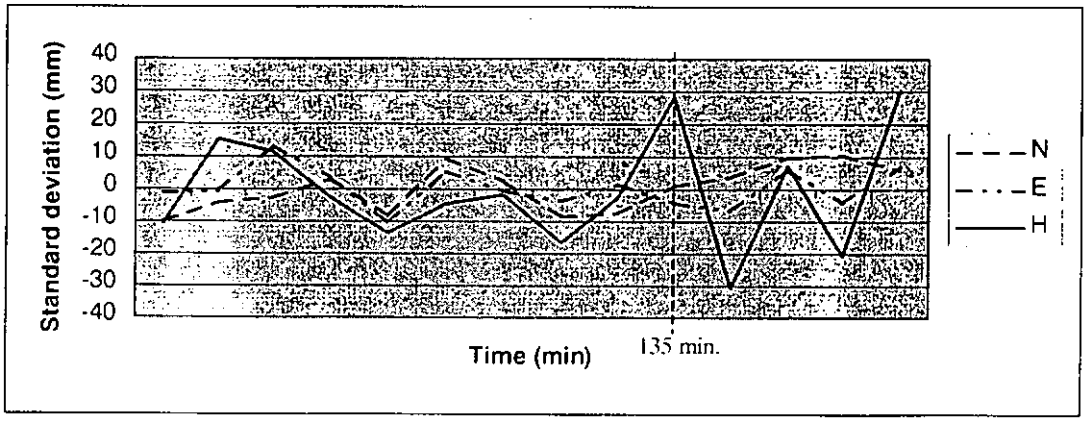

Figure 3.12
Standard deviation of the different epochs

In Figure 3.12, the differences range from approximately ± 10 mm in horizontal, to approximately ± 30 mm in vertical. The dramatic changes at and after 135 minutes are due to decrease in the number of satellites by one.

Tests and examples are then extended to different baselines. Details of the baselines are shown in Table 3.4 and results of the baselines are shown in Table 3.5.

Table 3.4
Information of samples

File	number of satellites	number of epochs	number of DD measurements	baseline length	PDOP
H1021	6	6	30	3m	3
H202	7	6	36	3m	3
H206	6~7	6	32	3m	3
AA16	6	6	30	~1.6km	3
AA22	7	6	36	~2.2km	3
KYC10	4	6	18	~10.6km	6
KYC11	6	6	30	~10.8km	3

Table 3.5
Processing result of samples

File	number of candidates (1st search)	1st Max. AFV	Final Max. AFV	1st AFR	2nd AFR	3rd AFR	dX	dY	dZ
H1021	16	0.9936	0.9952	4.2816	1.1391	1.0061	0.0000	0.0060	0.0060
H202	10	0.9616	0.9827	1.0722	1.0930	1.0042	-0.0030	-0.0030	-0.0020
H206	14	0.9807	0.9899	1.7957	1.4509	1.0117	-0.0120	0.0280	0.0030
AA16	5	0.9225	0.9299	1.0070	1.0085	1.0011	0.0159	-0.0263	0.0326
AA22	4	0.9332	0.9418	1.0507	1.0144	1.0004	0.0060	0.0130	-0.0130
KYC10	7	0.9223	0.9253	1.0140	1.0058	1.0021	0.6270	0.6640	1.0860
KYC11*	62*	0.9095	0.9191	1.0827	1.0042	1.0012	0.1270	1.0810	-0.1800

Note that "*" in file KYC11 means no solution found in the first 1 m^3 search volume, therefore the search volume was doubled to 8 m^3 search volume and a trial position yields AFV greater than 0.8 is considered as a candidate.

Processing results of the combined coarse and fine search technique on the baselines listed in Table 3.4 are shown in Table 3.5. The column "number of

candidates" in Table 3.5 is the number of local maxima with AFV greater than 0.9 in a given search volume. The 1st Max. AFV denotes the maximum AFV after the coarse searching in the first stage, and the Final Max. AFV is the maximum AFV obtained after the search using the fine resolution. AFR is the ambiguity function ratio described in section 2.5.6. AFRs obtained in the three searching stages are shown in columns five to seven of Table 3.5. Differences of the AFM positions from the GPSurvey solutions (processed with 30 minutes or more measurements) are shown in the last three columns of the table. The large differences of KYC10 and KYC11 are probably due to the un-modelled atmospheric effect. The three-dimensional plots of AF and the trial positions are shown in Figure 3.13, which the Z coordinates are fixed. The figure shows that a correct local maximum is prominent to the other local maxima in each plot (except the long baselines KYC10 and KYC11).

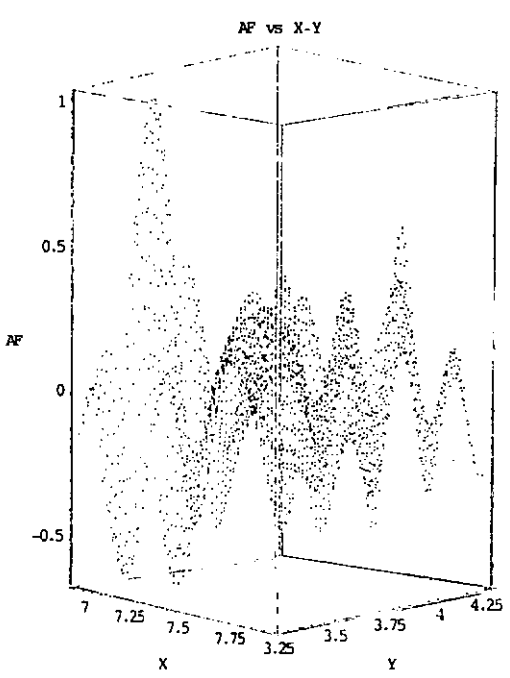

(a)

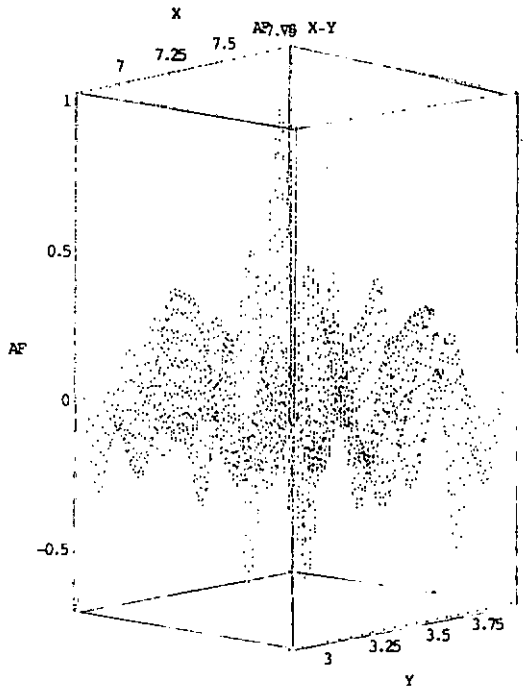

(b) cont.

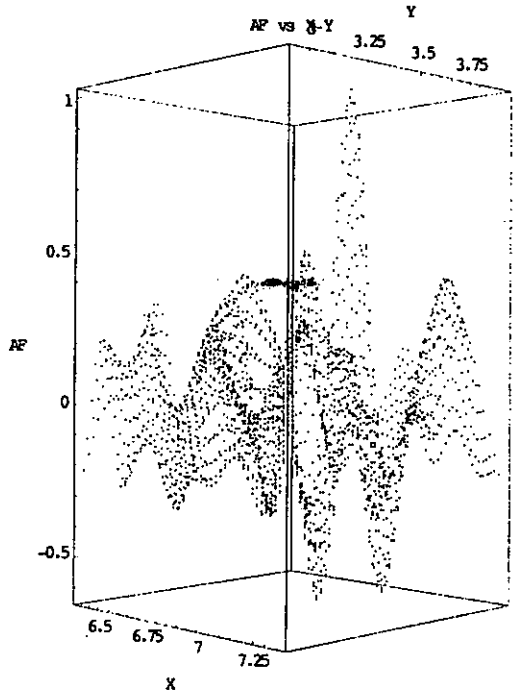
AF vs X-Y
Y
3.25
3.5
3.75
1
0.5
AF
0
-0.5
6.5
6.75
7
7.25
X

(c)

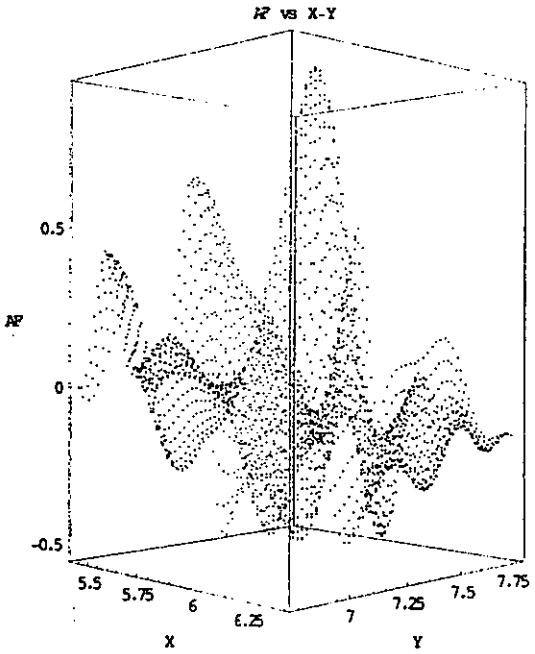
AF vs X-Y
0.5
AF
0
-0.5
5.5
5.75
6
6.25
X
7
7.25
7.5
7.75
Y

(d)

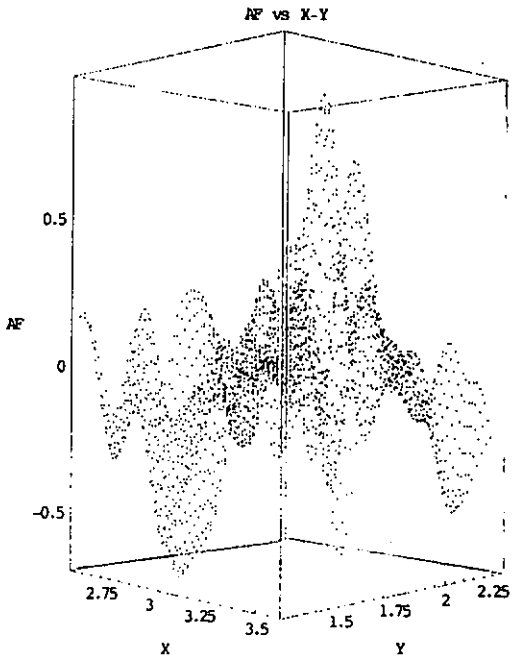
AF vs X-Y
0.5
AF
0
-0.5
2.75
3
3.25
3.5
X
1.5
1.75
2
2.25
Y

(e)

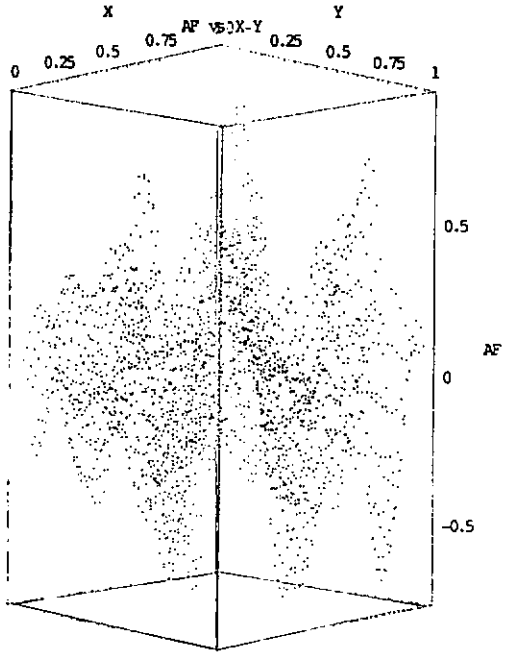
X
Y
AF vs X-Y
0
0.25
0.5
0.75
0.25
0.5
0.75
1
0.5
AF
0
-0.5

(f)

cont.

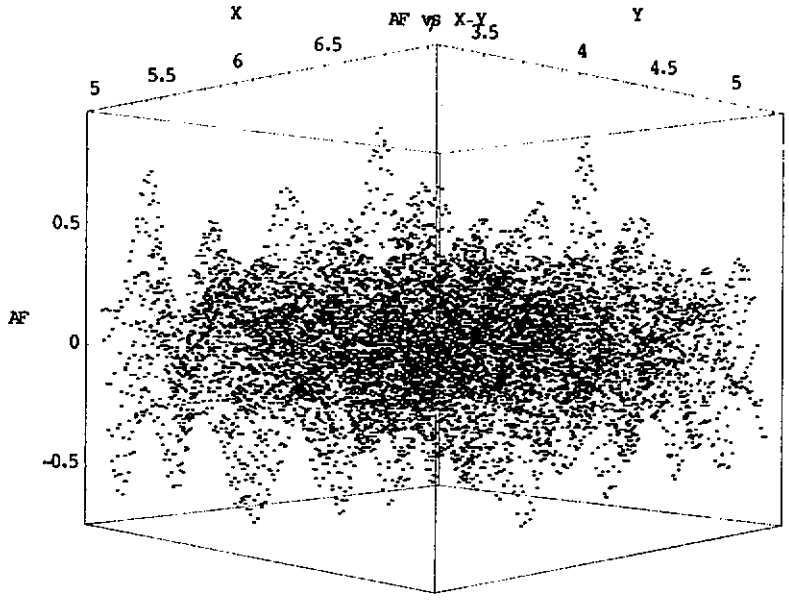

(g)

Figure 3.13
AF vs the trial positions in search volumes, (a) 3 m baseline of H1021; (b) 3 m baseline of H202; (c) 3 m baseline of H206; (d) 1.6 km baseline of AA16; (e) 2.2 km baseline of AA22; (f) 10.6 km baseline of KYC10; (g) 10.8 km baseline of KYC11 (8 m^3 search volume)

The above results (see Table 3.1-3, 3.5) show that the combined coarse and fine search technique can greatly reduce the processing time of AFM and successfully isolate the correct local maximum from the other local maxima in short baselines.

3.1.2 Search by Linear Combination of Carrier Phase Data

Linear combinations of carrier phases can increase the efficiency of AFM search by reducing the number of measurements to a half (the original L1 and L2 observables are linear combined to one observable). Linear combinations of carrier phases are briefly described in section 2.4. Widelane linear combination of carrier

phases is tested in this section because of the reduced number of measurements and its long wavelength. The 86.2 cm long wavelength widelane makes ambiguity resolution easier to achieve since the change of widelane ambiguity value becomes noticeable. What would be the effect of widelane observable applied to AFM?

The 2.2 km baseline in the new airport (see Table 3.4: AA22) was selected to test the effect of widelane observable to AFM solution. The widelane processing result was compared with the AFM result of the original L1 and L2 carrier phase observables in Table 3.5. The results are summarized in Table 3.6.

Table 3.6
Comparison of widelane and the original L1 and L2 AFM processing results

	original L1 and L2 observables	widelane observable
number of candidates (AF>0.9)	4	802
First maximum AF	0.9332	0.9902
Final maximum AF	0.9418	0.9922
First AFR	1.0507	1.0064
Second AFR	1.0144	1.0121
Third AFR	1.0004	1.0008
Coordinate differences from known (in meter)		
X	0.0060	0.1110
Y	0.0130	0.0780
Z	-0.0130	-0.1860
Processing time in sec. (without threshold test)	678	591

Illustrations of ambiguity function of the two observables over the same 1 m^3 search volume and 20 mm search resolution are shown in Figure 3.14.

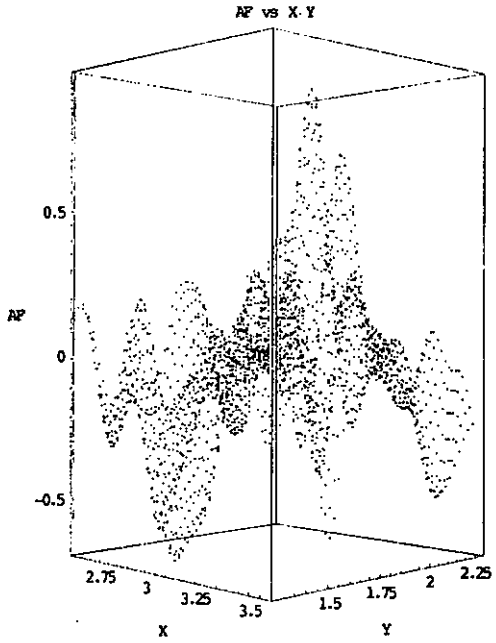
AF vs X Y
0.5
AF
0
-0.5
2.75
3
3.25
3.5
X
1.5
1.75
2
2.25
Y

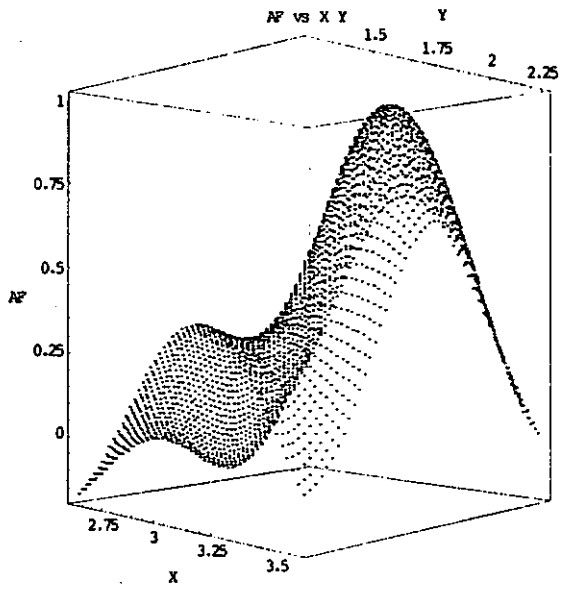
AF vs X Y
Y
1.5
1.75
2
2.25
1
0.75
0.5
AF
0.25
0
2.75
3
3.25
3.5
X

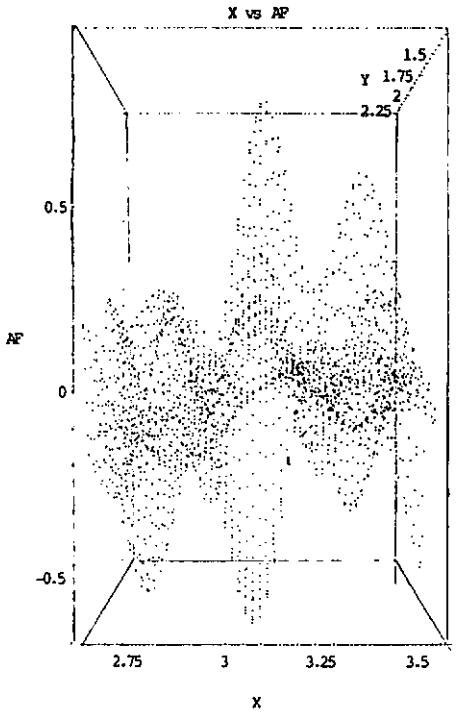
X vs AF
1.5
Y 1.75
2
2.25
0.5
AF
0
-0.5
2.75
3
3.25
3.5
X

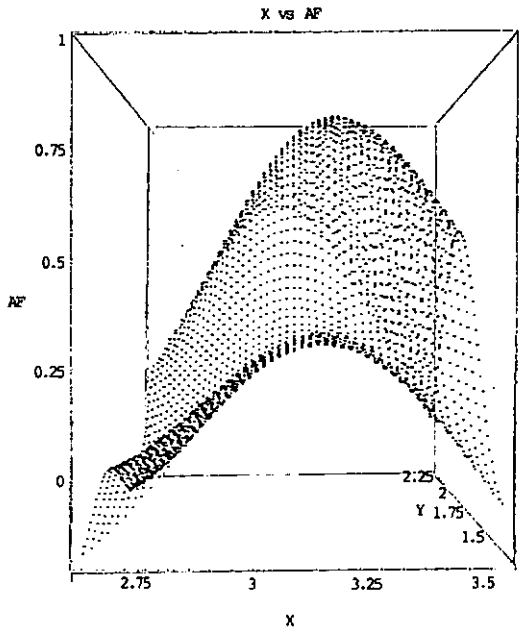
X vs AF
1
0.75
0.5
AF
0.25
0
2.25
2
Y 1.75
1.5
2.75
3
3.25
3.5
X

cont.

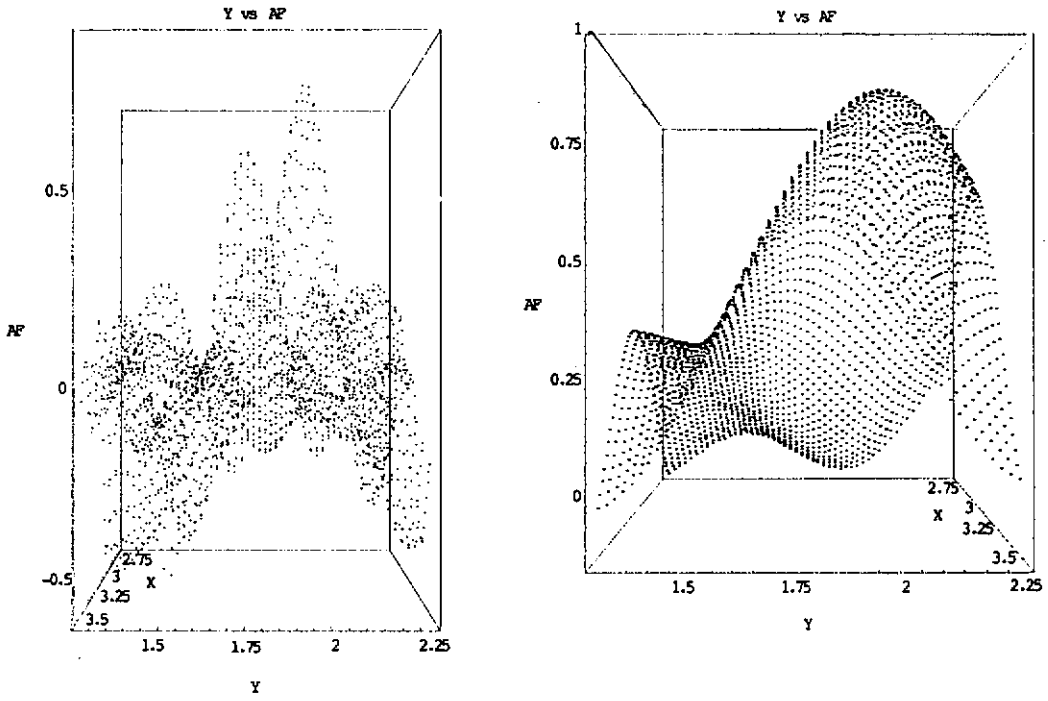

Figure 3.14
Illustrations of ambiguity function over the same 1 m^3 search volume by using the original L1 and L2 carrier phase observables (left-hand side), and widelane linear combination of carrier phases (right-hand side).

The test shows that the long wavelength property of widelane has significant improvement in the AFM search efficiency. It reduces about 13 percent of the processing time. The processing time of large AFM search volume with widelane observable may be further reduced by lowering the search resolution. Nevertheless, the number of candidates with AFV>0.9 significantly increases from 4 to 802 (see Table 3.6). These candidates form a wide-spreading local maximum (see the right-hand side of Figure 3.14) so it lowers the ambiguity function ratio (AFR) between the best position and the second best position (see Table 3.6) that makes validation less confident. Moreover, the positioning accuracy is seriously decreased when comparing the AFM processing result of widelane with that of the original L1 and L2 carrier phases. It is easy to see that the maximum in the left-hand side of Figure 3.14

is a little bit shifted to the right when using widelane observable, it can be seen in the right-hand side of Figure 3.14. The lower positioning accuracy of widelane observable is probably due to the fact that the linear combination of carrier phases amplified the un-modelled biases and errors such as multipath error and measurement noise [Hofmann-Wellenhof et al., 1994, pp. 96 and 127].

3.1.3 Validation Criteria

Validation of AFM can be done by comparing of the maximum normalized AFV (AFV_{2ndMax}) produced by the second best position with the maximum normalized AFV (AFV_{Max}) produced by the best position. It is called ambiguity function ratio (AFR):

$$AFR = \frac{AFV_{2ndMax}}{AFV_{Max}} \tag{3.16}$$

The numerator AF_{2ndMax} is less than the denominator AF_{Max}, the AFR is therefore larger than one. If the AFR is significantly larger than one, the second best position is then considered to be further apart from the best position. Acceptance of the best position is decided by the test statistic of AFR against the tabulated value of F distribution. The F-test is then used to decide whether the best position can be distinguished from the other candidates, especially the second best position.

The null hypothesis is

$$H_0 : AFR = 1 \tag{3.17}$$

The alternative hypothesis is

$$H_a : AFR > 1 \tag{3.18}$$

If the null hypothesis is accepted, it is concluded that the best position may not be distinguished from the second best position and other candidates. The "correct" position is obtained when the AFR has passed the F-test at a specified confidence level, i.e.:

$$AFR > F_{\alpha,m1,m2} \tag{3.19}$$

where AFR is the ratio of the second maximum AFV to the maximum AFV, and $F_{\alpha,m1,m2}$ is the F-value of specified significance level with m_1 degree of freedom for the position of the second maximum AFV and m_2 degree of freedom for the position of the maximum AFV. α is normally taken as 0.05, it represents 95% confidence level.

This project uses six-epoch double difference (DD) measurements and here assumes the number of satellites as 6. The degree of freedom is 27 (6 epochs x 5 DD measurements – 3 positioning parameters). Therefore, the tabulated (with interpolation) F value in 95% confidence from [Wolf and Ghilani, 1997] is 1.905.

However, most AFRs in Table 3.5 are less than the critical F value 1.905. It means that the best position is not significantly distinguished from the second best position. This is not true since the search resolution may be too fine and thus the best position and the second best position are in the same local maximum. As described in section 3.1.1 (pp. 68), the first search resolution is 20 mm, the second search resolution is 5mm and the final search resolution is 1mm. The second best position may be only 20 mm apart from the best position in the first search. Therefore, the AFVs of the two positions are very close, which lower the AFR. The AFRs of the second search and the third search are not important for validation because the best positions and the second best positions of the second search and the third search belong to the same local maximum in the range of ± 5 mm. However, they can give some quality information about the second and the third searches. The greater the AFR the better its quality.

The first search is very important since it separates the best local maximum from the other local maxima in the whole search volume so that fine search can be carried out in this local maximum. Since the first search resolution may be too high, so the best position and the second best position belong to the same local maximum that makes ratio test not sound, which the AFRs (see Table 3.5) are less than the critical F value. In order to make ratio test meaningful, the first search resolution is changed to 50 mm. It will not miss the "correct" local maximum because six epochs' measurements should sufficiently suppress the wrong local maxima and constructively produce the "correct" local maximum. Table 3.7 shows the results of first search with 50 mm and 20 mm search resolutions. Illustrations of the local

maxima of the two search resolutions in the same 1 m^3 search volume are shown in Figure 3.15. The "correct" local maximum has not missed.

Table 3.7
AFM processing results of the 5 cm and 2 cm first search resolutions

	5 cm search resolution	2 cm search resolution
Number of candidates (AF>0.9)	1	4
First AFR	1.2477	1.0507
Second AFR	1.3325	1.0144
Third AFR	1.0144	1.0004
Forth AFR	1.0004	--
First Max. AF	0.9081	0.9332
Final Max. AF	0.9418	0.9418
Processing time in sec.	93	678

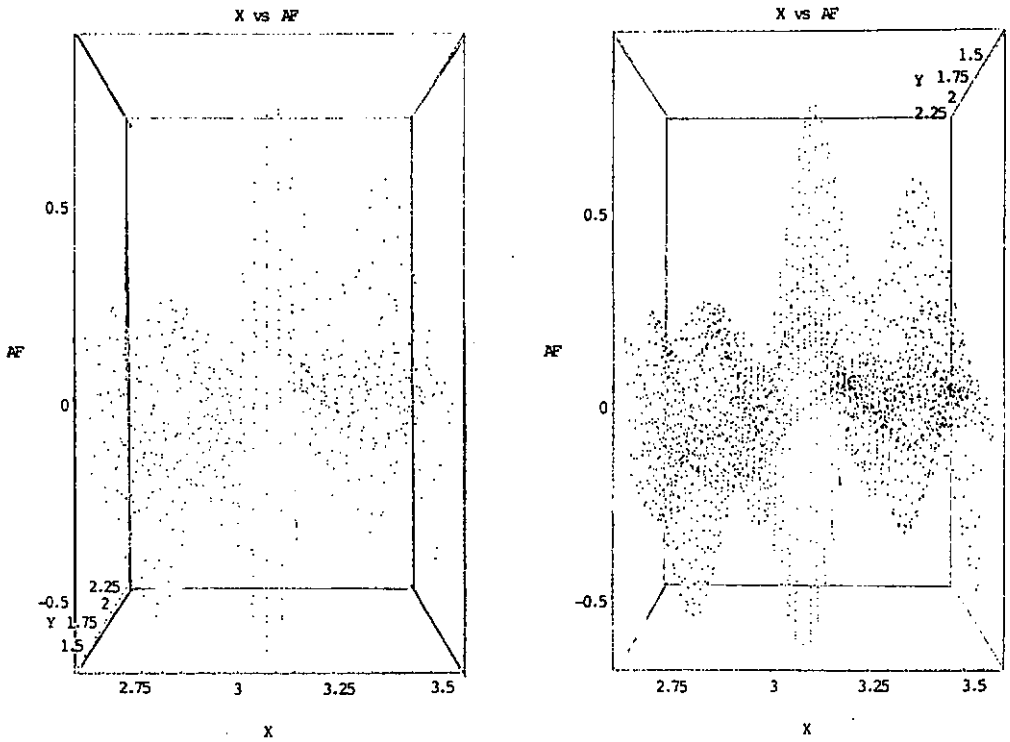

cont.

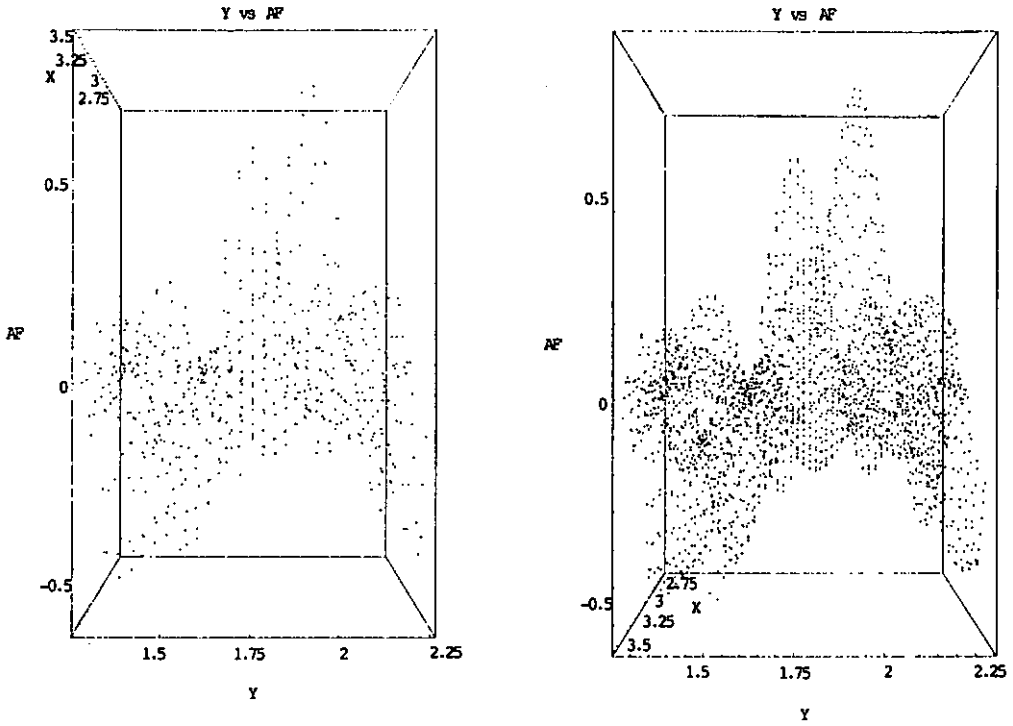

Figure 3.15
Illustrations of ambiguity function over the same 1 m^3 search volume by using the 5 cm search resolution (left-hand side), and 2 cm search resolution (right-hand side).

The profiles of the two search resolutions are very similar, the difference is the separation between candidates, i.e. in 5 cm search resolution, the neighbour candidates are 5 cm apart, the neighbour candidates are 2 cm apart in 2 cm search resolution. The best position is therefore at least 5 cm apart from the second best position in 5 cm search resolution. It yields the greater first AFR when comparing with the 2 cm search resolution, it can be found in Table 3.7. However, this first AFR of 1.2477 is far from the critical F value 1.905. Teunissen [1998] pointed out that this kind of test statistic does not have an F-distribution since the nominator and denominator of the test statistic are not independent.

Validation of AFM solution can be done by least squares adjustment of the best position and the second best position [Corbett and Cross, 1995]. Before carrying out the least squares adjustment, the integer ambiguities must be computed using the best position determined by AFM; this ambiguity resolution by AFM will be described in next section. The computed ambiguities are applied to the measurements. Least squares adjustments are then carried out using the best position and the second best position as known parameters. Carrier phase fixed solutions of the two positions are solved and a posteriori variances (of the best position and the second best position) and the best estimated positions are determined. Ratio of the a posteriori variance determined by the second best position to the a posteriori variance determined by the best position is validated by F-test.

The null hypothesis is:

$$H_0 : \hat{\sigma}^2_{0(\min)} = \hat{\sigma}^2_{0(2nd\ \min)} \tag{3.20}$$

with the alternative hypothesis:

$$H_a : \hat{\sigma}^2_{0(\min)} < \hat{\sigma}^2_{0(2nd\ \min)} \tag{3.21}$$

where

$$\hat{\sigma}^2_0 = \frac{v^T W v}{(n-m)} \tag{3.22}$$

where $\hat{\sigma}_0^2$ is the a posteriori variance,

v is the residual vector,

W is the weight matrix, and

$(n\text{-}m)$ is the degree of freedom.

The test statistic (ratio of the second minimum a posteriori variance to the minimum a posteriori variance) is:

$$F_{\alpha,m_1,m_2} < \frac{\hat{\sigma}^2_{0(2nd\ \min)}}{\hat{\sigma}^2_{0(\min)}} \tag{3.23}$$

where F_{α,m_1,m_2} is the F-value of specified significance level with m_1 degree of freedom for the second best position and m_2 degree of freedom for the best position. If the solution has passed the F-test, the best position is accepted. It implies the best position can be distinguished from the second best position and the other candidates.

Validation by F-test is verified using the 2.2 km baseline in the new airport (see Table 3.4), which is the same baseline used to verify the AFR (ambiguity function ratio) test in pp. 78-82. Least squares adjustment on the baseline was carried out. The minimum and the second minimum a posteriori variance are determined as 2.604817129 and 2.604817186 respectively. The variance ratio is therefore about one. Even the search resolution is 5 cm, which the best position and the second best position are separated at least 5 cm, the test statistic is still very close to one. It is

probably due to the low degree of freedom of the six-epoch measurement. F-test is therefore too tight for validation of the short observation time-span's solutions. Besides, Teunissen [1998] pointed out that this kind of test statistic does not have an F-distribution since the nominator and denominator of the test statistic are not independent.

3.1.4 Integer Ambiguity Resolution and Cycle Slip Correction

Lacking statistic information available for quality assurance is one shortcoming of AFM. It can be solved by applying least squares adjustment after AFM processing, which has been described in previous section (pp. 83-85). However, this process requires fixing the integer ambiguities and cycle slips prior to the least squares adjustment. Integer ambiguities can be computed by the correct position, determined by AFM. It is ambiguity resolution (AR) by AFM. The following real example shows how AFM is used for ambiguity resolution and cycle slip correction. Integer ambiguities of each DD observations in all measurement epochs are computed (see Table 3.8) using the "correct" position determined by AFM. It does not like the conventional method of initial integer ambiguity resolution. It has an extra benefit of absorption of any cycle slip, so applying the computed integer ambiguity to all DD observations will repair any cycle slip as well.

Cycle slip simulation has done by manually editing of a DD observation. In Table 3.8, the first L1 DD observation of the forth epoch (highlighted in the column L1 of Table 3.8) has changed from "-238502.485" to "-238505.485" (highlighted in the

column L1 of Table 3.9). A cycle slip of 3 cycles is imposed on the DD observation. The computed DD integer ambiguity changed from "-238521.0" to "-238524.0" (highlighted in the column Integer ambiguity of L1 of Table 3.8 and Table 3.9) after cycle slip simulation. However, the DD observation without ambiguity (highlighted in the column N corrected DDL1 of Table 3.8 and Table 3.9) remains unchanged. That shows integer ambiguity absorbs any cycle slip.

Table 3.8
Real example on ambiguity resolution by AFM

Correct position:								
	-2418121.582	5385913.609	2405587.207	*Integer ambiguity of L1*		*Integer ambiguity of L2*	*N corrected*	
Epoch	*L1*	L2	N (L1)		N (L2)		*DD L1*	*DD L2*
1	-238502.431	-88268.496	-238521.018	-238521	-88282.979	-88283	18.569	14.504
	-259412.861	109963.428	-259406.994	-259407	109968.000	109968	-5.861	-4.572
	-217168.623	-114791.663	-217186.970	-217187	-114805.959	-114806	18.377	14.337
	-915124.358	-683084.172	-915154.971	-915155	-683108.026	-683108	30.642	23.828
	-340283.686	-258608.088	-340277.059	-340277	-258602.924	-258603	-6.686	-5.088
	-572491.861	-378392.875	-572501.005	-572501	-378400.000	-378400	9.139	7.125
2	-238502.446	-88268.523	-238521.017	-238521	-88282.994	-88283	18.554	14.477
	-259412.841	109963.450	-259406.984	-259407	109968.014	109968	-5.841	-4.550
	-217168.596	-114791.653	-217186.975	-217187	-114805.974	-114806	18.404	14.347
	-915124.347	-683084.159	-915154.983	-915155	-683108.031	-683108	30.653	23.841
	-340283.694	-258608.100	-340277.051	-340277	-258602.924	-258603	-6.694	-5.100
	-572491.838	-378392.869	-572501.004	-572501	-378400.011	-378400	9.162	7.131
3	-238502.461	-88268.528	-238521.013	-238521	-88282.984	-88283	18.539	14.472
	-259412.838	109963.463	-259406.996	-259407	109968.015	109968	-5.838	-4.537
	-217168.570	-114791.619	-217186.981	-217187	-114805.965	-114806	18.430	14.381
	-915124.340	-683084.091	-915154.993	-915155	-683107.977	-683108	30.660	23.909
	-340283.712	-258608.085	-340277.052	-340277	-258602.896	-258603	-6.712	-5.085
	-572491.817	-378392.842	-572501.006	-572501	-378400.003	-378400	9.183	7.158
4	-238502.485	-88268.545	-238521.025	-238521	-88282.992	-88283	18.515	14.455
	-259412.819	109963.475	-259406.995	-259407	109968.013	109968	-5.819	-4.525
	-217168.543	-114791.602	-217186.980	-217187	-114805.969	-114806	18.457	14.398
	-915124.309	-683084.137	-915154.983	-915155	-683108.039	-683108	30.691	23.863
	-340283.740	-258608.112	-340277.064	-340277	-258602.910	-258603	-6.740	-5.112
	-572491.801	-378392.836	-572501.009	-572501	-378400.011	-378400	9.199	7.164
5	-238502.492	-88268.561	-238521.013	-238521	-88282.993	-88283	18.508	14.439
	-259412.809	109963.489	-259406.996	-259407	109968.018	109968	-5.809	-4.511
	-217168.521	-114791.567	-217186.990	-217187	-114805.959	-114806	18.479	14.433
	-915124.278	-683084.099	-915154.969	-915155	-683108.014	-683108	30.722	23.901
	-340283.753	-258608.105	-340277.064	-340277	-258602.893	-258603	-6.753	-5.105
	-572491.783	-378392.821	-572501.010	-572501	-378400.011	-378400	9.217	7.179
6	-238502.510	-88268.578	-238521.009	-238521	-88282.993	-88283	18.490	14.422
	-259412.798	109963.494	-259406.999	-259407	109968.013	109968	-5.798	-4.506
	-217168.495	-114791.556	-217186.985	-217187	-114805.964	-114806	18.505	14.444
	-915124.280	-683084.113	-915154.988	-915155	-683108.042	-683108	30.720	23.887
	-340283.772	-258608.139	-340277.058	-340277	-258602.907	-258603	-6.772	-5.139
	-572491.755	-378392.801	-572501.004	-572501	-378400.008	-378400	9.245	7.199

Table 3.9
Real example on ambiguity resolution and cycle slip correction by AFM

Correct position:								
	-2418121.582	5385913.609	2405587.207	*Integer ambiguity of L1*		*Integer ambiguity of L2*		
							N corrected	
Epoch	*L1*	L2	N (L1)		N (L2)		*DD L1*	*DD L2*
1	-238502.431	-88268.496	-238521.018	-238521	-88282.979	-88283	18.569	14.504
	-259412.861	109963.428	-259406.994	-259407	109968.000	109968	-5.861	-4.572
	-217168.623	-114791.663	-217186.970	-217187	-114805.959	-114806	18.377	14.337
	-915124.358	-683084.172	-915154.971	-915155	-683108.026	-683108	30.642	23.828
	-340283.686	-258608.088	-340277.059	-340277	-258602.924	-258603	-6.686	-5.088
	-572491.861	-378392.875	-572501.005	-572501	-378400.000	-378400	9.139	7.125
2	-238502.446	-88268.523	-238521.017	-238521	-88282.994	-88283	18.554	14.477
	-259412.841	109963.450	-259406.984	-259407	109968.014	109968	-5.841	-4.550
	-217168.596	-114791.653	-217186.975	-217187	-114805.974	-114806	18.404	14.347
	-915124.347	-683084.159	-915154.983	-915155	-683108.031	-683108	30.653	23.841
	-340283.694	-258608.100	-340277.051	-340277	-258602.924	-258603	-6.694	-5.100
	-572491.838	-378392.869	-572501.004	-572501	-378400.011	-378400	9.162	7.131
3	-238502.461	-88268.528	-238521.013	-238521	-88282.984	-88283	18.539	14.472
	-259412.838	109963.463	-259406.996	-259407	109968.015	109968	-5.838	-4.537
	-217168.570	-114791.619	-217186.981	-217187	-114805.965	-114806	18.430	14.381
	-915124.340	-683084.091	-915154.993	-915155	-683107.977	-683108	30.660	23.909
	-340283.712	-258608.085	-340277.052	-340277	-258602.896	-258603	-6.712	-5.085
	-572491.817	-378392.842	-572501.006	-572501	-378400.003	-378400	9.183	7.158
4	-238505.485	-88268.545	-238521.025	-238524	-88282.992	-88283	18.515	14.455
	-259412.819	109963.475	-259406.995	-259407	109968.013	109968	-5.819	-4.525
	-217168.543	-114791.602	-217186.980	-217187	-114805.969	-114806	18.457	14.398
	-915124.309	-683084.137	-915154.983	-915155	-683108.039	-683108	30.691	23.863
	-340283.740	-258608.112	-340277.064	-340277	-258602.910	-258603	-6.740	-5.112
	-572491.801	-378392.836	-572501.009	-572501	-378400.011	-378400	9.199	7.164
5	-238502.492	-88268.561	-238521.013	-238521	-88282.993	-88283	18.508	14.439
	-259412.809	109963.489	-259406.996	-259407	109968.018	109968	-5.809	-4.511
	-217168.521	-114791.567	-217186.990	-217187	-114805.959	-114806	18.479	14.433
	-915124.278	-683084.099	-915154.969	-915155	-683108.014	-683108	30.722	23.901
	-340283.753	-258608.105	-340277.064	-340277	-258602.893	-258603	-6.753	-5.105
	-572491.783	-378392.821	-572501.010	-572501	-378400.011	-378400	9.217	7.179
6	-238502.510	-88268.578	-238521.009	-238521	-88282.993	-88283	18.490	14.422
	-259412.798	109963.494	-259406.999	-259407	109968.013	109968	-5.798	-4.506
	-217168.495	-114791.556	-217186.985	-217187	-114805.964	-114806	18.505	14.444
	-915124.280	-683084.113	-915154.988	-915155	-683108.042	-683108	30.720	23.887
	-340283.772	-258608.139	-340277.058	-340277	-258602.907	-258603	-6.772	-5.139
	-572491.755	-378392.801	-572501.004	-572501	-378400.008	-378400	9.245	7.199

3.2 Investigation into LAMBDA

Teunissen [1995b] developed a processing algorithm which uses Least-squares AMBiguity Decorrelation Adjustment (LAMBDA) method to improve the efficiency of ambiguity resolution. This algorithm followed the steps, i) float solution, ii) integer ambiguity estimation and iii) fixed solution. These steps are similar to classic static approach described in section 2.5.1. The main characteristic of the algorithm is the integer ambiguity estimation by LAMBDA method. The LAMBDA method consists of:

(i) the decorrelation of the ambiguities by a reparametrization of the original ambiguities to new ambiguities, and

(ii) the actual ambiguity estimation

Lambda method requires the variance-covariance matrix of ambiguities and the approximate values of ambiguities derived from the least squares float solution. The variance-covariance matrix provides information for decorrelation of ambiguities, and the approximate values of ambiguities are used to transform to the less correlated ambiguities for performing the actual ambiguity estimation. The decorrelation process involves decomposition of the variance-covariance matrix of ambiguity parameters and Z-transformation of the original ambiguities a to the less correlated transformed ambiguities z. The integer ambiguity estimation is then done by search of the integer transformed ambiguities in a less correlated bounded search volume. Finally, the estimated integer transformed ambiguities $\check{z}$ are inversely Z-transformed to the original least squares ambiguity vector $\hat{a}$ for least squares fixed solution.

Jonge and Tiberius [1996] suggested many computational schemes for Lambda method. In this research, the author adopts a procedure that is relatively simple and efficient. The procedure is outlined in Figure 3.16.

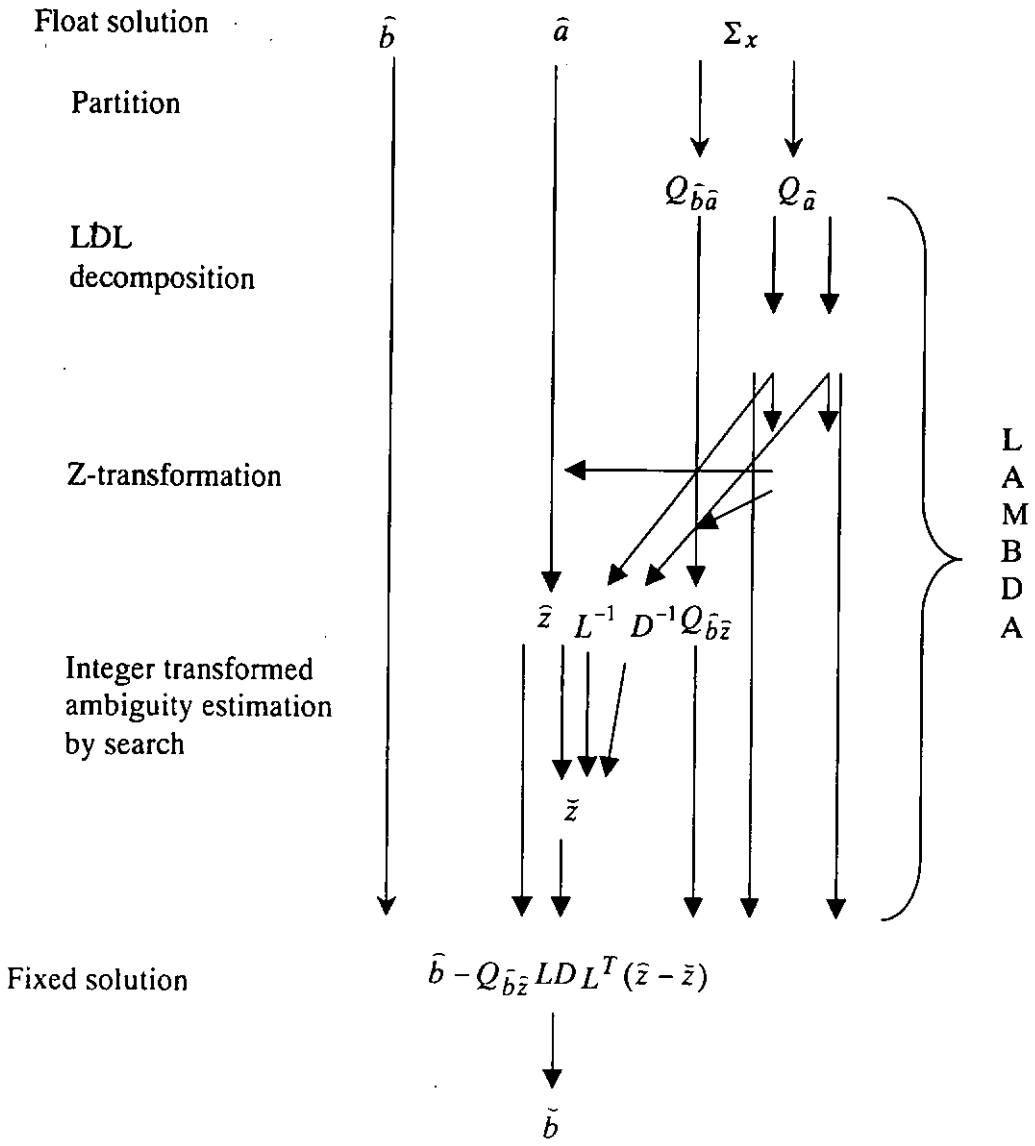

Figure 3.16
Outline of LAMBDA method

Approximate position parameters $\hat{b}$, approximate real ambiguity $\hat{a}$ and variance-covariance matrix of parameters are determined in the least squares float solution. This information is input to LAMBDA procedure as listed in Figure 3.16, and the best estimated position parameters and integer ambiguities are determined.

The following sections will investigate the principle, efficiency and accuracy of the LAMBDA method with a worked example. Measurement of an about 10 km baseline (KYC10 in Table 3.4) was selected as the worked example because of its highly correlated DD ambiguities. Six epochs of measurement are used. Because of this short observation time, the spectrum of DD ambiguity conditional variances will always show a discontinuity when passing the third conditional variance (see Appendix II) [Teunissen, 1998]. In the example, only four satellites and L1 carrier phase data are available. Such condition reduces the number of very small conditional variances and thus the transformed spectrum is not flat already.

Variance-covariance matrix of the unknown parameters $\Sigma_{\hat{x}}$ is determined by the combined code and carrier phase float solution:

$$\Sigma_{\hat{x}} = \left[\begin{array}{ccc|ccc} 0.4666 & -0.2477 & -0.1515 & 1.6992 & -0.3927 & -0.7749 \\ -0.2477 & 0.6117 & 0.3206 & -1.0690 & -1.3443 & 0.2023 \\ -0.1515 & 0.3206 & 0.4214 & 0.0930 & 0.3192 & 0.8572 \\ \hline 1.6992 & -1.0690 & 0.0930 & 8.3520 & 1.9074 & -0.6973 \\ -0.3927 & -1.3443 & 0.3192 & 1.9074 & 9.0707 & 4.0560 \\ -0.7749 & 0.2023 & 0.8572 & -0.6973 & 4.0560 & 3.3790 \end{array}\right] \quad (3.24)$$

and the approximate ambiguities are determined as:

$$\hat{a} = [-4581612.6609 \quad -35106603.4968 \quad -6024070.0418]^T \tag{3.25}$$

Given that variance-covariance of parameters $\Sigma_{\hat{x}}$ is:

$$\Sigma_{\hat{x}} = \begin{bmatrix} Q_{\hat{b}} & Q_{\hat{b}\hat{a}} \\ Q_{\hat{a}\hat{b}} & Q_{\hat{a}} \end{bmatrix} \tag{3.26}$$

where $Q_{\hat{b}}$ denotes the variance-covariance matrix of position parameters (X, Y and Z),

$Q_{\hat{b}\hat{a}}$ denotes the variance-covariance matrix of position parameters and DD ambiguities,

$Q_{\hat{a}\hat{b}}$ denotes the variance-covariance matrix of DD ambiguities and position parameters, and

$Q_{\hat{a}}$ denotes the variance-covariance of DD ambiguities.

The corresponding variance-covariance matrix can be partitioned from the variance-covariance matrix of parameters as:

$$Q_{\hat{b}} = \begin{bmatrix} 0.4666 & -0.2477 & -0.1515 \\ -0.2477 & 0.6117 & 0.3206 \\ -0.1515 & 0.3206 & 0.4214 \end{bmatrix} \tag{3.27}$$

$$Q_{\hat{b}\hat{a}} = \begin{bmatrix} 1.6992 & -0.3927 & -0.7749 \\ -1.0690 & -1.3443 & 0.2023 \\ 0.0930 & 0.3192 & 0.8572 \end{bmatrix} \tag{3.28}$$

$$Q_{\hat{a}} = \begin{bmatrix} 8.3520 & 1.9074 & -0.6973 \\ 1.9074 & 9.0707 & 4.0560 \\ -0.6973 & 4.0560 & 3.3790 \end{bmatrix} \tag{3.29}$$

where the determinant of $Q_{\hat{a}}$ is 91.0955.

With the variance-covariance matrix of position parameters $Q_{\hat{b}}$, position parameters and DD ambiguities $Q_{\hat{b}\hat{a}}$, DD ambiguities, and the approximate DD ambiguity vector $\hat{a}$, the integer ambiguity estimation by LAMBDA method can now proceed.

3.2.1 L^TDL Decomposition

Z-transformation matrix is required to decorrelate the DD ambiguities. Formation of Z-transformation matrix is based on the lower triangular matrix L and diagonal matrix D of the variance-covariance matrix of DD ambiguities. Since the variance-covariance matrix of DD ambiguities $Q_{\hat{a}}$ is a positive definite matrix, $Q_{\hat{a}}$ can be factorised into a product $L^T DL$, where L is lower triangular matrix with 1's along the diagonal and D is a diagonal matrix whose diagonal entries are all positive:

$$Q_{\hat{a}} = L^T DL \tag{3.30}$$

this decomposition gives,

$$L = \begin{bmatrix} 1 & 0 & 0 \\ 0.6531 & 1 & 0 \\ -0.2064 & 1.2003 & 1 \end{bmatrix} \tag{3.31}$$

$$D = \begin{bmatrix} 6.4156 & 0 & 0 \\ 0 & 4.2021 & 0 \\ 0 & 0 & 3.3790 \end{bmatrix} \tag{3.32}$$

Once the L and D have been determined, Z-transformation matrix can be computed.

3.2.2 Ambiguity Transformation

This is the most critical part of LAMBDA method since the efficiency of the method relies on this decorrelation step. The decorrelation is done by Z-transformation of the original ambiguities to less correlated transformed ambiguities:

$$z = Z^T a \tag{3.33}$$

where z is the transformed ambiguity vector, Z is the Z-transformation matrix, and a is the original ambiguity vector.

And the variance-covariance matrix of ambiguities is transformed by:

$$Q_{\hat{z}} = Z^T Q_{\hat{a}} Z \tag{3.34}$$

where $Q_{\hat{z}}$ denotes the transformed variance-covariance matrix of ambiguities,

Z denotes the Z-transformation matrix, and

$Q_{\hat{a}}$ denotes the original variance-covariance matrix of ambiguities.

The Z-transformation matrix is determined by the integer Gauss transformation and the conditional variances are reordered by permutation matrix to mitigate the discontinuity when passing the conditional variance. Teunissen [1998] described the location and/or size of the discontinuity depends on the model of observation equations and observation time-span.

The Z-transformation matrix of the example is:

$$Z = \begin{bmatrix} 1 & 0 & 0 \\ -1 & 1 & 0 \\ 1 & -1 & 1 \end{bmatrix} \tag{3.35}$$

Therefore, the approximate ambiguity vector (eqn. 3.25) is transformed by the Z-transformation matrix (eqn. 3.35) according to eqn. 3.33, and yields:

$$\hat{z} = [24500920.7941 \quad -29082533.4550 \quad -6024070.0418]^T \tag{3.36}$$

where $\hat{z}$ is the real transformed ambiguity vector.

And the variance-covariance matrix of ambiguities $Q_{\hat{a}}$ (eqn. 3.29) is transformed by eqn. 3.34:

$$Q_{\hat{z}} = \begin{bmatrix} 7.4802 & -1.7329 & -1.3743 \\ -1.7329 & 4.3377 & 0.6770 \\ -1.3743 & 0.6770 & 3.3790 \end{bmatrix} \tag{3.37}$$

where $Q_{\hat{z}}$ denotes the transformed variance-covariance matrix of ambiguities. The determinant of $Q_{\hat{z}}$ equals 91.0955, it is the same as the determinant of $Q_{\hat{a}}$. The identical determinant of $Q_{\hat{z}}$ and $Q_{\hat{a}}$ is due to the volume-preserving property of Z, which the determinant equals one.

In order to investigate the decorrelation effect, the standard deviation σ of the original and transformed ambiguities, as well as the correlation coefficient ρ are determined. The correlation coefficient ρ_{ij} is a standardized covariance that never exceeds 1 [Strang and Borre, 1997]:

$$\rho_{ij} = \frac{\sigma_{ij}}{\sqrt{\sigma_i^2 \sigma_j^2}} = \frac{\sigma_{ij}}{\sigma_i \varsigma_j} \text{ and } \left|\rho_{ij}\right| \leq 1 \tag{3.38}$$

Recall eqn. 3.29:

$$Q_{\hat{a}} = \begin{bmatrix} 8.3520 & 1.9074 & -0.6973 \\ 1.9074 & 9.0707 & 4.0560 \\ -0.6973 & 4.0560 & 3.3790 \end{bmatrix} \tag{3.29}$$

The standard deviations and correlation coefficients of $Q_{\hat{a}}$ are:

$\sigma_{\hat{a}1} = 2.890$ $\quad \rho_{\hat{a}1\hat{a}2} = 0.228$

$\sigma_{\hat{a}2} = 3.012$ $\quad \rho_{\hat{a}1\hat{a}3} = -0.366$

$\sigma_{\hat{a}3} = 1.838$ $\quad \rho_{\hat{a}2\hat{a}3} = 1.200$

After the decorrelation process:

$\sigma_{\hat{z}1} = 2.735$ $\quad \rho_{\hat{z}1\hat{z}2} = -0.232$

$\sigma_{\hat{z}2} = 2.083$ $\quad \rho_{\hat{z}1\hat{z}3} = -0.184$

$\sigma_{\hat{z}3} = 1.838$ $\quad \rho_{\hat{z}2\hat{z}3} = 0.200$

The result shows the transformed ambiguities are less correlated than the original ambiguities. However, its effect is not as significant as in [Teunissen, 1995b; Jonge and Tiberius, 1996; Teunissen, 1998]. It is because that the float solution (see pp. 91) includes pseudorange data, which flattened the transformed spectrum, and the baseline is quite long, which biased by atmospheric effect.

After this procedure, the less correlated real transformed ambiguities are then delivered to a bounded search volume for integer transformed ambiguity estimation.

3.2.3 Integer Ambiguity Estimation

This procedure aims to find the most likely integer candidates for the transformed ambiguities by means of a sequential conditional least squares estimation. The candidates are determined by search in a bounded volume, which satisfies:

$$(\hat{z}-z)^T Q_{\hat{z}}^{-1}(\hat{z}-z) \leq \chi^2 \tag{3.39}$$

where $\hat{z}$ denotes the real approximate transformed ambiguity vector,

z denotes the integer estimated transformed ambiguity vector,

$Q_{\hat{z}}$ denotes the transformed variance-covariance matrix of ambiguities, and

χ^2 denotes the bounds, not chi-square in standard statistic textbook.

For the computational details of this step, please refer to [Jonge and Tiberius, 1996; Teunissen, Jonge, and Tiberius, 1996]. A candidate fulfils the transformed integer minimization of eqn. 3.40 is considered as the best estimate.

$$(\hat{z}-z)^T Q_{\hat{z}}^{-1}(\hat{z}-z) = \min \tag{3.40}$$

The best and the second best estimated integer transformed ambiguity vectors of the example have been determined as:

$$\breve{z}_1 = [24500921 \quad -29082533 \quad -6024070]^T \tag{3.41}$$

$$\breve{z}_2 = [24500921 \quad -29082534 \quad -6024070]^T \tag{3.42}$$

Note that the best estimated integer transformed ambiguities are equal to the nearest integers of the approximate real transformed ambiguities (see eqn. 3.36) in the example. It means that by setting the approximate real transformed (decorrelated) ambiguities to the nearest integer in ambiguity transformation step has the same solution as the best estimated integer transformed ambiguities in the step of integer ambiguity estimation by search.

Once the transformed integer minimization problem has solved, the best estimated position parameters (X, Y and Z) can be determined by fixed solution in the last step of Figure 3.16, or by ordinary fixed solution with the back transformed ambiguities. The later approach is more common in practice. It is to transform the best estimated (and second best estimated) integer transformed ambiguity vector $\breve{z}$ back to the best estimated original DD integer ambiguity vector $\breve{a}$:

$$\breve{a} = (Z^T)^{-1}\breve{z} \tag{3.43}$$

and then perform least squares fixed solution.

The best and second best estimated original DD integer ambiguity sets of this example are listed in Table 3.10. In the table, another two ambiguity sets determined

by GPSurvey are also presented for comparison. These ambiguities are computed by the determined position of GPSurvey's solution. The fourth column is based on about 30 minutes' observation, whereas the fifth column is determined based on six-epoch measurement, which is the same observation time as the example. Moreover, the original DD ambiguities determined by the combined code and phase float solution are set to the nearest integer and shown in the sixth column.

Table 3.10
Comparison of integer ambiguity sets determined by LAMBDA to GPSurvey

	LAMBDA		GPSurvey		Combined code and phase solution (nearest integer)
Ambiguities	Best	2nd Best	~30 min.	6 epochs	
a_1	-4581612	-4581613	-4581611	-4581602	-4581613
a_2	-35106603	-35106604	-35106603	-35106594	-35106603
a_3	-6024070	-6024070	-6024071	-6024066	-6024070

The best estimated ambiguities a_1 and a_3 determined by LAMBDA are different from the GPSurvey's solution with about 30 minutes' observation by one cycle, however, the other solutions are a few cycles different. The coordinate differences to the GPSurvey's solution with about 30 minutes' observation are presented in Table 3.11.

Table 3.11
Coordinate differences

Position parameters	LAMBDA		GPSurvey	Combined code and phase solution (nearest integer)
	Best	2nd Best	6 epochs	
X	-0.3399	-0.5320	0.778	-0.4574
Y	0.4673	0.8445	-0.864	0.6330
Z	0.4111	0.5404	1.614	0.4327

The large differences in Table 3.11 are probably due to the atmospheric effect of the 10.6 km baseline and only four observing satellites; the solution of GPSurvey is L1 ionospheric-free fixed solution with Hopfield tropospheric model. The test indicates that the best estimated position by LAMBDA is the best solution (see Table 3.10 and 3.11). LAMBDA is also considered as a very efficient method, as it requires a few millisecond processing time in the example. Another example on LAMBDA method can be found in pp. 171-172 of Appendix II, which the baseline length is 1.6 km but the variance-covariance matrix of ambiguities has already flattened by the combined code and carrier phase float solution.

3.2.4 Validation Criteria

According to [Teunissen, 1995; Jonge and Tiberius, 1996; Teunissen, Jonge, and Tiberius, 1996; Teunissen, 1998], the LAMBDA method has no standard way to validate the solutions. They only suggest finding the best and second best estimates, which yield the minimum and second minimum residuals respectively, but haven't investigated any variance ratio test or other validation procedure for LAMBDA. In this stage, validation can therefore be done by variance ratio test or eqn. 2.25.

Variance ratio of the above example is 1.0557, however, the tabulated value of F distribution in 95% confidence is 2.403. Again, the F-test may not be suitable if the degree of freedom is low, due to short observation time-span and few observing satellites (only four in the example). Teunissen [1998] stated that this kind of test

statistic does not have an F-distribution since the nominator and denominator of the test statistic are not independent.

CHAPTER 4

THE IMPROVED GPS DATA PROCESSING ALGORITHMS

Three improved GPS data processing algorithms are proposed in this chapter. They are Combined Ambiguity Function Method and Least Squares Method with Signal-to-Noise Ratio Weighting (CALMS), Signal-to-Noise Ratio Weighted Ambiguity Function Technique (SWAT), and integrated LAMBDA and CALMS algorithm. CALMS and SWAT algorithms aim to improve the GPS positioning accuracy. The integrated LAMBDA and CALMS algorithm is proposed to improve data processing efficiency as well as to process GPS data without *a priori* position of roving receiver.

4.1 Concepts of the Proposed GPS Data Processing Algorithms

The three processing algorithms are based on AFM because of its advantages of AFM applied to deformation monitoring discussed in section 2.6. The concept of AFM is described and investigated in section 3.1 in details.

As described in section 2.1.5, multipathing is the major source of error in relative positioning and cannot be eliminated by differencing techniques. CALMS and SWAT are derived with the relationship between multipath and SNR described in section 2.2. They use SNR to form a stochastic model for mitigation of multipath error and therefore improve GPS differential positioning accuracy in both horizontal and vertical components. CALMS applies the stochastic model in weight matrix of

least squares adjustment while SWAT applies the model as a multiplying factor in AFM. The details of CALMS and SWAT are described in section 4.2 and 4.3. Moreover, the efficient LAMBDA method is integrated with the CALMS method. Solutions of LAMBDA and CALMS may be used as independent check and validation of solution. The integrated algorithm therefore improves GPS data processing accuracy, efficiency and reliability. Its procedure is described in section 4.4.

4.2 Combined Ambiguity Function Method and Least Squares Method with Signal-to-Noise Ratio Weighting (CALMS)

A flowchart of the main steps involved within the CALMS (Combined AFM (Ambiguity Function Method) and LSM (Least Squares Method) Method with Signal-to-Noise Ratio (SNR) weighting) GPS processing algorithm is presented in Figure 4.1.

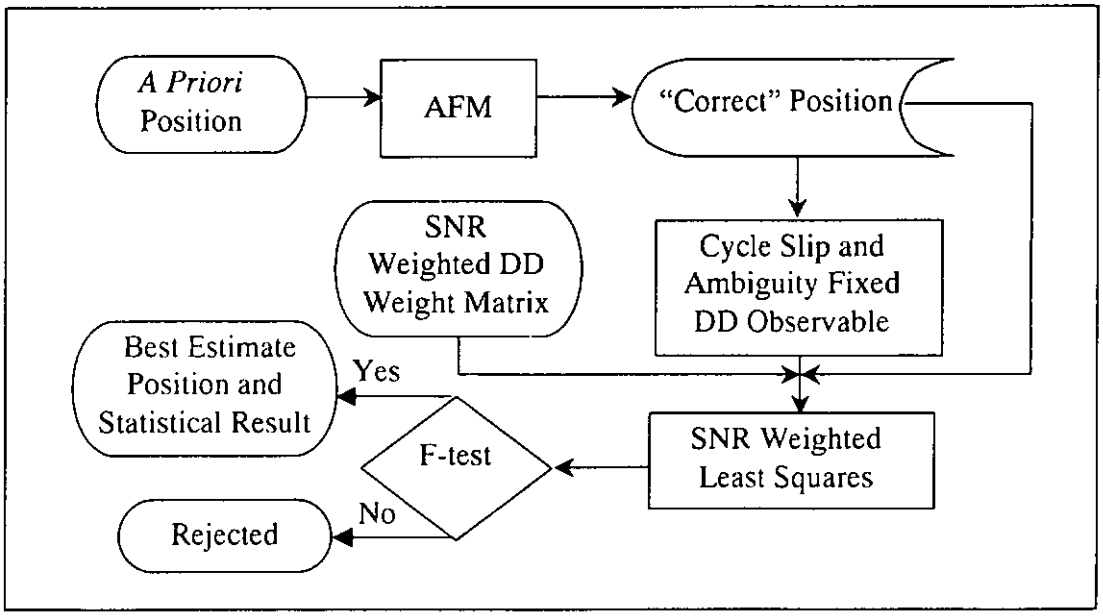

Figure 4.1
Outline of the CALMS GPS data processing algorithm

The first part of CALMS processing algorithm uses AFM to process DD measurements of L1 and L2, as described in section 3.1. *A priori* position for AFM is first determined from the last deformation monitoring solution. Then AFM is carried out to determine a very good "correct" position. This position is used as *a priori* position for SNR weighted least squares adjustment. The "correct" position is also employed in ambiguity resolution and cycle slip correction. The details of this procedure are described in [Lau, 1997] and section 3.1.4.

The second part and kernel of CALMS is the SNR weighting least squares of the carrier phase measurements. As described section 2.2, the SNR determines how well the carrier-tracking loops in the GPS receiver can track the signals and hence the precision of the carrier-phase measurements. Introduction of SNR weighting variance into least squares adjustment is similar to that of distance in a levelling network and elevation angle in GPS data processing algorithms.

CALMS is based on DD carrier phase observations, which can significantly reduce common biases of both receivers in short baselines, for example, satellite orbit bias, satellite clock offset, receiver clock offset, and part of ionospheric and tropospheric delay. Both L1 and L2 DD carrier phase measurements are used in the SNR weighted least squares adjustment. Unlike GLONASS, GPS has the same L1 and L2 frequencies for all satellites. The benefit of taking both L1 and L2 into SNR weighted least squares adjustment is that the CALMS takes interference into account and allocates suitable weight for interfered band. However, experimental result shows that L1 and L2 SNR weighted least squares have the same result as using L1

only. This is because both L1 and L2 have about the same signal-to-noise ratio during observation, which means no interference in either frequency.

As described in section 2.1.5 (eqn. 2.4 and 2.5), multipath is related to each receiver and satellite in view; SNR weight is applied to each receiver and satellite, therefore four SNRs are taken into account for each DD observation. This is done by the procedure similar to the formation of DD observation. Instead of undifferenced phase observation, the SNR matrix is obtained by multiplication of modified DD operator (called SNR operator below) and SNR of all satellites in view for both receivers in epoch(s). The SNR operator is formed by changing the differencing operators of double difference (DD) operator to positive, i.e. –1 to 1. This is because multipath error is not common for both receivers of a baseline so it cannot be eliminated. Therefore, SNR weight of a DD measurement must take all constituent SNRs into account, that is, four SNRs for a DD measurement (two satellites and two receivers). Besides, the matrix multiplication in the formation of an SNR matrix is modified; in constituent SNRs of a DD measurement, the dot product is obtained by multiplication rather than addition of multiplied elements. This adaptive matrix multiplication procedure can easily eliminate the loss of lock and zero SNR measurement during processing and effectively reflects the weight of DD measurement. The SNR matrix is expressed as

$$\sum_{SNR} = D \cdot S \tag{4.1}$$

where $\sum_{SNR}$ is the SNR matrix,

D is the SNR operator, and

S is a column matrix with all SNRs arranged in the sequence as undifferenced phase measurements.

To determine the correlation, the variance-covariance propagation law is applied, leading to

$$Q_{SNR} = \sigma^2 \cdot \sum_{SNR} \cdot \sum_{SNR}^{T} \tag{4.2}$$

where Q_{SNR} is the SNR cofactor matrix,

σ^2 is the *a priori* variance; it is taken as unity, and

$\sum_{SNR}$ is the SNR matrix.

An example of a single epoch SNR cofactor matrix is given below. It is a real data set observed at two stations on the roof of The Hong Kong Polytechnic University on 5/20/98; the mask angle was set to 10°, which was intended to show the SNR of a low-elevation angle satellite clearly:

SNR operator (D):

$$\begin{bmatrix}
1 & 1 & 0 & 0 & 0 & 0 & 0 & 0 & 0 & 1 & 1 & 0 & 0 & 0 & 0 & 0 & 0 & 0 \\
1 & 0 & 1 & 0 & 0 & 0 & 0 & 0 & 0 & 1 & 0 & 1 & 0 & 0 & 0 & 0 & 0 & 0 \\
1 & 0 & 0 & 1 & 0 & 0 & 0 & 0 & 0 & 1 & 0 & 0 & 1 & 0 & 0 & 0 & 0 & 0 \\
1 & 0 & 0 & 0 & 1 & 0 & 0 & 0 & 0 & 1 & 0 & 0 & 0 & 1 & 0 & 0 & 0 & 0 \\
1 & 0 & 0 & 0 & 0 & 1 & 0 & 0 & 0 & 1 & 0 & 0 & 0 & 0 & 1 & 0 & 0 & 0 \\
1 & 0 & 0 & 0 & 0 & 0 & 1 & 0 & 0 & 1 & 0 & 0 & 0 & 0 & 0 & 1 & 0 & 0 \\
1 & 0 & 0 & 0 & 0 & 0 & 0 & 1 & 0 & 1 & 0 & 0 & 0 & 0 & 0 & 0 & 1 & 0 \\
1 & 0 & 0 & 0 & 0 & 0 & 0 & 0 & 1 & 1 & 0 & 0 & 0 & 0 & 0 & 0 & 0 & 1
\end{bmatrix} \tag{4.3}$$

S matrix with the reference satellite at first for both receivers (9 satellites for each receiver):

$$\begin{bmatrix} 27 & 11 & 27 & 11 & 24 & 15 & 14 & 18 & 20 & 26 & 10 & 26 & 11 & 23 & 14 & 13 & 15 & 22 \end{bmatrix}^T \tag{4.4}$$

SNR cofactor matrix:

$$\begin{bmatrix} 5.963 & 38.054 & 6.559 & 29.923 & 11.384 & 9.866 & 14.636 & 23.852 \\ 38.054 & 242.860 & 41.860 & 190.960 & 72.649 & 62.963 & 93.406 & 152.220 \\ 6.559 & 41.860 & 7.215 & 32.915 & 12.522 & 10.853 & 16.100 & 26.237 \\ 29.923 & 190.96 & 32.915 & 150.160 & 57.126 & 49.509 & 73.448 & 119.690 \\ 11.384 & 72.649 & 12.522 & 57.126 & 21.733 & 18.835 & 27.942 & 45.535 \\ 9.866 & 62.963 & 10.853 & 49.509 & 18.835 & 16.324 & 24.216 & 39.464 \\ 14.636 & 93.406 & 16.100 & 73.448 & 27.942 & 24.216 & 35.925 & 58.545 \\ 23.852 & 152.220 & 26.237 & 119.690 & 45.535 & 39.464 & 58.545 & 95.407 \end{bmatrix} \times 10^9 \tag{4.5}$$

Element (2,2) has the largest SNR variance as it is the product of the reference satellite (SNR=27 for reference receiver and SNR=26 for roving receiver) and the third satellite (SNR=27 for reference receiver and SNR=26 for roving receiver). It reflects that the corresponding DD measurement has the largest weight for least squares adjustment.

The SNR cofactor matrix is closely related to the elevation angle since SNR is almost directly proportional to elevation angle in not too noisy environments. Sleewaegen [1997] has shown this linear relationship between standard derivation of

multipath and satellite elevation angle. The elevation angle of satellites and the corresponding SNRs of the above example are shown in Table 4.1.

Table 4.1
Elevation angle of satellites and SNRs

SV #	Elevation angle (°)	SNR of L1(reference receiver, roving receiver)
2	17	11, 10
4	48	27, 26
5	21	11, 11
7	55	27, 26
10	40	24, 23
13	25	15, 14
16	22	14, 13
18	30	18, 15
24	39	20, 22

The SNR cofactor matrix is a symmetric matrix where the elements are variances or covariances of double-differenced SNR. The full SNR cofactor matrix for all epochs is a block diagonal matrix since SNRs are correlated in the same epoch but uncorrelated to other epochs. It is exactly the same dimension as DD cofactor matrix and DD weight matrix. The SNR weighted DD weight matrix is formed by multiplication of corresponding variance or covariance between SNR cofactor matrix and DD weight matrix.

$$\text{DD weight matrix} = Q^{-1} = \begin{bmatrix} \frac{\sigma_0^2}{\sigma_1^2} & \frac{\sigma_0^2}{\sigma_1\sigma_2} & \cdots & \frac{\sigma_0^2}{\sigma_1\sigma_n} \\ \frac{\sigma_0^2}{\sigma_2\sigma_1} & \frac{\sigma_0^2}{\sigma_2^2} & \cdots & \frac{\sigma_0^2}{\sigma_2\sigma_n} \\ \vdots & \vdots & \ddots & \vdots \\ \frac{\sigma_0^2}{\sigma_n\sigma_1} & \frac{\sigma_0^2}{\sigma_n\sigma_2} & \cdots & \frac{\sigma_0^2}{\sigma_n^2} \end{bmatrix} \tag{4.6}$$

where σ_0^2 is the *a priori* variance of the GPS relative phase measurement (most geodetic receiver manufacturers claim it as $(5\text{ mm})^2$),

σ_n^2 is the variance of DD measurements,

$\sigma_{i=1..n}\sigma_{j=1..n}$ is the covariance of DD measurements and

n is the number of satellites at the epoch.

$$\text{SNR cofactor matrix} = \begin{bmatrix} \sigma_{12}^{12}\sigma_{12}^{12} & \sigma_{12}^{12}\sigma_{12}^{13} & \cdots & \sigma_{12}^{12}\sigma_{12}^{1n} \\ \sigma_{12}^{13}\sigma_{12}^{12} & \sigma_{12}^{13}\sigma_{12}^{13} & \cdots & \sigma_{12}^{13}\sigma_{12}^{1n} \\ \vdots & \vdots & \ddots & \vdots \\ \sigma_{12}^{1n}\sigma_{12}^{12} & \sigma_{12}^{1n}\sigma_{12}^{13} & \cdots & \sigma_{12}^{1n}\sigma_{12}^{1n} \end{bmatrix} \tag{4.7}$$

where $\sigma_{12}^{1n}\sigma_{12}^{1n}$ is the covariance of SNR measurements of the two (reference and roving) receivers of a baseline, and

n is the number of satellites at the epoch.

Taking elements in SNR cofactor matrix as S with reference satellite denoted as (^{1}), reference receiver denoted as ($_1$), and roving receiver denoted as ($_2$) omitted; eqn. 4.7 becomes:

$$\text{SNR cofactor matrix} = \begin{bmatrix} S^{22} & S^{23} & \cdots & S^{2n} \\ S^{32} & S^{33} & \cdots & S^{3n} \\ \vdots & \vdots & \ddots & \vdots \\ S^{n2} & S^{n3} & \cdots & S^{nn} \end{bmatrix} \tag{4.8}$$

$$\text{SNR weighted DD weight matrix} = \begin{bmatrix} \frac{\sigma_0^2}{\sigma_1^2} S^{22} & \frac{\sigma_0^2}{\sigma_1 \sigma_2} S^{23} & \cdots & \frac{\sigma_0^2}{\sigma_1 \sigma_{n-1}} S^{2n} \\ \frac{\sigma_0^2}{\sigma_2 \sigma_1} S^{32} & \frac{\sigma_0^2}{\sigma_2^2} S^{33} & \cdots & \frac{\sigma_0^2}{\sigma_2 \sigma_{n-1}} S^{3n} \\ \vdots & \vdots & \ddots & \vdots \\ \frac{\sigma_0^2}{\sigma_{n-1} \sigma_1} S^{n2} & \frac{\sigma_0^2}{\sigma_{n-1} \sigma_2} S^{n3} & \cdots & \frac{\sigma_0^2}{\sigma_{n-1}^2} S^{nn} \end{bmatrix} \quad (4.9)$$

This SNR-weighted DD weight matrix is the weight matrix for least squares adjustment of DD measurements. The full SNR-weighted DD weight matrix for n epochs is a block diagonal matrix:

$$W_{SNR} = \begin{bmatrix} W_1 & 0 & 0 & 0 \\ 0 & W_2 & 0 & 0 \\ 0 & 0 & \ddots & 0 \\ 0 & 0 & 0 & W_n \end{bmatrix} \quad (4.10)$$

where $W_{i,i=1,2,\ldots n}$ are the block matrix as shown in eqn. 4.9.

SNR-weighted least squares is performed as usual:

$$\hat{x} = (A^T W_{SNR} A)^{-1} A^T W_{SNR} l \quad (4.11)$$

where $\hat{x}$ is the best estimates,

A is the design matrix,

W_{SNR} is the SNR-weighted DD weight matrix, and

l is the vector of observational residuals.

This algorithm is derived for short-baseline (<10 km) application; however, it can easily be modified to provide the ionospheric-free solution for long-baseline processing. The formation of ionospheric-free observable can be found in [Leick 1995] or eqn. 2.24.

4.3 Signal-To-Noise Ratio Weighted Ambiguity Function Technique (SWAT)

A flowchart of the main steps involved in the SWAT (Signal-to-noise ratio Weighted Ambiguity function Technique) GPS processing algorithm is presented in Figure 4.2. Although this algorithm is also derived for short-baseline data processing, SWAT can easily be modified to include ionospheric correction; Mader [1992] describes the formation of equivalent ionospheric-free observable for AFM.

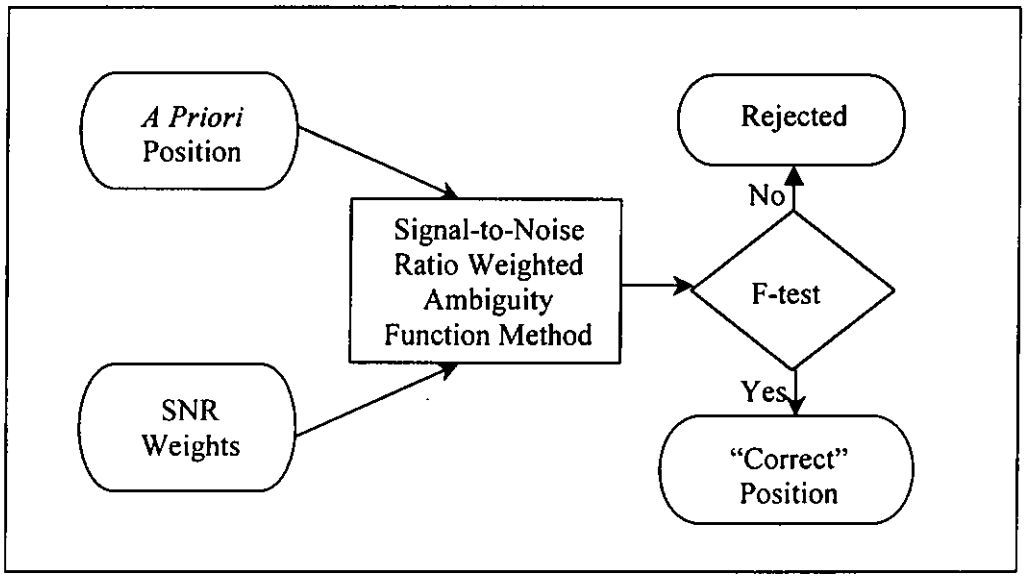

Figure 4.2
Outline of the SWAT GPS data processing algorithm

The *a priori* position is used to construct a search volume for the SNR weighted ambiguity function search. An example of a search volume is shown in Figure 4.3. In Figure 4.3, the *a priori* position, which was determined by the solution of last measurement, becomes the *a priori* position of AFM, which is the centre of the search volume.

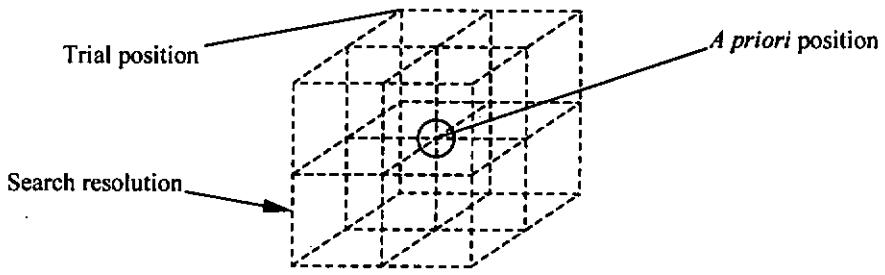

Figure 4.3
Search volume of AFM

Lau [1997] stated that incorrect position might be obtained by AFM when serious un-modelled errors are present in the measurements. Therefore, SWAT GPS data processing algorithm uses the SNR weighted AFM to mitigate multipath as well as interference. SWAT is the modification of the original AFM formula presented in eqn. 3.13 to

$$AF(X,Y,Z) = \sum_{L=1}^{2} \sum_{R=1}^{i} \sum_{S=1}^{j} \boldsymbol{S} \cos\{2\pi[\frac{f_L}{c} \rho_{km,c}^{pq}(t) - \varphi_{km,L,b}^{pq}(t)]\} \qquad (4.12)$$

where $\boldsymbol{S}$ is the SNR factor and the other notations are the same as eqn. 3.13.

SNR factor (S) is a multiplying factor. It determines the weight for ambiguity function of each measurement to the AFV by the measured SNR. S factor is direct and linear related to the measured SNR in the specific bounds:

$$S = \frac{DSNR - refSNR^4}{USNR^4 - refSNR^4} \times 0.2 + 1 \tag{4.13}$$

where *DSNR* is the SNR of the DD measurement,

refSNR is the reference SNR,

USNR is the upper bound of SNR, which is receiver dependent,

0.2 is the SNR interval between the *USNR* and *refSNR* , and

1 is an additive constant that equals the theoretical maximum of AFV.

Graphical representation of eqn. 4.13 is shown in Figure 4.4. The power of four in eqn. 4.13 is because that a DD measurement contains four SNRs (from the reference satellite and a satellite to the reference receiver, and the reference satellite and a satellite to the roving receiver).

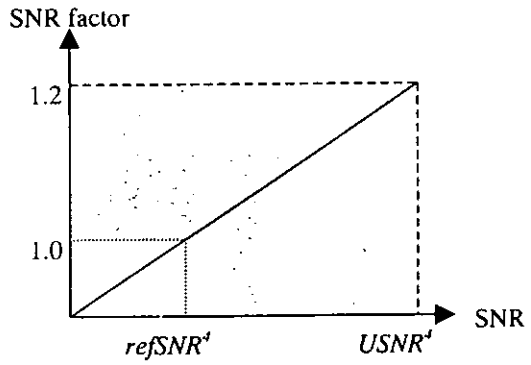

Figure 4.4
Interpolation of the SNR factor

Moreover, *DSNR* is obtained according to Lau and Mok [1999a] and the above section by:

$$\sum_{SNR} = D \cdot S \tag{4.14}$$

where $\sum_{SNR}$ is the column SNR matrix,

D is the SNR operator, and

S is a column matrix with all SNRs arranged in the sequence as undifferenced phase measurements.

The elements of the SNR matrix are the corresponding *DSNR*s. Details and principle for the formation of SNR matrix (eqn. 4.14) are described in [Lau and Mok, 1999a] and the above section. The procedure of SWAT is the same as that of AFM described in section 3.1. "Correct" position is obtained when the AF ratio of the best position (maximum AF) and the second best position (second maximum AF) passed F-test, which was described in section 3.1.3 and [Han and Mok, 1997; Lau and Mok, 1999a].

4.4 Integrated GPS Data Processing Algorithm

Frei and Beutler [1989] stated that optimized GPS data processing algorithm should be fast, reliable, self-contained, flexible, self-controlled and automatic.

However, the above two GPS data processing algorithms rely on the *a priori* position, which is determined in the solution of last measurement, to construct an AFM search volume. Besides, the algorithms require the input of signal-to-noise ratio for each measurement (satellite and epoch) in order to form a stochastic model. It does not mean that the algorithms are not self-contained and automatic since RINEX Version 2.0 format ought to have signal strength provided, ranging from 0 to 9 [Strang and Borre, 1997, pp. 593]. Moreover, the receiver manufacturers can add the signal-to-noise ratios in their in-house observation file. Therefore, the processing algorithms can read the observations as well as signal-to-noise ratios and apply them into processing. The processing algorithms become self-contained and automatic.

In order to make a processing algorithm really self-contained, self-controlled and automatic, the *a priori* position for CALMS search volume should be determined by the observations. It means that no *a priori* position, which is determined by the solution of previous measurement, is required to input. It can be done by carrying out code solution and/or float solution before CALMS procedure. Since the processing time of CALMS depends on the search volume (see section 3.1), the accurate *a priori* position can greatly reduce the CALMS search volume and so lessens the processing time. It is necessary for fast and precise GPS data processing algorithm.

LAMBDA method is selected as a part of the integrated GPS data processing algorithm to provide an accurate *a priori* position for CALMS searching. The reason for using LAMBDA is that, LAMBDA is considered to be an efficient GPS processing method suitable for processing data observed in short time. Since LAMBDA method requires an approximate coordinates of the unknown point,

approximate values of integer ambiguities, and the variance-covariance of unknown parameters (see in section 3.2), a float solution is hence required to perform prior to the use of LAMBDA method.

The integrated processing algorithm contains two stand-alone processing methods, they are LAMBDA and CALMS method. The incorporated LAMBDA method not only increases the processing efficiency but also serves as an independent solution for validating the position determined by CALMS that increases the reliability. As a result, this integrated GPS data processing is fast, reliable, self-contained, flexible, self-controlled and automatic.

4.4.1 Outline

The main steps for the integrated GPS data processing algorithm is shown in Figure 4.5. The algorithm consists of five processing steps, shown as the square boxes with numbers in Figure 4.5. The five processing steps are

1) Initial position determination by DD C/A code solution,

2) Carrying out combined of C/A code and L1 carrier phase float solution,

3) Position determination by LAMBDA method,

4) Position determination by CALMS method, and

5) Validation of positioning result using F-statistical test.

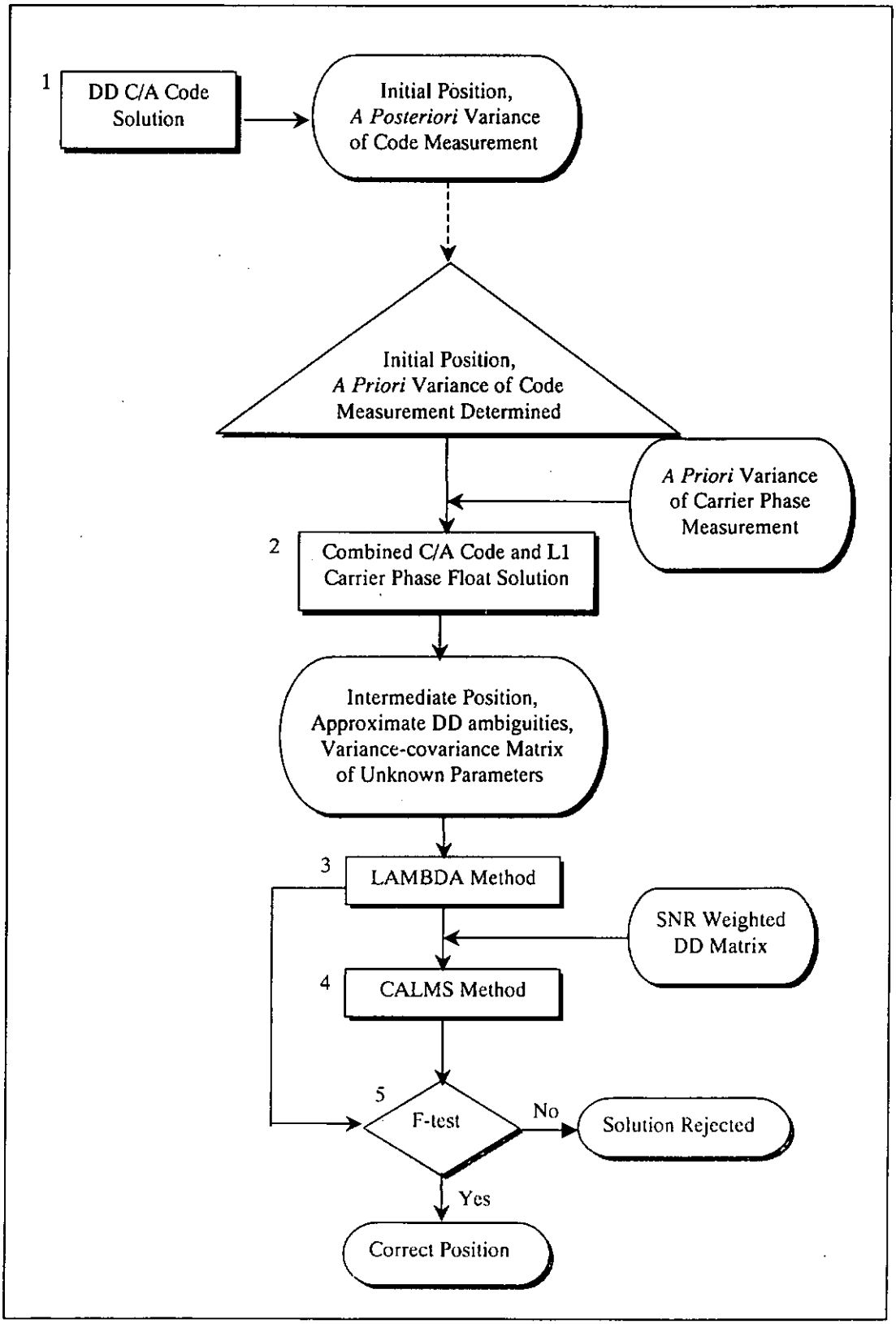

Figure 4.5
Outline of the integrated GPS data processing algorithm

4.4.2 C/A Code Solution and Combined C/A Code and L1 Carrier Phase Float Solution

The first part of the integrated processing algorithm is the DD C/A code solution. This part is to find the initial position of the unknown point and the *a posteriori* variance of DD C/A code solution by least squares. The next step is the combined C/A code and L1 carrier phase float solution. Model of the float solution is shown below.

Linear observation equations of relative code and phase measurement [Hofmann-Wellenhof et al., 1994] are shown in eqn. (4.15) and (4.16) respectively:

$$P_{AB}^{pq}(t)-\rho_{AB}^{pq}(t)=\left[-\frac{X^q(t)-X_B}{\rho_B^q(t)}+\frac{X^p(t)-X_B}{\rho_B^p(t)}\right]\Delta X_B-\left[-\frac{Y^q(t)-Y_B}{\rho_B^q(t)}+\frac{Y^p(t)-Y_B}{\rho_B^p(t)}\right]\Delta Y_B$$
$$-\left[-\frac{Z^q(t)-Z_B}{\rho_B^q(t)}+\frac{Z(t)-Z_B}{\rho_B^p(t)}\right]\Delta Z_B \qquad (4.15)$$

$$\lambda\varphi_{AB}^{pq}(t)-\rho_{AB}^{pq}(t)=\left[-\frac{X^q(t)-X_B}{\rho_B^q(t)}+\frac{X^p(t)-X_B}{\rho_B^p(t)}\right]\Delta X_B-\left[-\frac{Y^q(t)-Y_B}{\rho_B^q(t)}+\frac{Y^p(t)-Y_B}{\rho_B^p(t)}\right]\Delta Y_B$$
$$-\left[-\frac{Z^q(t)-Z_B}{\rho_B^q(t)}+\frac{Z(t)-Z_B}{\rho_B^p(t)}\right]\Delta Z_B+\lambda N_{AB}^{pq} \qquad (4.16)$$

where $P_{AB}^{pq}(t)$ denotes the measured DD pseudorange at epoch t.

$\rho_{AB}^{pq}(t)$ denotes the computed DD topocentric distance.

X, Y and Z denote the Cartesian coordinates,

$\rho_B^p(t)$ and $\rho_B^q(t)$ denote the topocentric distance from the unknown point B to the satellite p and q respectively,

ΔX_B, ΔY_B, ΔZ_B denote the corrections in Cartesian coordinates of point B,

λ denotes the carrier wavelength,

$\varphi_{AB}^{pq}(t)$ denotes the DD phase measurement at epoch t, and

N_{AB}^{pq} denotes the DD integer ambiguity.

Design matrix (A):

$$\begin{bmatrix}
a_{XB}^{12}(t_1) & a_{YB}^{12}(t_1) & a_{ZB}^{12}(t_1) & \lambda & 0 & 0 & 0 & 0 \\
a_{XB}^{13}(t_1) & a_{YB}^{13}(t_1) & a_{ZB}^{13}(t_1) & 0 & \lambda & 0 & 0 & 0 \\
a_{XB}^{14}(t_1) & a_{YB}^{14}(t_1) & a_{ZB}^{14}(t_1) & 0 & 0 & \lambda & 0 & 0 \\
\vdots & \vdots & \vdots & 0 & 0 & 0 & \ddots & 0 \\
a_{XB}^{1S}(t_1) & a_{YB}^{1S}(t_1) & a_{ZB}^{1S}(t_1) & 0 & 0 & 0 & 0 & \lambda \\
a_{XB}^{12}(t_1) & a_{YB}^{12}(t_1) & a_{ZB}^{12}(t_1) & 0 & 0 & 0 & 0 & 0 \\
a_{XB}^{13}(t_1) & a_{YB}^{13}(t_1) & a_{ZB}^{13}(t_1) & 0 & 0 & 0 & 0 & 0 \\
a_{XB}^{14}(t_1) & a_{YB}^{14}(t_1) & a_{ZB}^{13}(t_1) & 0 & 0 & 0 & 0 & 0 \\
\vdots & \vdots & \vdots & 0 & 0 & 0 & 0 & 0 \\
a_{XB}^{1S}(t_1) & a_{YB}^{1S}(t_1) & a_{ZB}^{1S}(t_1) & 0 & 0 & 0 & 0 & 0 \\
\vdots & \vdots & \vdots & \vdots & \vdots & \vdots & \vdots & \vdots \\
a_{XB}^{12}(t_n) & a_{YB}^{12}(t_n) & a_{ZB}^{12}(t_n) & \lambda & 0 & 0 & 0 & 0 \\
\vdots & \vdots & \vdots & 0 & \ddots & \ddots & \ddots & 0 \\
a_{XB}^{1S}(t_n) & a_{YB}^{1S}(t_n) & a_{ZB}^{1S}(t_n) & 0 & 0 & 0 & 0 & \lambda \\
a_{XB}^{12}(t_n) & a_{YB}^{12}(t_n) & a_{ZB}^{12}(t_n) & 0 & 0 & 0 & 0 & 0 \\
\vdots & \vdots & \vdots & \vdots & \vdots & \vdots & \vdots & \vdots \\
a_{XB}^{1S}(t_n) & a_{YB}^{1S}(t_n) & a_{ZB}^{1S}(t_n) & 0 & 0 & 0 & 0 & 0
\end{bmatrix} \tag{4.17}$$

where a_{XB}, a_{YB} and a_{ZB} are the partial derivatives with respect to the receiver positions (shown inside the square brackets in eqn. 4.15),

1 denotes the reference satellite in double difference,

S denotes the number of satellites,

t is the measurement epochs from 1 to n, and

λ is the wavelength of L1 carrier phase.

$$\text{Unknown vector (X):} \begin{bmatrix} \Delta X_B \\ \Delta Y_B \\ \Delta Z_B \\ N_{AB}^{12} \\ N_{AB}^{13} \\ \vdots \\ N_{AB}^{1S} \end{bmatrix} \tag{4.18}$$

Misclosure vector:

$$l = \begin{bmatrix} l_{AB}^{12}(t_1) \\ l_{AB}^{13}(t_1) \\ l_{AB}^{14}(t_1) \\ \vdots \\ l_{AB}^{1S}(t_1) \\ l_{AB}^{12}(t_1) \\ l_{AB}^{13}(t_1) \\ l_{AB}^{14}(t_1) \\ \vdots \\ l_{AB}^{1S}(t_1) \\ \vdots \\ l_{AB}^{12}(t_n) \\ \vdots \\ l_{AB}^{1S}(t_n) \\ l_{AB}^{12}(t_n) \\ \vdots \\ l_{AB}^{1S}(t_n) \end{bmatrix} \tag{4.19}$$

and the weight matrix (W):

$$\begin{bmatrix}
w_{AB,L1}^{12,12} & w_{AB,L1}^{12,13} & w_{AB,L1}^{12,14} & \cdots & w_{AB,L1}^{12,1S} & 0 & 0 & 0 & \cdots & 0 & \cdots & 0 & \cdots & 0 & 0 & \cdots & 0 \\
w_{AB,L1}^{13,12} & w_{AB,L1}^{13,13} & w_{AB,L1}^{13,14} & \cdots & w_{AB,L1}^{13,1S} & 0 & 0 & 0 & \cdots & 0 & \cdots & 0 & \cdots & 0 & 0 & \cdots & 0 \\
w_{AB,L1}^{14,12} & w_{AB,L1}^{14,13} & w_{AB,L1}^{14,14} & \cdots & w_{AB,L1}^{14,1S} & 0 & 0 & 0 & \cdots & 0 & \cdots & 0 & \cdots & 0 & 0 & \cdots & 0 \\
\vdots & \vdots & \vdots & \ddots & \vdots & 0 & 0 & 0 & \cdots & 0 & \cdots & 0 & \cdots & 0 & 0 & \ddots & \vdots \\
w_{AB,L1}^{1S,12} & w_{AB,L1}^{1S,13} & w_{AB,L1}^{1S,14} & \cdots & w_{AB,L1}^{1S,1S} & 0 & 0 & 0 & \cdots & 0 & \cdots & 0 & \cdots & 0 & 0 & \cdots & 0 \\
0 & 0 & 0 & 0 & 0 & w_{AB,C}^{12,12} & w_{AB,C}^{12,13} & w_{AB,C}^{12,14} & \cdots & w_{AB,C}^{12,1S} & 0 & 0 & 0 & 0 & 0 & 0 & 0 \\
0 & 0 & 0 & 0 & 0 & w_{AB,C}^{13,12} & w_{AB,C}^{13,13} & w_{AB,C}^{13,14} & \cdots & w_{AB,C}^{13,1S} & 0 & 0 & 0 & 0 & 0 & 0 & 0 \\
0 & 0 & 0 & 0 & 0 & w_{AB,C}^{14,12} & w_{AB,C}^{14,13} & w_{AB,C}^{14,14} & \cdots & w_{AB,C}^{14,1S} & 0 & 0 & 0 & 0 & 0 & 0 & 0 \\
0 & 0 & 0 & 0 & 0 & \vdots & \vdots & \vdots & \ddots & \vdots & 0 & 0 & 0 & 0 & 0 & 0 & 0 \\
0 & 0 & 0 & 0 & 0 & w_{AB,C}^{1S,12} & w_{AB,C}^{1S,13} & w_{AB,C}^{1S,14} & \cdots & w_{AB,C}^{1S,1S} & 0 & 0 & 0 & 0 & 0 & 0 & 0 \\
0 & 0 & 0 & 0 & 0 & 0 & 0 & 0 & 0 & 0 & \ddots & \vdots & 0 & 0 & 0 & 0 & 0 \\
0 & 0 & 0 & 0 & 0 & 0 & 0 & 0 & 0 & 0 & \cdots & w_{AB,L1}^{12,12} & \cdots & w_{AB,L1}^{12,1S} & 0 & 0 & 0 \\
0 & 0 & 0 & 0 & 0 & 0 & 0 & 0 & 0 & 0 & 0 & \vdots & \ddots & \vdots & 0 & 0 & 0 \\
0 & 0 & 0 & 0 & 0 & 0 & 0 & 0 & 0 & 0 & 0 & w_{AB,L1}^{1S,12} & \cdots & w_{AB,L1}^{1S,1S} & 0 & 0 & 0 \\
0 & 0 & 0 & 0 & 0 & 0 & 0 & 0 & 0 & 0 & 0 & 0 & 0 & 0 & w_{AB,C}^{12,12} & \cdots & w_{AB,C}^{12,1S} \\
0 & 0 & 0 & 0 & 0 & 0 & 0 & 0 & 0 & 0 & 0 & 0 & 0 & 0 & \vdots & \ddots & \vdots \\
0 & 0 & 0 & 0 & 0 & 0 & 0 & 0 & 0 & 0 & 0 & 0 & 0 & 0 & w_{AB,C}^{1S,12} & \cdots & w_{AB,C}^{1S,1S}
\end{bmatrix} \tag{4.20}$$

where *L1* denotes L1 carrier phase observable and *C* denotes C/A code observable. Eqn. 4.20 can be simplified as a block matrix:

$$W = \begin{bmatrix}
W_{L1} & 0 & 0 & 0 & 0 & 0 & 0 \\
0 & W_C & 0 & 0 & 0 & 0 & 0 \\
0 & 0 & W_{L1} & 0 & 0 & 0 & 0 \\
0 & 0 & 0 & W_C & 0 & 0 & 0 \\
0 & 0 & 0 & 0 & \ddots & 0 & 0 \\
0 & 0 & 0 & 0 & 0 & W_{L1} & 0 \\
0 & 0 & 0 & 0 & 0 & 0 & W_C
\end{bmatrix} \tag{4.21}$$

The initial position of the code solution becomes the approximate position of the combined C/A code and L1 carrier phase float solution. Moreover, the *a posteriori* variance of DD C/A code solution becomes the *a priori* variance of code measurements in combined code and carrier phase float solution. For more about *a priori* variance and *a posteriori* variance, please see Allan [1993] and Mikhail [1976]. On the other hand, the *a priori* variance of DD carrier phase measurements is 2.5E-5, which is the square of standard error (± 5 mm) of carrier phase measurement. The weight of measurement is:

$$weight = \frac{1}{\sigma_o^2} \tag{4.22}$$

where σ_o^2 is the *a priori* variance of the measurements.

The relative weight between DD code measurement and DD carrier phase measurement is very important as it would affect the accuracy of the estimated unknown point in combined code and carrier phase float solution. Strang and Borre [1997] have given an example for the weights of code and carrier phase measurements. They take the standard error of code measurement as ± 0.3 m and carrier phase measurement as ± 5 mm. On the other hand, Trimble Navigation Limited stated that the standard errors of code and carrier phase for 4000SSi receiver are ± 0.5 m and ± 5 mm respectively. However, the standard error of code measurement in short observation time-span (six epochs' measurements - one minute' measurements with ten second measurement interval) is different. A

versatile method is adopted in this algorithm, the standard error (or *a priori* variance) of code measurement is obtained from the *a posteriori* variance of code solution. The products of the combined C/A code and L1 carrier phase solution are the intermediate position (X, Y and Z) and the DD ambiguities. Experimental result shows that the accuracy of the intermediate position in the six-epochs' combined C/A code and L1 carrier phase solution is about 0.1 m for a 2.2 km baseline, however, its positioning accuracy depends on the satellite geometry, and the effect of multipath and other biases and errors.

The least squares float solution is carried out by:

$$\hat{x} = (A^T W A)^{-1} A^T W l \tag{4.23}$$

Eqn. 4.23 is linearized by iteration until the $\Delta V^T W V$ is less than a very small positive critical value (1E-16 is selected in the project) [Leick, 1995, pp. 114].

Outputs of the combined C/A code and L1 carrier phase float solution are intermediate position, approximate DD ambiguities and variance-covariance matrix of parameters.

4.4.3 Position Determination by LAMBDA

Input parameters for this step are:

i) the approximate position of the unknown,

ii) the approximate DD ambiguities, and

iii) the variance-covariance of DD ambiguities, which are determined by the combined C/A code and L1 carrier phase float solution.

Details of this procedure can be found in section 3.2. Outputs are the best estimated DD ambiguities and position of the unknown point. The final solution (best estimated position) of this step is based on integer ambiguity estimation and fixed solution. It is therefore more precise and accurate than the combined C/A code and L1 carrier phase float solution. The precise and accurate position determined by LAMBDA method can hence reduce the search volume of the following step – CALMS method. The smaller CALMS search volume will have less trial positions and thus reduces AFM processing time.

4.4.4 Position Determination by CALMS

The integrated processing algorithm adopted CALMS method rather than SWAT. It is because that CALMS method is a combination of position and ambiguity domain processing algorithm, which the integer ambiguities are constrained [Han and Rizos, 1997a].

The procedures for this step are the same as that described in section 4.2. The position determined by the LAMBDA method is used to construct a search volume to be processed by CALMS method. The position determined by LAMBDA method becomes the *a priori* position of CALMS method.

As described in the introduction (Chapter 1), the project is constrained to short baseline. The integrated processing algorithm does not need to incorporate any

ionospheric-free solution and tropospheric model or correction. However, it can be easily modified to include ionospheric-free solution (see [Leick, 1995; Mader, 1992] or eqn. 2.24) when processing long baseline, provided that dual-frequency observables are available.

4.4.5 Validation of Positioning Results

Step 5 is the validation of solutions determined by CALMS and LAMBDA using F statistical test. AFR of the CALMS solutions in the integrated processing algorithm is computed based on the recommendation of Han and Mok [1997] and Mok [1998] as:

$$AFR = \frac{\sum_{T=1}^{i}\sum_{L=1}^{j}\sum_{R=1}^{k}\sum_{S=1}^{l} 1-AFV_{2ndMax}}{\sum_{T=1}^{i}\sum_{L=1}^{j}\sum_{R=1}^{k}\sum_{S=1}^{l} 1-AFV_{Max}} \tag{4.24}$$

where AFR is the ratio of the second maximum AFV to the maximum AFV,

L is the number of carrier phases from 1 to j,

R is the number of receivers from 1 to k,

S is the number of satellites from 1 to l,

T is number of measurement epochs from 1 to i,

AFV_{2ndMax} is the second maximum AFV of all measurements at a trial position,

AFV_{Max} is the maximum AFV of all measurements at a trial position, and

1 is the theoretical maximum AFV of each measurement.

with the null hypothesis is

$$H_0 : AFR = 1 \tag{4.25}$$

and the alternative hypothesis is

$$H_a : AFR > 1 \tag{4.26}$$

The solution is accepted when the AFR has passed the F-test at the 95% confidence level, i.e.:

$$AFR > F_{\alpha,m1,m2} \tag{4.27}$$

Validations of LAMBDA ambiguity fixed solution and CALMS ambiguity fixed solution are done by ratio test between the best and the second best solution against F distribution or a critical value. The ratio test is:

$$\frac{\left(V^T PV\right)_{2ndBest}}{\left(V^T PV\right)_{Best}} > F_{\alpha,m1,m2} \tag{4.28}$$

where V denotes the residual vector of the fixed solution,

P denotes the weight matrix of the fixed solution,

$m1$ and $m2$ denotes the degree of freedom of the fixed best and second best solution respectively, and

$F_{\alpha,m1,m2}$ denotes the corresponding F distribution.

In addition to the above validation procedures, another ratio test is performed between the *a posteriori* variance determined by the LAMBDA integer ambiguity fixed solution and the *a posteriori* variance determined by CALMS integer ambiguity fixed solution. This test validates the equality of the variances of two populations on the basis of the ratio between sample variances. Let $\hat{\sigma}_L^2$ with m_1 degree of freedom be the *a posteriori* variance from the LAMBDA integer ambiguity fixed solution, and $\hat{\sigma}_C^2$ while m_2 degree of freedom be the *a posteriori* variance from the CALMS integer ambiguity fixed solution. The F value is determined as:

$$F_{m1,m2} = \frac{\hat{\sigma}_L^2}{\hat{\sigma}_C^2} \tag{4.29}$$

Test the hypothesis that $\hat{\sigma}_L^2 = \hat{\sigma}_C^2$ against the alternative that $\hat{\sigma}_L^2 \neq \hat{\sigma}_C^2$ using the level of significance of 0.05. It is a two-tailed test since the only concern is whether the two *a posteriori* variances are statistically equal. The null hypothesis is accepted if $F_{m1,m2}$ computed is close to one. This F-test let us know the agreement of the

LAMBDA solution with the CALMS solution. If alternative hypothesis cannot be rejected (F_{m_1,m_2} is significantly greater or less than one), the solution of the integrated processing algorithm is considered as unreliable.

CHAPTER 5

EXPERIMENTAL TESTING

5.1 Purpose of Test

Experimental testing aims to verify the improvement of the proposed GPS data processing algorithms on accuracy, reliability and efficiency. It can also be used as a calibration test to examine the performance of the processing algorithms applied to deformation monitoring.

5.2 Testing Sites

5.2.1 Campus of The Hong Kong Polytechnic University

The roof of core H inside the Hong Kong Polytechnic University is selected as a site for test data collection. The collected data are utilized to test the accuracy and reliability of the processing algorithms. Identification of this site is HKPU in the following description.

To assess the effectiveness of CALMS and SWAT, a site in a severe multipath environment was deliberately selected. A set of data was collected in HKPU in order to verify that the test site has severe multipath effect. The data were processed using GPSurvey. Figure 5.1 shows the L1 phase residual of SVN 4 (Figure 5.1(a)) and 24

(Figure 5.1(b)) for two consecutive days. The phase residual patterns of the two satellites in the two days are very similar. The high correlation in the phase residual patterns has obviously shown the presence of multipath at this site. Figure 5.1 is extracted from the processing report of GPSurvey.

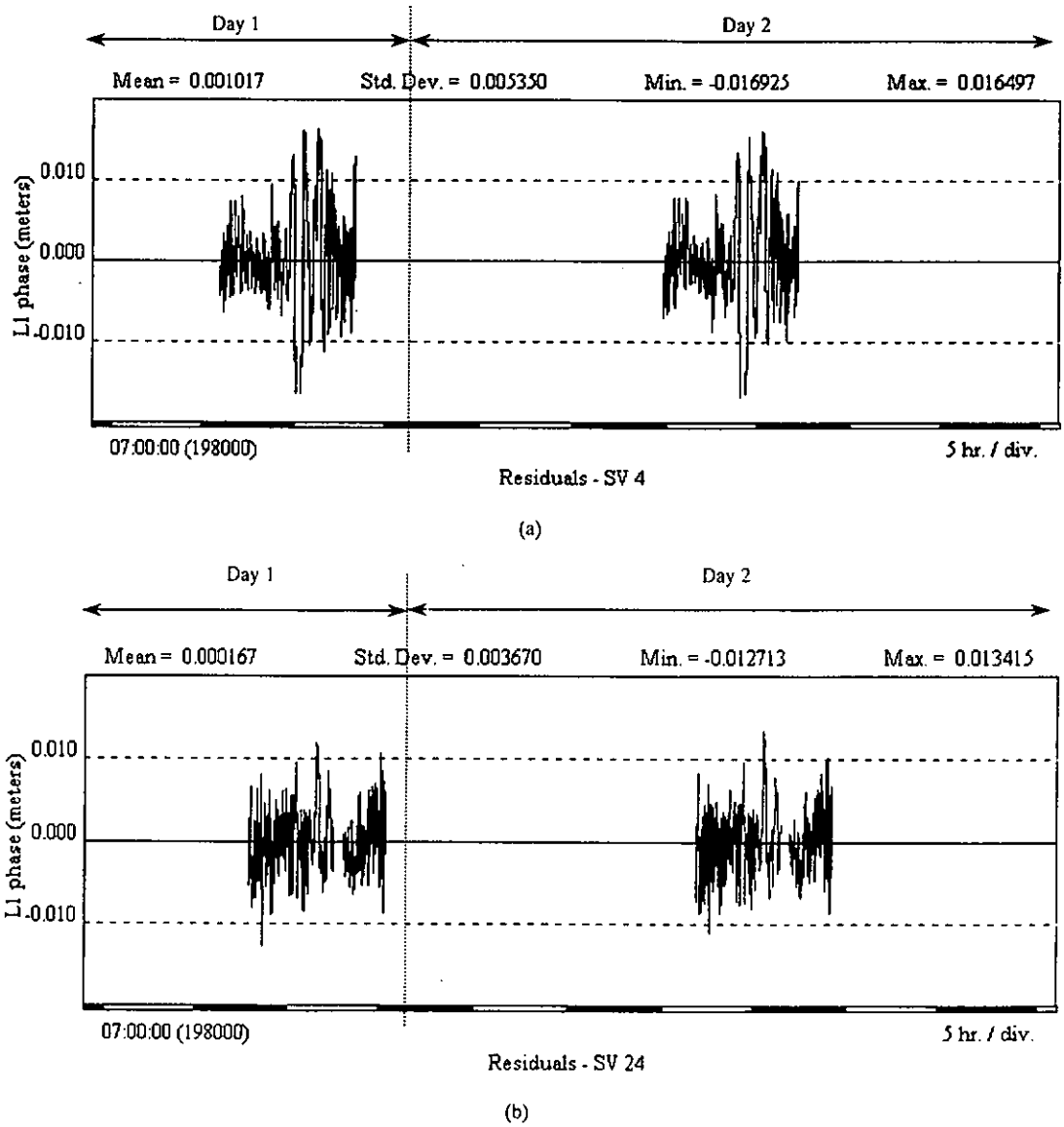

Figure 5.1
Highly correlated phase residual of two consecutive days showing the presence of multipath

5.2.2 Construction Site of the Hong Kong New Airport at Chek Lap Kok

The new airport is built on a newly reclaimed island. The Airport Authority (AA) has therefore established good deformation monitoring network, monitoring stations and settlement markers to perform deformation monitoring in this reclaimed area. Background of deformation monitoring in the new airport can be found in section 1.4. Engineering site in the new airport was selected for collection of testing data.

Figure 5.2
Fieldwork in the new airport

5.2.3 Construction Site of MTRC in Tseung Kwan O

Tseung Kwan O is also a reclaimed area; some locations in this area have recorded about 85 cm settlement recently.

Mass Transit Railway Corporation (MTRC) is building a railway and depot in this area (see Figure 5.3). Deformation monitoring and other construction activities

are massively carried out in this engineering site. A set of test data is collected in this site. Identification of this site is TKO in the following description.

Figure 5.3
Construction site of MTRC in Tseung Kwan O

5.3 Facilities Used for Test

Trimble 4000SSi geodetic receiver was used for test data collection This receiver has 12 channels and is able to track dual frequency (L1 and L2) carrier phases, P code observations on L1 and L2 frequencies, and C/A code observations on L1. It was connected with Trimble compact L1/L2 antenna with groundplane.

GPSurvey, Trimble commercial GPS data processing software, is used to process the collected measurements and determine the solutions. These solutions are employed to verify the solutions of the processing algorithms.

5.4 Design of Experiment

The test data collected in the three sites are processed by the proposed processing algorithms and GPSurvey. Six-epoch solutions of the processing algorithms are compared with GPSurvey's solutions of about an hour observation in order to find out the positioning accuracies of the processing algorithms and reliabilities. Moreover, CALMS and SWAT solutions are compared with their original non-SNR weighted solutions for determination of the improvements on positioning accuracies and reliabilities.

To have a more independent and thorough investigation on the positioning accuracy and reliability of CALMS and SWAT method, a X-Y-Z stage (see Figure 5.4) was used. The X-Y-Z stage can shift in X, Y and Z direction in 0.1 mm precision. This test can be a simulation of deformation monitoring or calibration of the methods. It was done by taking measurements in a position (Position 1) for an hour and then moving to another position (Position 2), which has no movement in X, Y direction and 1.5 cm in Z direction. The computed shifts of CALMS and SWAT were compared with the known shifts, i.e. 0 cm in X,Y and 1.5 cm in Z. This difference can be described as "absolute" difference. Besides, the integrity of CALMS and SWAT were tested with sidereal day-to-day repeatability; the Positions 1 and 2 of core H at HKPU were observed in two consecutive days at the same sidereal time.

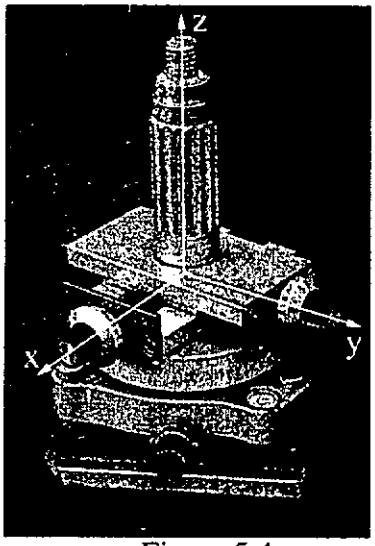

Figure 5.4
X-Y-Z stage

5.5 Description of Test Data Sets

The length of the baseline in core H is about three metres. Data set collected in core H was observed in ten seconds interval for an hour and the mask angle was set to 15°. Trimble 4000SSi was used to collect test data in core H. The GDOP was about two and the number of satellite was six to eight. The six-epoch processing results of CALMS and SWAT were compared with Trimble GPSurvey's result, which was observed for two days.

Another data set was collected in The Hong Kong New Airport at Chek Lap Kok (Figure 5.2); the length of the baseline is about 1.6 km and the receiver setting is the same as in core H. The number of satellites and GDOP were six to eight and two to three, respectively. The six-epoch processing results of CALMS and SWAT were compared with GPSurvey solution of about an hours' observation.

Two baselines in MTRC construction site in Tseung Kwan O were selected for testing the processing algorithms. One baseline length is about 3.3 km and the other one is about 4.5 km. Testing data sets in this site were observed to satellites with 15° mask angle and in ten seconds measurement interval for about an hour. Test data set of the 3.3 km baseline, called TKO33, was observed to 6-7 satellites with GDOP ranging from three to four. Test data set of the 4.5 km baseline is called TKO45. It was observed to 6-7 satellites with GDOP ranging from three to four.

The test data sets include different satellite geometry and environments. They are summarized in Table 5.1. The tests and comparisons performed on the test data sets are summarized in Table 5.2.

Table 5.1
Summary of test data sets

Site/Baseline name	Observation date (dd/mm/yy)	Baseline length (km)	Mask angle (°)	Measurement interval (s)	No. of satellites	GDOP
HKPU	16,17/06/98	0.003	15	10	6-8	2-3
new airport	20/06/98	1.6	15	10	6-8	2-3
TKO33	21/07/99	3.3	15	10	6-7	3-4
TKO45	23/07/99	4.5	15	10	6-7	3-4

Table 5.2
Tests and comparisons performed on the test data sets

Test on or comparsion with / Baseline name	HKPU	new airport	TKO33	TKO45
GPSurvey's solution	✓	✓	✓	✓
known shifts on X-Y-Z stage	✓	✓		
sidreal day-to-day repeatability's solution	✓			

CHAPTER 6

RESULTS AND ANALYSES

6.1 Combined Ambiguity Function Method and Least Squares Method with Signal-to-Noise Ratio Weighting (CALMS)

Figure 6.1 shows the differences (in plane coordinate) of the known 3m baseline in HKPU at Position 1; differences at Position 2 (next sidereal day) are shown in Figure 6.2. In the following presentation, LS means conventional least squares, CALMS is the combined AFM with SNR weighted least squares method, and GPSurvey is the GPS processing software of Trimble. The results are summarized in Table 6.1 and 6.2.

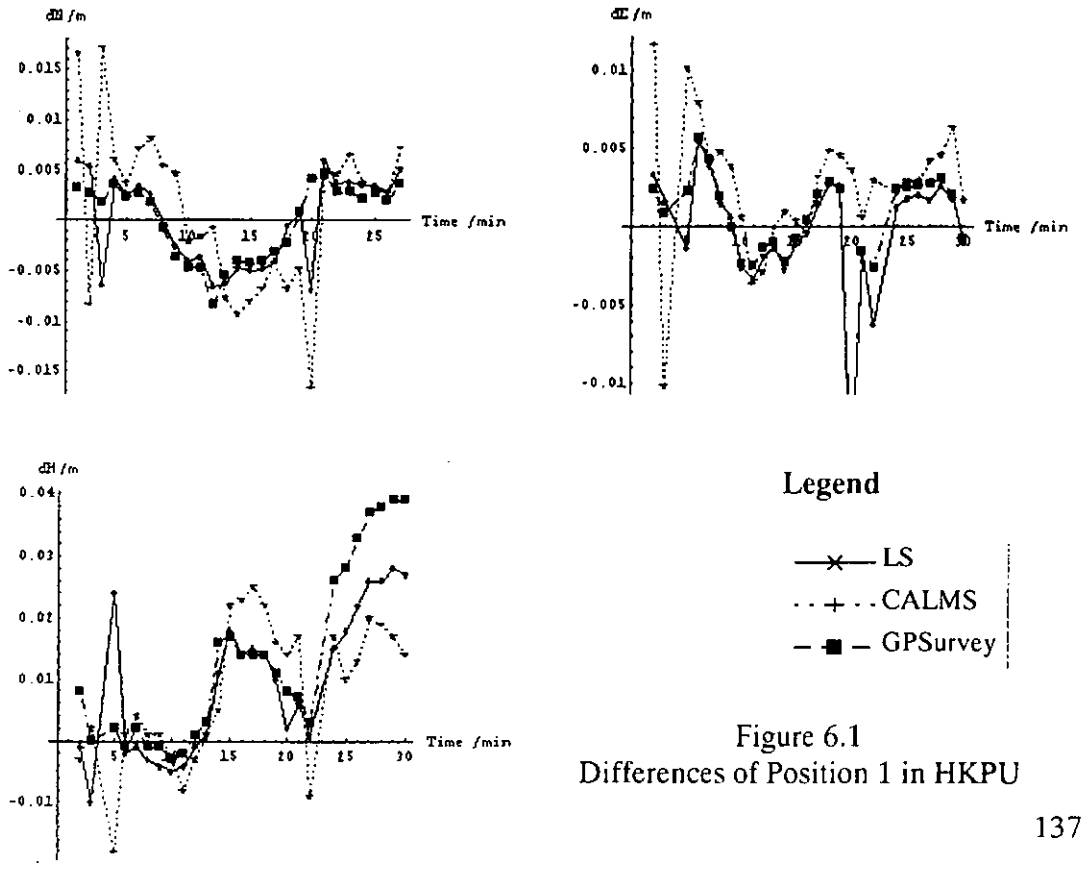

Figure 6.1
Differences of Position 1 in HKPU

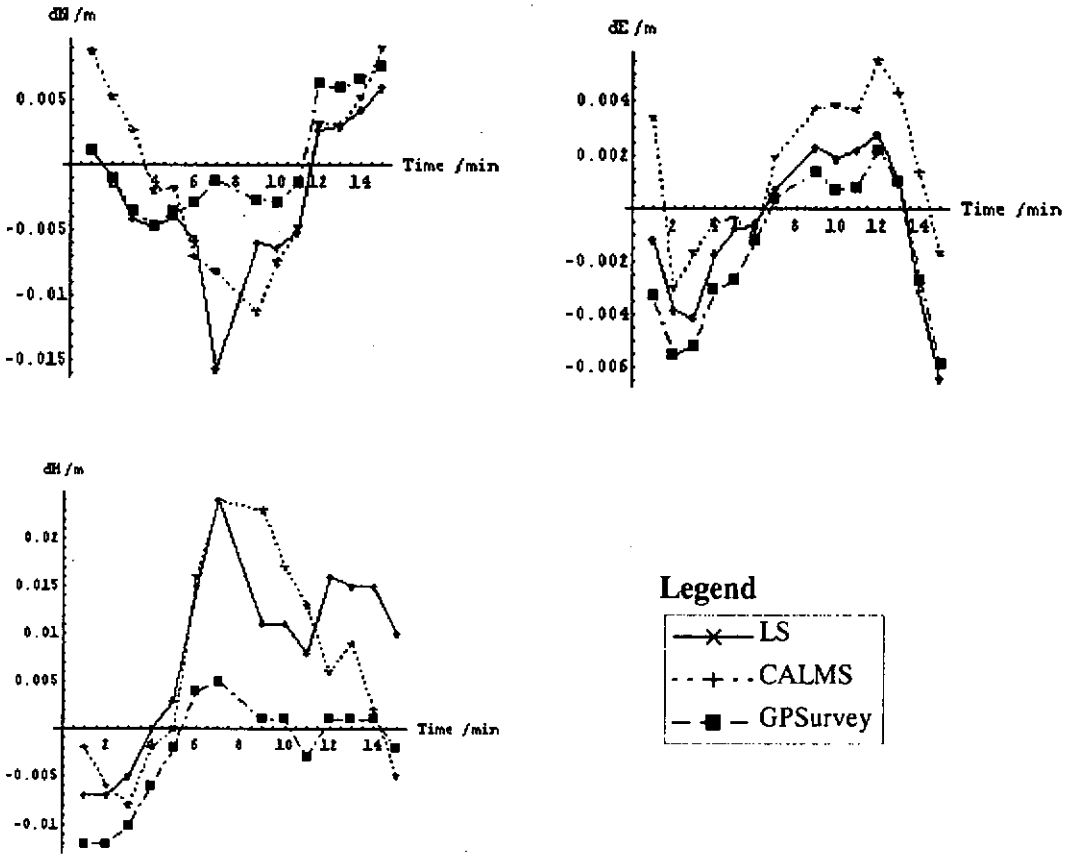

Figure 6.2
Differences of Position 2 in HKPU

Table 6.1
Summary of differences of processing algorithms at Position 1 in HKPU

Mean	dN (m)	dE (m)	dH (m)
LS	-0.00092	-0.000186	0.009
CALMS	0.00092	0.00263	0.008
GPSurvey (1 min.)	-0.00031	0.00067	0.006
RMS			
LS	0.00447	0.00397	0.01175
CALMS	0.00793	0.00425	0.01147
GPSurvey (1 min.)	0.00387	0.00238	0.00806

Table 6.2
Summary of differences of processing algorithms at Position 2 in HKPU

Mean	dN (m)	dE (m)	dH (m)
LS	-0.00262	-0.00079	0.008
CALMS	-0.00043	0.00139	0.006
GPSurvey (1 min.)	0.00023	-0.00166	0.0126
RMS			
LS	0.00569	0.00281	0.00959
CALMS	0.00662	0.00276	0.01086
GPSurvey (1 min.)	0.00441	0.00275	0.00561

Figure 6.3 and 6.4 show the differences in plane coordinate (compared with 49 minutes solution of GPSurvey) of the about 1.6 km baseline in the new airport at Position 1 and 2 respectively. The results are summarized in Table 6.3 and 6.4.

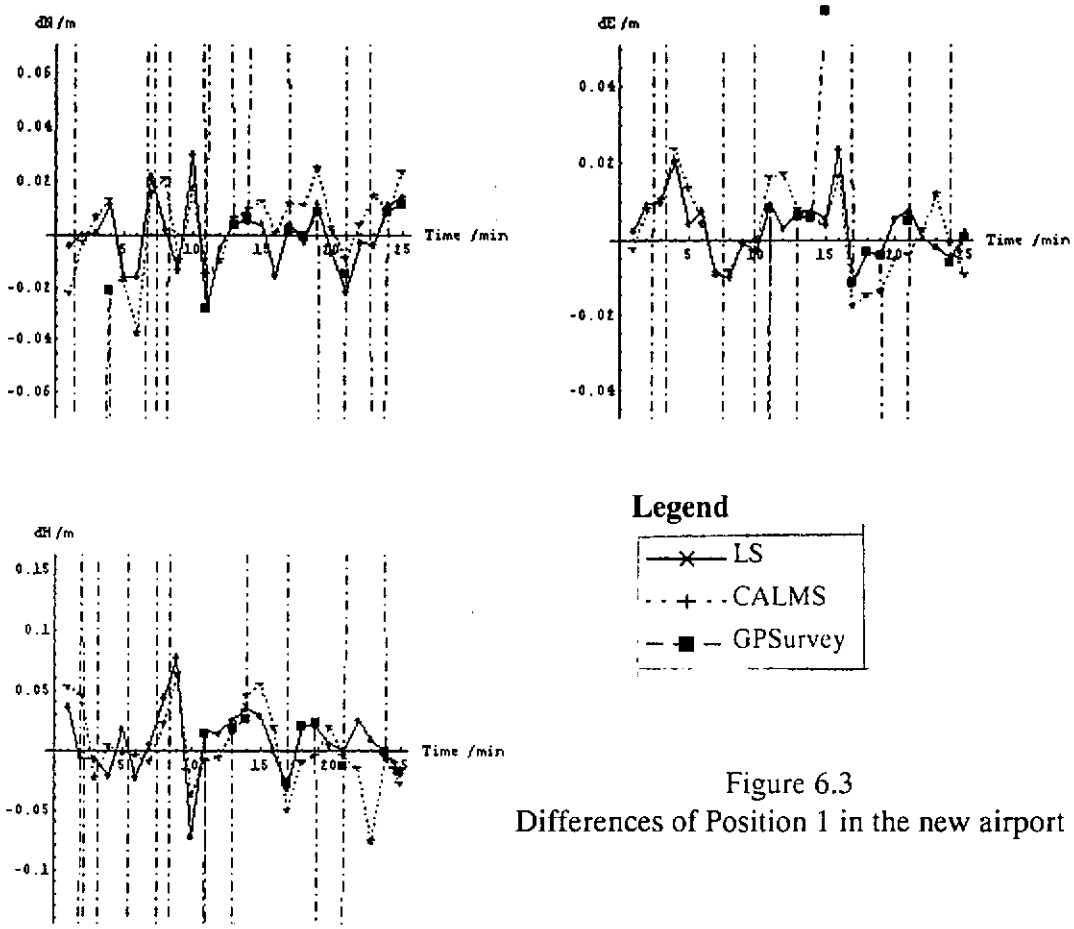

Figure 6.3
Differences of Position 1 in the new airport

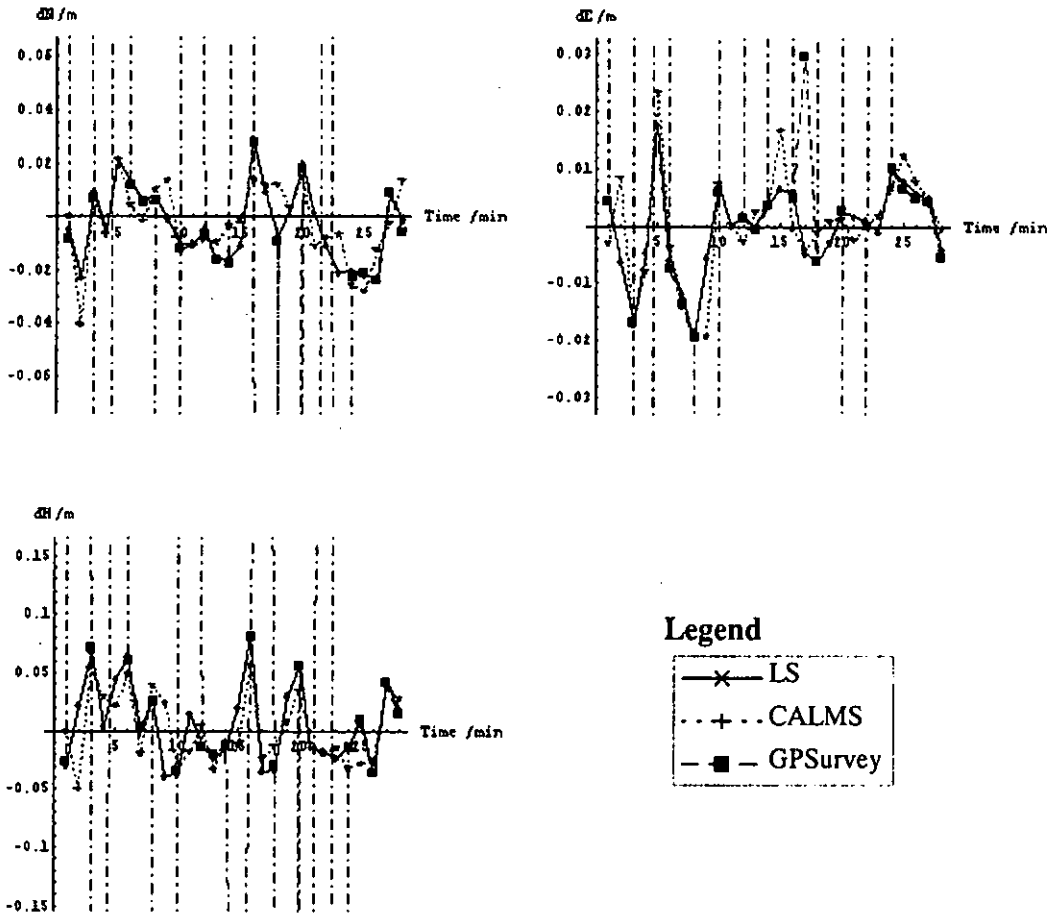

Figure 6.4
Differences of Position 2 in the new airport

Table 6.3
Summary of differences of processing algorithms at Position 1 in the new airport

Mean	dN (m)	dE (m)	dH (m)
LS	-0.00071	0.00309	0.008
CALMS	0.00314	0.00226	0.002
GPSurvey (1 min.)	0.00562	-0.2078	-0.0708
RMS			
LS	0.01351	0.00848	0.0291
CALMS	0.01540	0.01108	0.0335
GPSurvey (1 min.)	0.92386	1.34206	2.6464

Table 6.4
Summary of differences of processing algorithms at Position 2 in the new airport

Mean	dN (m)	dE (m)	dH (m)
LS	-0.00283	-0.00031	0.006
CALMS	-0.00218	0.00006	0.002
GPSurvey (1 min.)	-0.10294	0.07844	-0.0085
RMS			
LS	0.01423	0.00793	0.0355
CALMS	0.01434	0.00981	0.0303
GPSurvey (1 min.)	0.99722	1.40386	2.004

Table 6.5 and 6.6 show the mean of determined shift in HKPU and the new airport. It can check the processing result more independently because it considers the relative positions only.

Table 6.5
Determined shifts of processing algorithms in HKPU

Mean	shift N (m)	shift E (m)	shift H (m)
LS	-0.002522	-0.000604	0.014
CALMS	-0.001353	-0.001245	0.013
GPSurvey (1 min.)	0.00054	-0.00233	0.0065
Known	0.000	0.000	0.015

Table 6.6
Determined shifts of processing algorithms in the new airport

Mean	shift N (m)	shift E (m)	shift H (m)
LS	0.017933	-0.002911	0.013
CALMS	0.014734	-0.001714	0.015
GPSurvey (1 min.)	-0.10856	0.28624	0.077
GPSurvey (49 min.)	0.020055	0.000487	0.040
Known	0.000	0.000	0.015

Table 6.7 and 6.8 show the mean "absolute" differences in HKPU and the new airport.

Table 6.7
"Absolute" differences of processing algorithms in HKPU

Mean "absolute" difference	N (m)	E (m)	H (m)
LS	-0.002522	-0.000604	-0.001
CALMS	-0.001353	-0.001245	-0.002
GPSurvey (1 min.)	0.00054	-0.00233	-0.0085

Table 6.8
"Absolute" differences of processing algorithms in the new airport

Mean "absolute" difference	N (m)	E (m)	H (m)
LS	0.017933	-0.002911	-0.002
CALMS	0.014734	-0.001714	0.000
GPSurvey (1 min.)	-0.10856	0.28624	0.062
All observation			
GPSurvey (49 min.)	0.020055	0.000487	0.025

Table 6.9 and 6.10 show the differences in northing, easting, and height of the baseline TKO33 and TKO45, respectively.

Table 6.9
Summary of differences of the processing algorithms in TKO33

Mean	dN (m)	dE (m)	dH (m)
LS	-0.00078	-0.00285	0.004
CALMS	-0.00032	-0.00225	0.003
GPSurvey (1 min.)	0.00122	0.00476	-0.017
RMS			
LS	0.01960	0.01711	0.02928
CALMS	0.01515	0.01402	0.02243
GPSurvey (1 min.)	0.00598	0.02612	0.13726

Table 6.10
Summary of differences of the processing algorithms in TKO45

Mean	dN (m)	dE (m)	dH (m)
LS	-0.00122	0.00385	0.006
CALMS	-0.00582	0.00291	0.004
GPSurvey (1 min.)	0.00180	0.00807	-0.035
RMS			
LS	0.02805	0.02103	0.05360
CALMS	0.01644	0.02005	0.02698
GPSurvey (1 min.)	0.00643	0.04916	0.17554

The "absolute" differences in HKPU determined by LS and CALMS agreed in about 1 mm level (shown in Table 6.7). It is because that the environment of the two receivers for the 3 m baseline is about the same, as is the multipath. Most multipath may be eliminated by double difference for such short baseline. It cannot show the improvement of CALMS clearly. However, it shows the integrity of the technique as the "absolute" differences are 1mm in horizontal and 2 mm in vertical (shown in Table 6.7) for sidereal day-to-day repeatability result. The small differences may be due to slightly different weather and the sidereal day-to-day repeatability is not exactly 4 minutes in advance for the next day.

In the new airport's "absolute" result (Table 6.8), CALMS shows an 18% improvement in northing, a 41% improvement in easting, and a 15% improvement in height when comparing to conventional least squares.

From the result of TKO33 (Table 6.9), CALMS shows a 59% improvement in northing, a 21% improvement in easting, and a 30% improvement in height when comparing to conventional least squares.

According to the result of TKO45 (Table 6.10), CALMS shows a 52% improvement in northing, a 24% improvement in easting, and a 25% improvement in height when comparing to conventional least squares.

From the above results, the signal-to-noise ratio weighted least squares processing algorithm (CALMS) does improve the positioning accuracy even using 1 minute of data (6 epochs) in strong multipath environment. CALMS is a versatile algorithm which is not dependent on surveying environment, receiver type and number of receivers. Moreover, it is suitable for short observation time-span since the stochastic model of CALMS modelled the multipath error so that long observation time-span for averaging or smoothing multipath error is not required. The above result shows that the solution of CALMS is better than that of GPSurvey, which is processed with 30 to 49 minutes' observation.

The advantage of CALMS is that it would not be limited to the mentioned multipath properties such as non-Gaussian and measurement environment dependent.

6.2 Signal-to-Noise Ratio Weighted Ambiguity Function Technique (SWAT)

Figure 6.5 shows the differences in northing, easting and height of the known 3m baseline in HKPU at Position 1; differences at Position 2 (next sidereal day) are shown in Figure 6.6. In the following presentation, AFM means Ambiguity Function Method, SWAT is Signal-to-noise ratio Weighted Ambiguity Function Technique, and GPSurvey is GPS processing software of Trimble. The results are summarized in Table 6.11 and 6.12.

Table 6.11
Summary of differences of processing algorithms at Position 1 in HKPU

Mean	dN (m)	dE (m)	dH (m)
AFM	0.00175	-0.002	0.01
SWAT	0.00126	-0.00185	0.01
GPSurvey (1 min.)	-0.00031	0.00067	0.006
RMS			
AFM	0.0038	0.00259	0.00947
SWAT	0.00362	0.00249	0.00781
GPSurvey (1 min.)	0.00387	0.00238	0.00806

Table 6.12
Summary of differences of processing algorithms at Position 2 in HKPU

Mean	dN(m)	dE(m)	dH(m)
AFM	0.00019	-0.00225	0.0094
SWAT	0.00025	-0.00219	0.0095
GPSurvey (1 min.)	0.00023	-0.00166	0.0126
RMS			
AFM	0.00488	0.00117	0.00832
SWAT	0.00503	0.00115	0.00836
GPSurvey (1 min.)	0.00441	0.00275	0.00561

Figure 6.7 and 6.8 show the differences in northing, easting and height (compared with 49 minutes solution of GPSurvey) of the about 1.6 km baseline in the new airport at Position 1 and 2 respectively. Table 6.13 and 6.14 summarized the results.

Table 6.13
Summary of differences of processing algorithms at Position 1 in the new airport

Mean	dN (m)	dE (m)	dH (m)
AFM	0.01249	-0.00498	-0.0128
SWAT	0.01238	-0.00484	-0.0123
GPSurvey (1 min.)	0.00562	-0.2078	-0.0708
RMS			
AFM	0.02076	0.01021	0.0675
SWAT	0.01999	0.01011	0.0663
GPSurvey (1 min.)	0.92386	1.34206	2.6464

Table 6.14
Summary of differences of processing algorithms at Position 2 in the new airport

Mean	dN(m)	dE(m)	dH(m)
AFM	0.01614	0.00073	0.0184
SWAT	0.01415	-0.00035	0.0177
GPSurvey (1 min.)	-0.10294	0.07844	-0.0085
RMS			
AFM	0.01255	0.00935	0.0608
SWAT	0.01137	0.00747	0.0516
GPSurvey (1 min.)	0.99722	1.40386	2.004

Table 6.15 and 6.16 show the mean of determined shift in HKPU and the new airport. It can check the processing result more independently because it considers the relative positions only.

Table 6.15
Determined shifts of processing algorithms in HKPU

Mean	shift N (m)	shift E (m)	shift H (m)
AFM	-0.00155	-0.00025	0.0149
SWAT	-0.00101	-0.00034	0.0142
GPSurvey (1 min.)	0.00054	-0.00233	0.0065
Known	0.000	0.000	0.015

Table 6.16
Determined shifts of processing algorithms in the new airport

Mean	shift N (m)	shift E (m)	shift H (m)
AFM	0.00365	0.00571	0.046
SWAT	0.00177	-0.00449	0.044
GPSurvey (1min)	-0.10856	0.28624	0.077
GPSurvey (49min)	0.020055	0.000487	0.040
Known	0.000	0.000	0.015

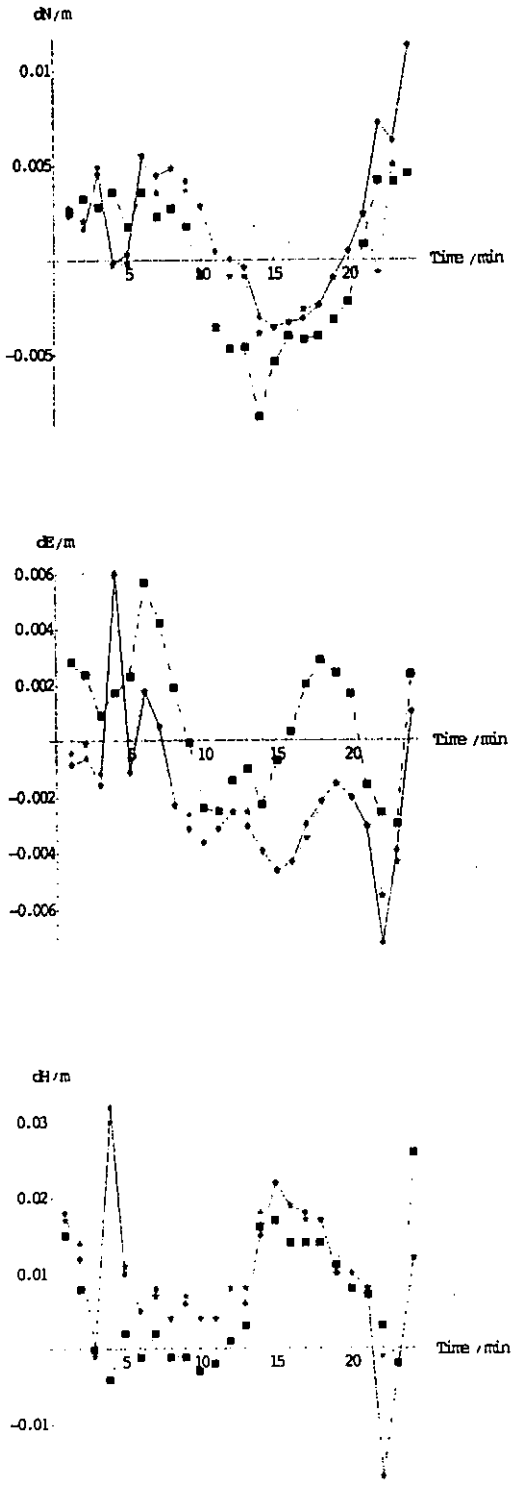

Figure 6.5
Differences of Position 1 in HKPU

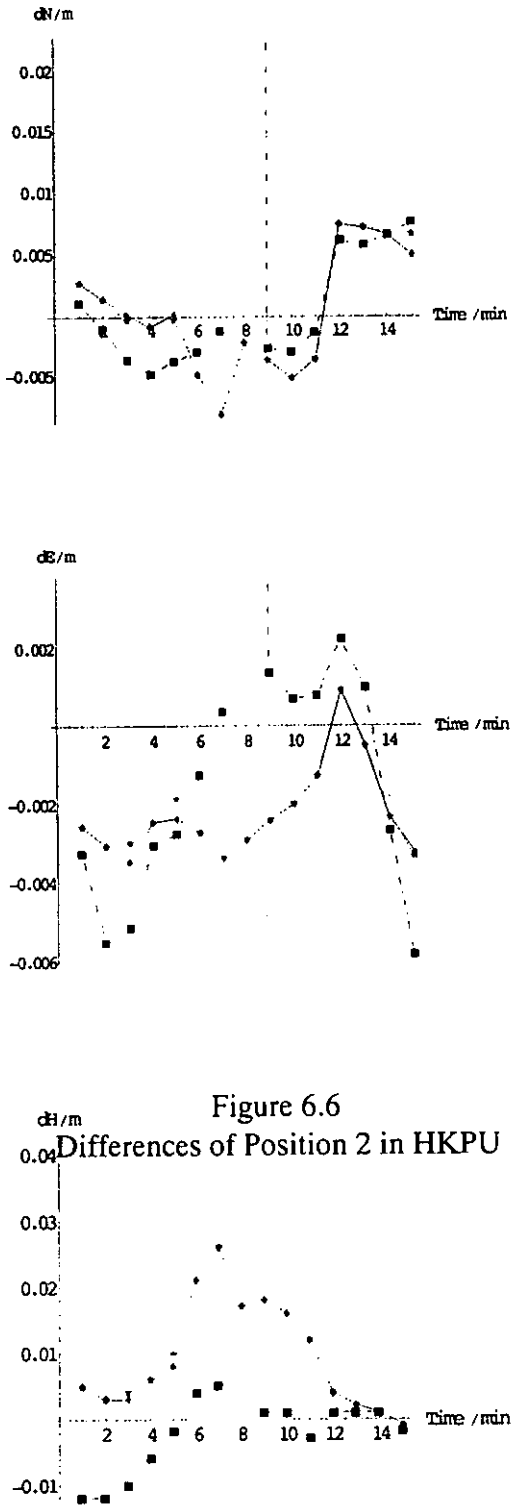

Figure 6.6
Differences of Position 2 in HKPU

Figure 6.6
Differences of Position 2 in HKPU

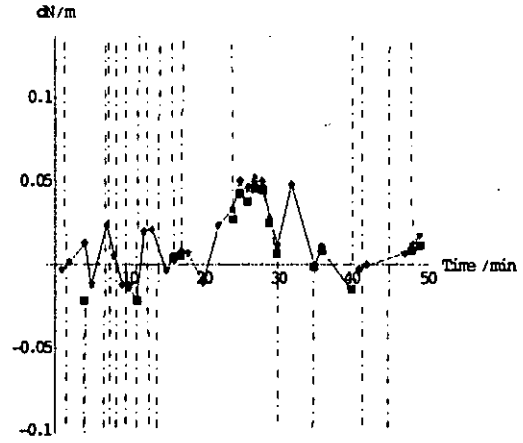

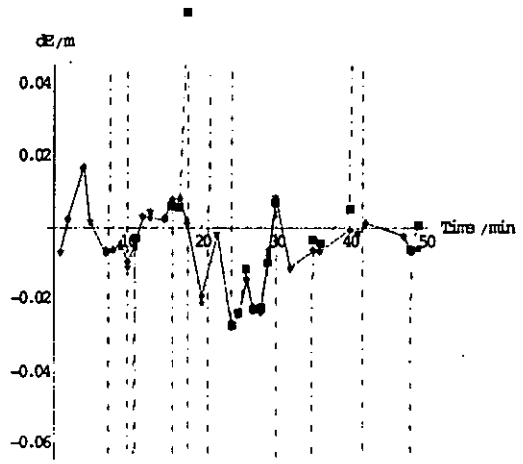

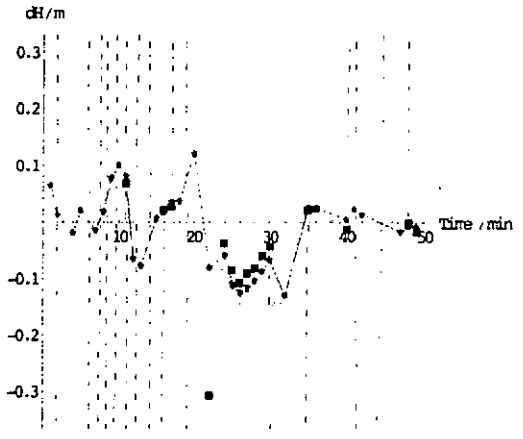

Figure 6.7
Differences of Position 1 in the new airport

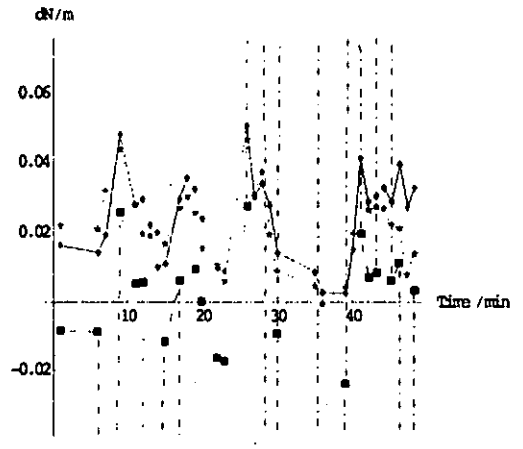

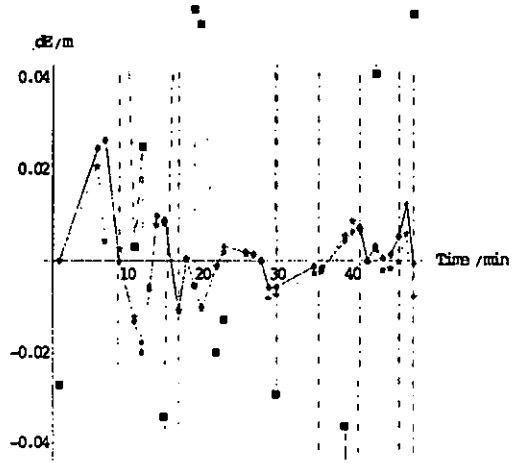

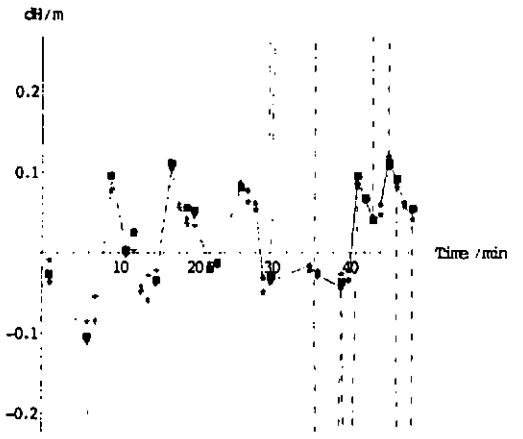

Figure 6.8
Differences of Position 2 in the new airport

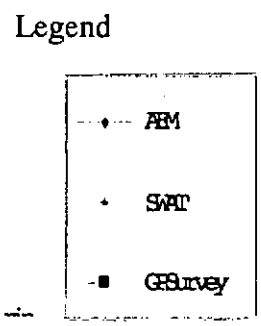

Table 6.17 and 6.18 show the mean "absolute" differences in HKPU and the new airport.

Table 6.17
"Absolute" differences of processing algorithms in HKPU

Mean "absolute" difference	N (m)	E (m)	H (m)
AFM	-0.00155	-0.00025	-0.0001
SWAT	-0.00101	-0.00034	-0.0008
GPSurvey (1 min.)	0.00054	-0.00233	-0.0085

Table 6.18
"Absolute" differences of processing algorithms in the new airport

Mean "absolute" difference	N (m)	E (m)	H (m)
AFM	0.00365	0.00571	0.031
SWAT	0.00177	-0.00449	0.029
GPSurvey (1min)	-0.10856	0.28624	0.062
All observation			
GPSurvey (49min)	0.020055	0.000487	0.025

Table 6.19 and 6.20 show the differences in northing, easting, and height of the baseline TKO33 and TKO45, respectively.

Table 6.19
Summary of differences of the processing algorithms in TKO33

Mean	dN (m)	dE (m)	dH (m)
AFM	-0.00076	-0.00319	0.004
SWAT	-0.00033	-0.00272	0.003
GPSurvey (1 min.)	0.00122	0.00476	-0.017
RMS			
AFM	0.01978	0.01782	0.02989
SWAT	0.01460	0.01420	0.02407
GPSurvey (1 min.)	0.00598	0.02612	0.13726

Table 6.20
Summary of differences of the processing algorithms in TKO45

Mean	dN (m)	dE (m)	dH (m)
AFM	-0.00128	0.00446	0.006
SWAT	-0.00051	0.00311	0.006
GPSurvey (1 min.)	0.00166	0.00755	-0.022
RMS			
AFM	0.02089	0.01850	0.05579
SWAT	0.01696	0.02628	0.03244
GPSurvey (1 min.)	0.00699	0.03562	0.18247

The "absolute" differences in HKPU determined by AFM and SWAT agreed in about 1-mm level (shown in Table 6.17). It is because the environment of the two receivers for the 3 m baseline is about the same, as is the multipath. Most multipath may be eliminated by double difference for such short baseline. It cannot show the improvement of SWAT clearly. However, it shows the integrity of the technique as the "absolute" differences are 1 mm in horizontal and vertical (shown in Table 6.17) for sidereal day-to-day repeatability result. The small differences may be due to

slightly different weather and the sidereal day-to-day repeatability is not exactly 4 minutes in advance for the next day.

In the new airport result (Table 6.18), SWAT shows 52% accuracy improvement in northing, 21% in easting and 13% in height when comparing to conventional ambiguity function method (AFM) and known displacements on the X, Y, Z stage. Besides, the reliability of SWAT is increased by about 15%, which shows in RMS errors of Table 6.13 and 6.14.

From the result of TKO33 (Table 6.19), SWAT shows a 55% improvement in northing, a 15% improvement in easting, and a 14% improvement in height when comparing to AFM.

According to the result of TKO45 (Table 6.20), SWAT is determined to have a 60% improvement in northing, a 30% improvement in easting, and a 9% improvement in height when comparing to AFM.

From the above results, the signal-to-noise ratio weighted ambiguity function technique processing algorithm (SWAT) does improve the positioning accuracy even using 1 minute of data (6 epochs) in strong multipath environment. SWAT is a versatile algorithm that is not dependent on surveying environment, receiver type and number of receivers. Moreover, it is suitable for short observation time-span since the stochastic model of SWAT modelled the multipath error so that long observation time-span for averaging or smoothing multipath error is not required. The above result section shows that the solution of SWAT is better than that of GPSurvey, which processed with 30 to 49 minutes' observation.

6.3 The Integrated GPS Data Processing Algorithm

It was tested with the 1.6 km baseline in the new airport. The differences from the GPSurvey's solution (49 minutes observation time) in WGS-84 Cartesian coordinate system are shown in Figure 6.9. Figure 6.9 shows how the processing steps, which are code solution, combined code and carrier phase float solution, LAMBDA and CALMS, converge the solution. Finally, the solution (in plane coordinate system) is the same as shown in Figure 6.4 because the same test data set was used and the final step of the integrated processing algorithm is the same – CALMS.

In Figure 6.9, the solutions of LAMBDA are not always better than the combined code and carrier phase float solutions. Since LAMBDA method is an ambiguity domain processing algorithm (it is similar to the other ambiguity domain processing algorithms such as FARA and the classic approach described in section 2.5), a few measurements may result in incorrect ambiguity resolution. It can be seen in Table 3.10 and 3.11, Table 6.8, and Table 6.18, the commercial package GPSurvey also yields low positioning accuracy when processing six epochs' measurements. Tiberius and de Jonge [1995] have shown that correct ambiguity resolution (100% successful rate) by LAMBDA method for a 2.2 km baseline can be achieved with single-epoch dual frequency phase and code data from seven satellites. However, Tiberius et al. [1997] reported, "In all cases the standard deviations are far larger than the one cycle level". They tested the reliability of LAMBDA method for ambiguity resolution (AR) using single-epoch dual frequency and single frequency phase and/or code data from four to seven satellites, and found that all the AR results have greater than one

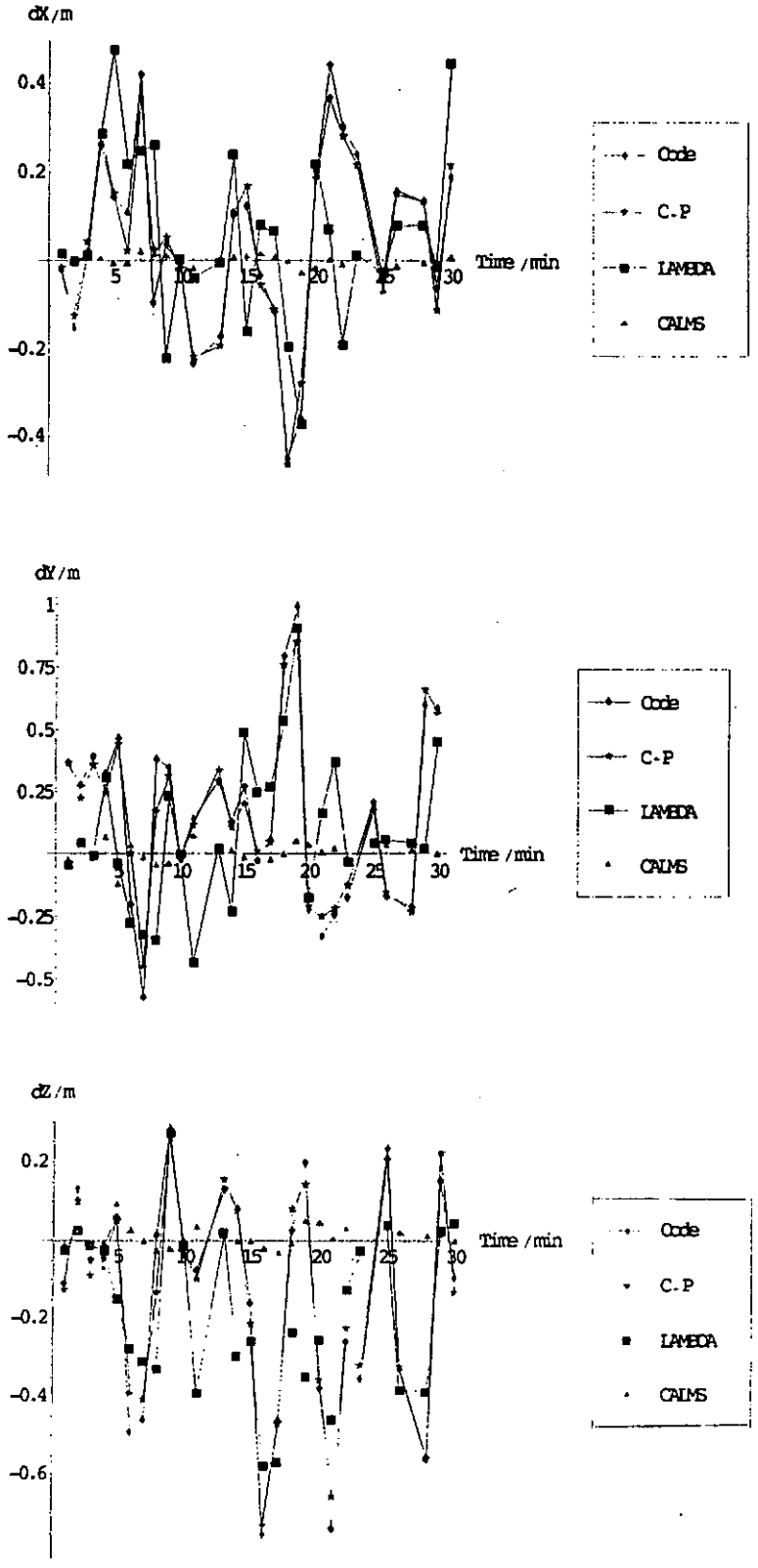

Figure 6.9
Differences and convergence of coordinate by the processing steps of the integrated GPS data processing algorithm

cycle standard deviation. They also tested a discrimination test, which is similar to eqn. 4.24 but they used a constant critical value 1.44 (lower than F-value for six-epoch solution of this project), and found that only 38% of cases resolved integer ambiguity correctly and passed the discrimination test even when using more than 31 epochs' data. Moreover, they discovered that 55% of the cases were accepted by the discrimination test, although the corresponding integer ambiguity solution disagreed with the "true value". In my test, the successful rate of LAMBDA is about 40% when using six-epoch single frequency code and phase data from six satellites. Goodness of LAMBDA solution depends on the correctness AR. Therefore, the final validation test of the integrated processing algorithm (see eqn. 4.29) seems not sound; the successful rate of the final validation test is about 33%. Since the above discussion showed that LAMBDA method cannot hundred percent resolve the integer ambiguity correctly in short observation time-span measurements, a position domain AFM (of CALMS) is required to overcome the correctness AR problem. The advantages of AFM have been discussed in section 2.6 and 3.1.

In the test, the LAMBDA solutions can still provide a correct AFM search volume (1 m^3 or doubled to 8 m^3) for CALMS. In fact, LAMBDA solution will not be apart from the correct solution by two metres (the extended 8 m^3 AFM search volume). Therefore, the final solution of CALMS is still reliable and accurate. It is due to the advantage of the combined AFM and LSM solution of CALMS that also constrained the ambiguity to integer. On the other hand, the processing time of the various processing steps in the integrated GPS data processing algorithm can be found in Appendix I.

CHAPTER 7

CONCLUSIONS

7.1 Summary of the Thesis

This thesis described the types of deformation and the importance of deformation monitoring in Chapter 1. Geo-technical and land surveying techniques of deformation monitoring were reviewed. Moreover, the state of the art of using GPS for deformation monitoring in Hong Kong was presented. Having discussion on the biases and errors of GPS and the present GPS data processing algorithms in Chapter 2 and 3, three improved processing algorithms were proposed in Chapter 4. They are the CALMS, SWAT, and an integrated algorithm. The proposed algorithms were tested with real data collected in the campus of the Hong Kong Polytechnic University, the construction site of the new Hong Kong International Airport, and Tseung Kwan O construction site of the Mass Transit Railway Corporation of Hong Kong. Details on the test data sets were described in Chapter 5. The test results were shown and analysed in Chapter 6. The improvement of the GPS data processing algorithms using six-epoch observation for the short baselines was presented.

7.2 Discussion and Conclusion

The proposed CALMS and SWAT are the GPS data processing algorithms applying Ambiguity Function Method (AFM) for static deformation monitoring.

They use the signal-to-noise ratio to improve the GPS positioning accuracy. CALMS uses SNR weighted least squares adjustment and SWAT uses SNR weighted ambiguity function technique. Test of the processing algorithms in Chapter 6 shows the effective improvement of positioning accuracy. It is demonstrated more precisely, accurately, and independently with the real data collected from simulated deformation monitoring (known shifts of X-Y-Z stage) in the new airport construction site. In fact, CALMS is more accurate and reliable than SWAT because CALMS has constrained the ambiguities to integer, which is contributed by the least squares adjustment (fixed solution) of CALMS. The fact is shown in the results of section 6.1 (Table 6.8) and 6.2 (Table 6.18).

The advantage of CALMS and SWAT is that they are not limited to the multipath properties described in section 2.1.5 such as non-Gaussian and measurement environment dependent. However, CALMS and SWAT require a good *a priori* position, it makes CALMS and SWAT not self-contained and automatic.

The integrated GPS data processing algorithm uses the information given in observation file to determine solution. It is therefore self-contained and automatic. The processing steps of the integrated processing algorithm converge the approximate solution to the best estimated solution step-by-step. The various processing steps are to optimize the processing time. The processing time for a 6-epoch observation is less than 90 seconds; the processing time depends on the number of measurements (satellites). Examples of processing time are shown in Appendix I. CALMS takes most of the processing time since it has to search all the

trial positions in a given search volume (1 m^3 or double to 8 m^3 in case of no solution found in 1 m^3) by trial and error process.

The quality assurance procedure is done by variance ratio test of the different processing steps (the LAMBDA fixed solution and CALMS fixed solution) against F-distribution. Although the experimental result in section 6.3 showed that this final validation test is biased to the unreliable LAMBDA solution, it can still provide us information about the quality (agreement) of solutions. Therefore, the final validation test will not reject the failed solutions, the final solution is given by the more reliable CALMS solution, which does not require ambiguity resolution. Reliability of the solution can also be found in the AFR and variance ratio between the best and second best solution of LSM (in CALMS) and LAMBDA method if the second best solution is available. LAMBDA method has only the best solution sometimes since the transformed spectrum has already been flattened by short-baseline constraint and the combined code and carrier phase solution [Teunissen, 1998]. An example of the variance ratio test can be found in Appendix I. In the example, the a posteriori variance of LAMBDA solution is 1.63002056184705 and that of CALMS solution is 1.63002053317381. The variance ratio is obviously very close to one, which means the solutions by LAMBDA and CALMS come from the same population in statistic point of view.

The integrated processing algorithm can be used to process single frequency data and single-epoch measurement. Because of short-baseline constraint, the processing algorithm does not need dual frequency data for ionospheric-free solution. The observables for the integrated processing algorithm are L1 phase and C/A code; it

does not need dual frequency data for any linear combination of carrier phases. However, the available dual frequency data can improve the positioning accuracy and reliability indeed.

The float solution, the second processing step of the integrated processing algorithm, has used the combined code (C/A) and carrier phase (L1) data. Moreover, all other least squares adjustments (in LAMBDA and CALMS) have constrained the ambiguities to integer and processed them as known parameters (fixed solution), the integrated processing algorithm therefore has the capability for single-epoch solution.

In conclusion, the integrated GPS data processing algorithm is:

- self-contained
- automatic
- self-controlled
- reliable
- fast and precise
- short observation time-span required (6-epoch observation in 10 or 15 seconds measurement interval)
- integer ambiguity constrained
- short baseline constrained
- change in satellite geometry constrained (very little or no for 6-epoch observation).

These factors are described as essential for GPS data processing algorithm according to Frei and Beutler [1989] and Han and Rizos [1997a].

7.3 Limitation of this Research

The proposed GPS data processing algorithms were investigated for short baseline (<10 km) only. They have been tested with less than 5 km baselines. However, baseline length should not affect the effectiveness of multipath mitigation of the proposed algorithms since multipath effect is environment dependent and independent to length of baseline; the problems of long baseline on GPS data processing are ionospheric effect, tropospheric effect, and orbital errors.

CALMS and SWAT methods require a good *a priori* position, which is always available in static deformation monitoring.

The proposed processing algorithms use signal-to-noise ratio to model multipath effect, however, signal-to-noise ratio is not available in RINEX file. RINEX 2.0 format ought to provide signal strength which ranges from 0 to 9, but most receiver manufacturers' utility programs that convert their code to RINEX do not provide signal strength. If signal strength is available in RINEX file, it is still not suitable or effective to model multipath effect. It is because the short range of signal strength (0-9) is not fine enough to model mulitpathing. Most receivers have SNR ranging from 0 to 30-50 displayed in receiver panel or output to NMEA-0183 GSV output format (adopted in this research). Therefore, the signal strength of RINEX format should be modified for better representation of the real signal-to-noise ratio.

7.4 Recommendation for Future Research

This research demonstrates the postprocessing of static data sets. However, the proposed processing algorithms can be applied to real-time kinematic (RTK) measurements. The single-epoch solutions with the proposed processing algorithms are worth investigation.

The proposed algorithms can be investigated for long-baseline application since the GPS biases and errors in long baselines, described in Chapter 2, can affect the effectiveness of ambiguity resolution in the integrated algorithm and AFM searching in the CALMS and SWAT method.

The third carrier phase observable will be available to civil user in the coming future. Advantages and disadvantages of the additional observable on ambiguity resolution, AFM searching, positioning accuracy and ionospheric correction should be investigated. Development of GPS data processing algorithm using the three carrier phase observables is necessary.

APPENDIX I

PROCESSING REPORTS

Process Time : 5:18:47 PM 3/29/99(Local Time)
Reference Station Observation File: k:\Data-BackUp\CALMS-AAresult\Aa-P2\62051711.98x
Unkouwn Station Observation File : k:\Data-BackUp\CALMS-AAresult\Aa-P2\4134171101.98x

****
Base Station WGS84 Cartensian Coordinates
****

X : -2395455.378
Y : 5395829.342
Z : 2405930.346

****
A Priori Position of Unknown Station in WGS84 Cartensian Coordinates
****

X : -2395802.436
Y : 5395061.725
Z : 2407295.140

****
Processing Information
****

Reference satellite : 10
Number of satellites : 6
Number of Epoch(s) : 6
Measurement Interval (seconds) : 10
Occupation Time : 1 minute(s) 0 seconds

****
*** Initial Unknown Position ***
*** By Code Solution ***
****

X : -2395793.8265
Y : 5395067.4878
Z : 2407296.0786

Number of Iteration : 3

A Posteriori Variance of Code Soultion : 0.1580478

****
*** Intermediate Unknown Position ***
*** Combined Code and Carrier Phase 'Float' Solution ***
****

X : -2395793.8223
Y : 5395067.4862
Z : 2407296.0622

Number of Iteration : 2

A Posteriori Variance of Combined Code and Carrier Phase Float Soultion : 2.640162E-05

****
*** LAMBDA ***
*** Combined Code and Carrier Phase 'Fixed' Solution ***
****

X : -2395793.7931
Y : 5395067.0775
Z : 2407296.1640

A Posteriori Variance: 1.63002056184705
Variance Ratio: 0 (no second best soluton)

****
*** Ambiguity Function Validation ***
****

Number of Local Maxima [AF of Candidates > 0.9 (or 0.8 if Warning Appears Above)]: 2

10 Maximum Candidates with AFV > 0.9 (or 0.8 if Warning Appears Above)

0.917404755015253
0.903515859503956
0
0
0
0
0
0
0
0

10 Minimum A Posteriori Variance

1.63002046450907
1.63002048360281
0
0
0
0
0
0
0
0

****
Ambiguity Function Result
****

First AFR : 1.168156
Second AFR : 1.14885
Third AFR : 1.009728
Final AFR : 1.000183
Maximum AF : 0.9477

WGS84 Cartensian Coordinates of Unknown station

X : -2395793.7950
Y : 5395067.0930
Z : 2407296.1780

****
Statistical Result
****

Number of Observations : 30

Number of Parameters : 3

A Posteriori Variance of unit weight : 1.63002053317381

Number of Iteration(s) : 3

F-test (at 95.0% confidence) : Passed

****
A Posteriori Variance-Covariance of Parameters
****

1.820408E-05 -2.518228E-05 -1.219756E-05
7.592419E-05 2.878107E-05
2.386704E-05

****
*** CALMS ***
Least Squares Result
****

X : -2395793.7951
Y : 5395067.0935
Z : 2407296.1780

WGS84 Geographic Coordinates of Unknown station

Lat : 22 19 14.2517257
Long : 113 56 40.6591849
Height : 5.958

Baseline slope distance (in metres) : 1600.322 Standard Deviation (m): 0.006384

Baseline Components (m): dx -338.415127 dy -762.264537 dz 1365.817954
Standard Deviations (m) : 0.004267 0.008713 0.000024

dn 1475.914839 de 618.628446 du 1.113429
0.003005 0.003277 0.009911

Solution Type : L1 fixed double difference
Code Solution Processing Time : 0.1601563 seconds

Float Solution Processing Time : 0.4375 seconds
LAMBDA Processing Time : 0.0625 seconds
AFM Processing Time : 1 minutes 7.609375 seconds
Total Time : 1 minute(s) 10.69141 seconds

Process Time : 00:38:13 29/03/99(Local Time)
Reference Station Observation File: h:\Data-BackUp\Swat1\981222A211.txt
Unkouwn Station Observation File : h:\Data-BackUp\Swat1\6205356111.txt

****
Base Station WGS84 Cartensian Coordinates
****

X : -2408856.098
Y : 5391044.469
Z : 2403591.685

****
A Priori Position of Unknown Station in WGS84 Cartensian Coordinates
****

X : -2418124.779
Y : 5386031.259
Z : 2405095.124

****
Processing Information
****

Reference satellite : 31
Number of Epoch(s) : 6
Measurement Interval (seconds) : 15
Occupation Time : 1 minute(s) 30 seconds

****
*** Initial Unknown Position ***
*** By Code Solution ***
****

X : -2418146.0571
Y : 5386069.9586
Z : 2405111.5935

Number of Iteration : 4

A Posteriori Variance of Code Soultion : 8.720272

****
*** Intermediate Unknown Position ***
*** Combined Code and Carrier Phase 'Float' Solution ***
****

X : -2418145.6424
Y : 5386068.5540
Z : 2405111.2707

Number of Iteration : 3

A Posteriori Variance of Combined Code and Carrier Phase Float Soultion : 2.689561E-05

```
**************************************************
***                  LAMBDA                    ***
***  Combined Code and Carrier Phase 'Fixed' Solution  ***
**************************************************

X :       -2418145.5249
Y :        5386068.3883
Z :        2405111.2491

A Posteriori Variance:     1.196881206243
Variance Ratio:          1.05574129419642

**********************************
***  Ambiguity Function Validation  ***
**********************************

Number of Local Maxima [AF of Candidates > 0.9 (or 0.8 if Warning Appears Above)]:  3

10 Maximum Candidates with AFV > 0.9 (or 0.8 if Warning Appears Above)

 0.930902687919496
 0.919801867762175
 0.905056492832757
 0
 0
 0
 0
 0
 0
 0

10 Minimum A Posteriori Variance

 1.19714986126418
 1.19008236264193
 1.19008252273458
 0
 0
 0
 0
 0
 0
 0

**********************
Ambiguity Function Result
**********************

First AFR      :  1.160655
Second AFR     :  1.002868
Third AFR      :  1.009497
Final AFR      :  1.000467
Maximum AF     :  0.9284
```

WGS84 Cartensian Coordinates of Unknown station

X : -2418145.3540
Y : 5386068.4320
Z : 2405111.4090

****
Statistical Result
****

Number of Observations : 18

Number of Parameters : 3

A Posteriori Variance of unit weight : 12.7018900531352

Number of Iteration(s) : 2

F-test (at 95.0% confidence) : Passed

****
A Posteriori Variance-Covariance of Parameters
****

2.168468E-04 -3.098848E-04 -2.845684E-04
1.248948E-03 1.304588E-03
1.728018E-03

****
Least Squares Result
****

X : -2418145.2800
Y : 5386068.2118
Z : 2405111.1717

WGS84 Geographic Coordinates of Unknown station

Lat : 22 17 57.47487209
Long : 114 10 41.93554464
Height : 5.5285

Baseline slope distance (in metres) : 10647.107 Standard Deviation (m): 0.017820

Baseline Components (m): dx -9289.181979 dy -4976.257161 dz 1519.486735
Standard Deviations (m) : 0.014726 0.035340 0.001728

dn 1688.288719 de 10511.695997 du -112.421643
0.012573 0.027389 0.047808

Solution Type : Ionospheric-free double difference
Code Solution Processing Time : 5.004883E-02 seconds
Float Solution Processing Time : 0.2800293 seconds

LAMBDA Processing Time	:	0.050048828125 seconds
AFM Processing Time	:	47.06982 seconds
Total Time	:	48.11011 seconds

APPENDIX II

LAMBDA PROCESSING LOG FILES

1.6 km baseline

Variance-covariance matrix of parameters

7.29E-03	-9.91E-03	-4.82E-03	3.41E-02	9.98E-03	-3.88E-03	-6.62E-03	7.12E-03
-9.91E-03	3.00E-02	1.13E-02	-5.72E-02	-6.92E-02	-1.77E-02	-9.98E-03	-1.65E-03
-4.82E-03	1.13E-02	9.51E-03	-2.80E-02	-4.20E-02	-9.11E-03	-7.51E-03	-3.41E-02
3.41E-02	-5.72E-02	-2.80E-02	0.16839	9.28E-02	-3.10E-04	-1.51E-02	4.33E-02
9.98E-03	-6.92E-02	-4.20E-02	9.28E-02	0.277018	9.21E-02	8.02E-02	0.106739
-3.88E-03	-1.77E-02	-9.11E-03	-3.10E-04	9.21E-02	3.97E-02	3.67E-02	1.75E-02
-6.62E-03	-9.98E-03	-7.51E-03	-1.51E-02	8.02E-02	3.67E-02	0.036645	2.56E-02
7.12E-03	-1.65E-03	-3.41E-02	4.33E-02	0.106739	1.75E-02	2.56E-02	0.214823

Variance-covariance matrix of ambiguities

0.16839	9.28E-02	-3.10E-04	-1.51E-02	4.33E-02
9.28E-02	0.277018	9.21E-02	8.02E-02	0.106739
-3.10E-04	9.21E-02	3.97E-02	3.67E-02	1.75E-02
-1.51E-02	8.02E-02	3.67E-02	0.036645	2.56E-02
4.33E-02	0.106739	1.75E-02	2.56E-02	0.214823

L matrix

1	0	0	0	0
1.411452	1	0	0	0
6.610616	5.352093	1	0	0
-0.604354	2.007524	1.031181	1	0
0.201732	0.496872	8.16E-02	0.119217	1

D matrix

5.41E-03	0	0	0	0
0	1.46E-02	0	0	0
0	0	2.58E-03	0	0
0	0	0	3.36E-02	0
0	0	0	0	0.214823

Complete LTDL

Original ambiguities

10642143
-1108689
247483.8
3764753
14633833

Z matrix

1	-1	-1	1	0
-3	2	1	-1	0
10	-3	1	-1	1
-4	-2	-3	4	-1
1	0	0	0	0

Complete Z-Transform
Complete Search (Five candidates)

16017869.38
-21131478.74
-22797607.25
26562360.2
-3517269.19

16017869.38

-21131478.74
-22797607.25
26562360.2
-3517269.19

16017869.38
-21131478.74
-22797607.25
26562360.2
-3517269.19

16017869.38
-21131478.74
-22797607.25
26562360.2
-3517269.19

16017869.38
-21131478.74
-22797607.25
26562360.2
-3517269.19

Best N set

16017869
-21131479
-22797607
26562360
-3517269

Second best N set

0
0
0
0
0

	Best	2nd best
Back transformed ambiguities	3764753	0
	-1108689	0
	14633831	0
	247484	0
	10642143	0

Back transformed ambiguities in original order	10642143
	-1108689
	247484
	3764753
	14633831

End Lambda

10.6 km baseline

Variance-coariance matrix of parameters

0.466569	-0.247674	-0.151531	1.699239	-0.392739	-0.774919
-0.247674	0.611658	0.32057	-1.069011	-1.344302	0.202257
-0.151531	0.32057	0.421397	9.30E-02	0.319205	0.857243
1.699239	-1.069011	9.30E-02	8.352007	1.907424	-0.697339
-0.392739	-1.344302	0.319205	1.907424	9.070673	4.056006
-0.774919	0.202257	0.857243	-0.697339	4.056006	3.379042

Variance-coariance matrix of ambiguities

8.352007	1.907424	-0.697339
1.907424	9.070673	4.056006
-0.697339	4.056006	3.379042

L matrix

1	0	0
0.653121	1	0
-0.206372	1.200342	1

D matrix

6.415625	0	0
0	4.20208	0
0	0	3.379042

Complete LTDL

Original ambiguities

-4581612.661
-35106603.5
-6024070.042

Z matrix

1	0	0
-1	1	0
1	-1	1

Complete Z-Transform

Complete Search (Five candidates)

24500921
-29082534
-6024070

24500920
-29082533
-6024070

24500922
-29082534
-6024070

24500920
-29082534
-6024070

24500921
-29082533
-6024070

Best N set

24500921
-29082533
-6024070

Second best N set

24500921
-29082534
-6024070

	Best	2nd best
Back transformed ambiguities	-4581612	-4581613
	-35106603	-35106604
	-6024070	-6024070

-4581612
-35106603
-6024070

Back transformed ambiguities in original

End Lambda

REFERENCES

Abdalla, K. A. and Fashir, H.H. (1991). "Modelling of Atmospheric Propagation Delays on Single Frequency GPS Signals." *IAG*, Vol. 109, pp.113-120.

Abidin, H. Z. (1993). "On the Construction of the Ambiguity Searching Space for On-The-Fly Ambiguity Resolution." *Navigation*, Vol. 40, Part 3, pp.321-338.

Abidin, H. Z., Wells, D. E. and Kleusbery, A. (1992). "Some aspects of "On-The-Fly" Ambiguity Resolution." *Proceedings of the Sixth International Geodetic Symposium on Satellite Positioning*, Columbus, Ohio, March 17-20, Vol. 2, pp.660-669.

Allan, A. L. (1993). *Practical Surveying and Computations*, 2nd ed., Butterworth-Heinemann.

Ashjaee, J., and Lorenz, R. (1992). "Precision GPS surveying after Y-code." *Proc. ION-GPS-92*, pp.657-659.

Ayson, I. and Lang, C. (1996). "Settlement monitoring and instrumentation during the construction of Hong Kong's new airport." *Proceedings: The 8th International Symposium on Deformation Measurements, Hong Kong*, June 25-28, pp.405-420.

Beutler G, Davidson DA, Langley RB, Santerre R, Vanicek P, Wells DE (1984). "Some theoretical and practical aspects of geodetic positioning using carrier phase difference observations of GPS satellites." University of New Brunswick, Canada, *Technical Report*, Vol. 109.

Blewitt, G. (1989). "Carrier phase ambiguity resolution for the Global Positioning System applied to geodetic baselines up to 2000 Km." *Journal of Geophysical Research*, Vol. 94, pp.10187-10203.

Bock, Y. (1998). "Medium Distance GPS Measurements." In Teunissen, P. J. G. and Kleusberg, A. (Eds), *GPS for Geodesy*, 2nd Edition, Springer, pp. 483-536.

Bock, Y, Gourevitch, S. A., Counselman, C. C., King, R.W., and Abbot, R. I. (1986). "Interferometric analysis of GPS phase observations." *Manuscripta Geodaetica*, Vol.11, Number 4, pp.282-288.

Bock, Yehuda and Shimada, S. (1990). "Continuously Monitoring GPS Networks for Deformation Measurements." *IAG*, Vol. 102, pp.40-56.

CED. (1998). "SLOPE MAINTENANCE A Prerequisite for A Safe Home." *World Wide Wed (WWW)*, http://www.info.gov.hk/ced/inf_9815.htm.

Chen, R. (1996). "Integration Analysis of the Finnish Permanent GPS Array and High Precise Local GPS Monitoring Networks." *Proceedings: The 8th International Symposium on Deformation Measurements*, Hong Kong, June 25-28, pp.37-46.

Chen, Y. Q., and Chrzanowski, A. (1986). "An Overview of the Physical Interpretation of Deformation Measurements." *Proceedings of Deformation Measurements Workshop*, 31 October-1 November 1986, Massachusetts Institute of Technology, pp. 207-220.

Cohen, C. E. (1996). "Attitude Determination." in Parkinson, B. W. et al. (ed.), *Global Positioning System: Theory and Applications, Progress in Astronautics and Aeronautics*, Vol. 164, AIAA, 1996, pp. 519-538.

Comp, C. J., and Axelrad, P. (1996). "An Adaptive SNR-Based Carrier Phase Multipath Mitigation Technique." *Proceedings of ION GPS-96*, Kansas City, September, 1996, pp. 683-697.

Corbett, S. J., Cross, P. A. (1995). "GPS Single Epoch Ambiguity Resolution." *Survey Review*, 33, 257 (July, 1995), pp. 149-160.

Coulon, B. and Caristan Y. (1990). "Monitoring Displacements by GPS: A Calibration Test." *IAG*, Vol. 102, pp.112-119.

Counselman, C. C., and Gourevitch, S. A. (1981). "Miniature interferometer terminals for earth surveying: Ambiguity and multipath with Global Positioning System." *IEEE Transactions on Geoscience and Remote Sensing*, Vol. GE-19(4), pp.244-252.

Cross, P. A. (1983). *Advanced least squares applied to position-fixing*. Working Paper No. 6, Department of Land Surveying, University of East London, pp.128-134.

Davis, J. L., Cosmo, M. L. and Elgered, G. (1995). "Using the Global Positioning System to Study the Atmosphere of the Earth: Overview and Prospects." *IAG*, Vol. 115, pp.233-242.

DeLoach, S. R. (1989). "Continuous Deformation Monitoring with GPS." *Journal of Surveying and Engineering*, Vol. 115, No. 1, pp.93-110

Divis, D. A. (1997). " L5: The Wait Continues." *GPS World*, Vol. 8, No. 9, September 1997, pp.12-16.

Dong, D. and Bock, Y. (1989). "Global Positioning System Network Analysis With Phase Ambiguity Resolution Applied to Crustal deformation Studies in California." *Journal of Geophysical Research*, Vol. 94, pp.3949-3966.

Erickson, C. (1992). "Investigations of C/A code and Carrier Measurements and Techniques for Rapid Static GPS Surveys." Reports of the Department of Geomatics Engineering of the University of Calgary, Vol. 20044

Euler, H. J., Sauermann, K. and Becker, M. (1990). "Rapid Ambiguity Fixing in small scale networks." *Proceedings of the Second International Symposium on Precise Positioning with the Global Positioning System*, Ottawa, Canada, September 3-7, pp.508-523.

Evans, Alan, G. and Hermann, B. R. (1990). "A Comparison of Several Techniques to Reduce Signal Multipath from the Global Positioning System." *IAG*, Vol. 102, pp.74-81.

Frei, E. (1991). "GPS-Fast Ambiguity Resolution Approach "FARA": theory and application." Presented paper at XX General assembly of IUGG, IAG-Symposium GM ¼, Vienna, August 11-24.

Frei, E. and Beutle, G. (1989). "Some Considerations concerning an adaptive, optimized technique to resolve the Initial Phase Ambiguities for Static and Kinematic GPS surveying-techniques." *Proceedings of the Fifth International Geodetic Symposium on Satellite Positioning*, Las Cruces, New Mexico, March 13-17, Vol. 2, pp.671-686.

Frei, E. and Beutler, G. (1990). "Rapid static positioning based on the fast ambiguity resolution approach 'FARA': Theory and first results." *Manuscripta Geodaetica*, 15 (6), pp.325-356.

Frei, E. and Schubernigg, M. (1992). "GPS Surveying Techniques using the "Fast Ambiguity Resolution Approach (FARA)." Paper presented at the 34th Australian Surveyors Congress and the 18th National Surveying Conference at Cairns, Australia, May 23-29, pp. 159-182.

Geiger, A., Hirter, H., Cocard, M., Bürki, B., Wiget, A., Wild, U and Schneider, D. (1995). "Mitigation of Tropospheric Effects in Local and Regional GPS Networks." *IAG*, Vol. 115, pp.263-267.

Geogiadou, Yola and Kleusberg, A. (1990). "Multipath Effects in Static and Kinematic GPS Surveying." *IAG*, Vol. 102, pp.82-89.

Goad, C. C. (1989). "Kinematic Survey of Clinton Lake Dam." *Journal of Surveying Engineering*, Vol. 115, No. 1, pp. 67-77.

Han, S. and Rizos, C. (1995). "On-The-Fly Ambiguity Resolution for Long Range GPS Kinematic Positioning." *IAG*, Vol. 115, pp.290-294.

Han, S. and Rizos, C. (1997a). "Comparing GPS Ambiguity Resolution Techniques.", *GPS World*. Vol.8, No. 10, October, 1997, pp. 54-60.

Han, S. and Rizos, C. (1997b). "GPS Ambiguity Resolution Techniques – Reliable Solutions Still a Challenge." *Geomatics Info Magazine*, Vol. 11, Number 11, pp.31-33.

Hartinger, H. and Brunner, F.K. (1998). "Experimental detection of deformations using GPS." *Proc. Symposium on Geodesy for Geotechnical and Structural Engineering*, Eisenstadt, pp. 145-152.

Hatch, R. (1986). "Dynamic differential GPS at the centimeter level." *Proceedings of the Fourth International Geodetic Symposium on Satellite Positioning*, Austin, Texas, April 28-May 2, Vol. 2, pp.1287-1298.

Hatch, R. (1991). "Instantaneous Ambiguity Resolution." Proceedings: Kinematic System in Geodesy, Surveying and Remote Sensing, IAG Symposium No. 107, Springer, New York, pp. 299-308.

Hein, G. W. and Riedl, B. (1995). "High Precision Deformation Monitoring Using Differential GPS." *IAG*, Vol. 115, pp.180-184.

Hilla, S. A. (1986). "Processing Cycle Slips in Nondifferenced Phase Data from the Macrometer V-1000 receiver." *Proceedings of the Fourth International Geodetic Symposium on Satellite Positioning*, Austin, Texas, April 28- May 2, Vol. 1, pp.647-661.

Hofmann-Wellenhof, B., Lichtenegger, H. and Collins, J. (1994). *GPS Theory and Practice*. 4th ed., Springer-Verlag – Wien New York.

Jakowski, N., Sardon, E., Engler, E., Jungstand, A. and Klähn, D. (1995). "About the Use of GPS Measurements for Ionospheric Studies." *IAG*, Vol. 115, pp.248-252.

Johannessen, R. (1997). "Interference: Sources and Symptoms." *GPS World*, Vol.8, No. 11, November, 1997, pp. 44-48.

Jonge de, P. and Tiberius, Ch. (1995). "Integer Ambiguity Estimation with the LAMBDA Method." *International Association of Geodesy Symposia 115*, pp.280-284.

Jonge de, P. J., Tiberius, C. C. J. M. (1996). The LAMBDA Method For Integer Ambiguity Estimation: Implementation Aspects. Delft Geodetic Computing Centre LGR Series No. 12.

Kennie, T. J. M. and Petrie, G. (1990). *Engineering Surveying Technology*. Blackie – Glasgow and London, pp. 166-169.

Komjathy, A., Langley, R. B., Vejrazka, F. (1995). "Assessment of two Methods to Provide Ionospheric Range Error Corrections for Single-Frequency GPS Users." *IAG*, Vol. 115, pp.253-257.

Krakiwsky, E. J. (1986). "An Overview of Deformations, Measurement Technologies, and Mathematical Modeling and Analysis." *Proceedings of Deformation Measurements Workshop*, 31 October-1 November 1986, Massachusetts Institute of Technology, pp. 7-33.

Landau, H., Euler, H. J. (1992). "On-the-fly Ambiguity Resolution for Precise Differential Positioning." Proceedings of ION GPS-92, Fifth International Technical Meeting of the Satellite Division of the Institute of Navigation, Albuquerque, New Mexico, September 16-18, pp. 607-613.

Langley, R. B. (1997). "GPS Receiver System Noise." *GPS World*, Vol.8, No. 6, June, 1997, pp. 40-45.

Lau, L. (1995). "GPS Theory Vs Practice." *Postgraduate Diploma Project Report*, Department of Geomatic Engineering (formerly Photogrammetry and Surveying), University College London.

Lau, L. (1997). "Investigation into the GPS Processing Algorithm for Deformation Monitoring." *M.Phil. Degree Progress Report*, Dept. of Land Surveying and Geo-Informatics, The Hong Kong Polytechnic University.

Lau, L. and Mok, E. (1999a). "Improvement of GPS Relative Positioning Accuracy By Using SNR." *Journal of Surveying Engineering*, Vol.125, No.4, November, 1999, pp. 185-202.

Lau, L. and Mok, E. (1999b). "Improvement of GPS Relative Carrier Phase Positioning Accuracy by SNR Weighted Ambiguity Function Technique." *Proceedings of the Institute of Navigation 55th Annual Meeting: Navigational Technology for the 21st Century*, jointly sponsored by the Institute of Navigation and Draper Laboratory, June 28-30, 1999, Royal Sonesta Hotel, Cambridge, MA, USA, pp. 323-332.

Lau, L. and Mok, E. (1999c). "Precise GPS Processing Algorithm for Short Observation Time-span in Urban Area." *Proceedings of the Institute of Navigation 55th Annual Meeting: Navigational Technology for the 21st Century*, jointly sponsored by the Institute of Navigation and Draper Laboratory, June 28-30, 1999, Royal Sonesta Hotel, Cambridge, MA, USA, pp. 533-540.

Leick, A. (1995). *GPS Satellite Surveying*. 2nd ed., Wiley-Interscience – New York Chichester Toronto Brisbane Singapore.

Levy, L. J. (1997). " The Kalman Filter: Navigation's Integration Workhorse." *GPS World*, Vol. 8, No. 9, September 1997, pp.65-71.

Lichtenegger, H. and Hofmann-Wellenhof, B. (1990). "GPS Data Preprocessing for Cycle-Slip Detection." *IAG*, Vol. 102, pp.57-68.

Lightsey, E. G. (1996). "Spacecraft Attitude Control Using GPS Carrier Phase." in Parkinson, B. W. et al. (ed.), *Global Positioning System: Theory and Applications, Progress in Astronautics and Aeronautics*, Vol. 164, AIAA, 1996, pp. 461-480.

Lindquister, U., Blewitt, G., Pogorelc, S., Roth, M., Caissg, M. and Tetreault (1989). "Design and Testing of a Continuously Monitoring GPS-Based System." *Transactions of American Geophysical Union*, Vol. 70, Part 1054.

Mader, G.L. (1992). "Rapid static and kinematic Global Positioning System solutions using the ambiguity function technique." *Journal of Geophysical Research* 97(B3), pp.3271-3283.

Mikhail, E. M. (1976). *Observations and Least Squares*, Harper & Row, Publishers, Inc..

Mittag, H. J., Rinne, H. (1993). *Statistical Methods of Quality Assurance.* 1st ed., Chapman and Hall, London.

Mok, E. (1998). "A Single Epoch GPS Processing Algorithm for Deformation Monitoring." *Proc. Symposium on Geodesy for Geotechnical and Structural Engineering*, International Association of Geodesy, Special Commission 4, April 20-22 1998, Eisenstadt, Vienna, pp159-166.

Mok, E. and Cross, P. A. (1996). "Optimum Rejection Threshold Determination for Ambiguity Function Testing." *Proceedings of Geoinformatics "96 Wuhan" – International Symposium on the Occasion of the 40th Anniversary of Wuhan Technical University of Surveying and Mapping (WTUSM)*, pp. 317-335.

Musman, S. (1995). "Deriving Ionospheric TEC from GPS Observations." *IAG*, Vol. 115, pp.258-262.

Ou, J. (1995). "On Atmospheric Effects on GPS Surveying." *IAG*, Vol. 115, pp.243-247.

Pachelski, W. (1995). "GPS Phases: Single Epoch Ambiguity and Slip Resolution." *IAG*, Vol. 115, pp.295-299.

Remondi, B. W. (1984). *Using the Global Positioning System (GPS) phase observable for relative geodesy: Modeling, processing, and results.* NOAA, Rockville, MD 20852, 1984, Reprint of doctoral dissertation, Center for Space Research, University of Texas at Austin.

Remondi, B. W. (1985). "Global Positioning System carrier phase: description and use." *Bulletin Geodesique*, 59(4), pp.361-377.

Remondi, B. W. (1991). "Kinematic GPS Results Without Static Initialization." National Information Center, Rockville, Maryland, NOOA Technical Memorandum NOS NGS-55.

Retscher, G. (1997). "Powerlines and Transmitting stations Impair RTK-GPS." *Geomatics Info Magazine*, Vol. 11, Number 11, pp.65-67.

Rizos, C., Galas, R. and Reigber, C (1996). "Design challenges in the development of a GPS-based volcano monitoring system." *Proceedings of The 8th FIG International Symposium on Deformation Measurements*, Hong Kong, June 25-28, pp.7-16.

Roddy, D. (1995). *Satellite Communications*. 2nd ed., McGraw-Hill.

Sleewaegen, J. M. (1997). "Multipath Mitigation, Benefits from Using the Signal-to-Noise Ratio." *Proceedings of ION GPS-97*, Kansas City, Missouri, September, 1997, pp. 531-540.

Spilker, J. J. and Natali, F. D. (1996). "Effects of Interference on the GPS C/A Receiver." in Parkinson, B. W. et al. (ed.), *Global Positioning System: Theory and Applications, Progress in Astronautics and Aeronautics*, Vol. 163, AIAA, 1996, pp. 745-756.

Strang, G. and Borre, K. (1997). *Linear Algebra, Geodesy, and GPS*. Wellesley-Cambridge Press.

Talbot, N. (1988). "Optimal Weighting of GPS Carrier Phase Observations based on the Signal-to-Noise Ratio." *International Symposium on Global Positioning Systems*, Queensland, 1988, pp. V.4.1-17.

Taylor, J. R. (1997). *An Introduction to Error Analysis*. Second Edition, University Science Books, Sausalito, California.

Teunissen, P. J. G. (1995a). "The Invertible GPS Ambiguity Transformation." *manuscripta geodaetica*, 20, pp. 489-497.

Teunissen, P. J. G. (1995b). "The Least-squares Ambiguity Decorrelation Adjustment: A Method for Fast GPS Integer Ambiguity Estimation." *Journal of Geodesy*, 70, pp. 65-82.

Teunissen, P. J. G. (1995c). "Size and Shape of L_1/L_2 Ambiguity Search Space." *IAG*, Vol. 115, pp.275-279.

Teunissen, P. J. G. (1998). "GPS Carrier Phase Ambiguity Fixing Concepts." In Teunissen, P. J. G. and Kleusberg, A. (Eds), *GPS for Geodesy*, 2nd Edition, Springer, pp. 319-388.

Teunissen, P. J. G., de Jonge, P. J. and Tiberius, C. C. J. M. (1996). " The Volume of the GPS Ambiguity Search Space and its Relevance for Integer Ambiguity Resolution. Proceedings of ION GPS-96, Part 1 of 2, Kansas City, Missouri, pp. 889-898.

Tiberius, C.C.J.M. and de Jonge, P.J. (1995). "Fast Positioning Using the LAMBDA Method." *Proceedings of the 4th International Symposium on Differential Satellite Navigation Systems DSNS'95*, Bergen, Norway, April 24-28, 1995, Paper No. 30.

Tiberius, C.C.J.M., Teunissen, P.J.G., de Jonge, P.J. (1997). "Kinematic GPS: Performance and Quality Control." *Proceedings of International Symposium on*

Kinematic Systems in Geodesy, Geomatics and Navigation KIS'97, 1997, pp. 289-299.

Uren, J. and Price, W. F. (1994), *Surveying for Engineers*, Third Edition, Macmillan, London, pp.554.

Van Nee, R.D.J. (1992). "Multipath Effects on GPS Code Phase Measurements." Navigation, *Journal of The Institute of Navigator*, Vol.39, No.2, pp. 177-190.

Wanninger, L. and Jahn, C. H. (1991). "Effects of Severe Ionospheric Conditions on GPS Data Processing." *IAG*, Vol. 109, pp.141-150.

Weill, L. R. (1997). " Conquering Multipath: The GPS Accuracy Battle." *GPS World*, Vol. 8, No. 4, April 1997, pp.59-66.

Wells, D. E., Beck, N., Delikaraoglou, D., Kleusberg, A., Krakiwsky, E. J., Lachapelle, G., Langley, R. B., Nakiboglu, M., Schwarz, K. P., Tranquilla, J. M., Vanicek, P. (1987). *Guide to GPS Positioning*. Canadian GPS Associates, Fredericton, New Brunswick, Canada.

Welsch, W. M. (1996). "Geodetic Analysis of Dynamic Processes: Classification and Terminology." *Proceedings: The 8th International Symposium on Deformation Measurements*, Hong Kong, June 25-28, pp.147-156.

Wolf, P. R. (1983). Elements of Photogrammetry. 2nd Edition, McGraw-Hill International Editions.

Wolf, P. R., Ghilani, C. D. (1997). *Adjustment Computations: Statistics and Least Squares in Surveying and GIS*. 3rd Ed., Wiley-Interscience, John Wiley & Sons, Inc..

Yang, X. and Brock, R. (1996). "Modeling GPS Satellite Geometry With RDOP." *Mult ASPRS/ACSM Annual Convention and Exposition Technical Papers*, Bethesda: ASPRS/ACSM, 1996, Vol. 2, pp. 172-181.

BIBLIOGRAPHY

Bentley, J. P. (1995). *Principles of Measurement Systems*. 3rd Edition, Longman Scientific & Technical, Longman Group UK Limited, England.

ICD-GPS-200C (1993). Interface control document, Revision C, Initial Release, 10 October 1993, Arinc Research Corporation, 2250 E. Imperial Highway, Suite 450, El Segundo, CA 90245-3509.

Jordon, D. W. and Smith P. (1997). *Mathematical Techniques: An Introduction for the Engineering, Physical*, Mathematical Sciences. 2nd edition, Oxford Toronto Melbourne, Oxford University Press.

Kreyszig, E. (1993). *Advanced Engineering Mathematics*. 7th edition, John Wiley & Sons, Inc., New York Chichester Brisbane Toronto Singapore.

Leon, S. J. (1994). *Linear Algebra With Applications*. 4th Edition, Macmillan College Publishing Company, Inc..

Thompson, E. H. (1969). *An Introduction to the Algebra of Matrices with Some Applications*. Adam Hilger, London.